*Economic Geology 100th Anniversary Volume*
pp. 39–75

# Coupling between Deformation, Fluid Pressures, and Fluid Flow in Ore-Producing Hydrothermal Systems at Depth in the Crust

Stephen F. Cox†

*Department of Earth and Marine Sciences and Research School of Earth Sciences, Australian National University, Canberra, ACT 0200, Australia*

## Abstract

At depths greater than several kilometers in the crust, elevated temperature, elevated confining pressure, and the presence of reactive pore fluids typically drive rapid destruction of permeability in fractured and porous rock. Ongoing deformation is required to regenerate permeability and facilitate the high fluid flux necessary to produce hydrothermal ore systems. A dominant influence on the development of fluid pathways in hydrothermal systems is provided by stress states, fluid pressures, and reactions that drive permeability enhancement and compete with permeability destruction processes.

Fluid redistribution within hydrothermal systems at depth in the crust is governed largely by hydraulic gradients between upstream fluid reservoirs and the downstream regions of permeable networks of active faults, shear zones, and related structures that drain reservoirs. Pressure-driven flow leads to generally upward migration of fluids, although permeability anisotropy and tortuous flow paths may cause a significant along-strike component to fluid migration. Devolatilization reactions in prograding metamorphic regimes play a key role, not only in fluid production but also in generating transitory elevated permeability in deep crustal reservoirs. Active deformation and the development of high pore-fluid factors (the ratio of fluid pressure to vertical stress) in fluid reservoirs also drive permeability enhancement via grain-scale microfracturing and pervasive development of meso- to macroscale hydraulic fracture arrays. In the upstream, high-temperature parts of hydrothermal systems, pervasive fluid flow through the crust may occur via episodic migration of fluid-pressure pulses. Recent observations suggest that propagating fluid-pressure pulses may create transient permeabilities as high as $10^{-13}m^2$ in the deep crust.

Flow focusing occurs wherever networks of active, high-permeability shear zones, faults, or other permeable structures, penetrate pressurized fluid reservoirs. These structures drain reservoirs and provide pathways for fluid redistribution to higher crustal levels. Contrasting styles of flow are expected between flow pathways in the aseismically deforming lower half of the crust and pathways within the seismogenic regime in the upper half of the crust. Below the seismic-aseismic transition, steady-state creep processes favor near-constant permeabilities and continuous fluid flow. In the seismogenic regime, large changes in fault permeability during the seismic cycle produce episodic flow regimes. In particular, large earthquake ruptures that propagate down from the upper crust into deeper level fluid reservoirs generate major, transitory perturbations to fluid pressure gradients. Episodic fluid redistribution from breached, overpressured (i.e., suprahydrostatic) reservoirs has the potential to generate large fluid discharge and high fluid/rock ratios around the downstream parts of fault systems after large rupture events. Hydrothermal self-sealing of faults, together with drainage of the hydraulically accessible parts of reservoirs between earthquakes, progressively shuts off flow along fault ruptures. Permeability enhancement due to rupture events may also drive transitory flow of fluids, derived from shallow crustal reservoirs, deep into fault zones after earthquakes.

As earthquakes migrate around fault systems in the upper, seismogenic part of the crust, permeability distribution and fluid pathways can evolve in complex ways. To achieve the necessary time-integrated fluid fluxes, the formation of large ore systems in this regime requires redistribution of fluid batches predominantly through small segments of fault systems during numerous rupture cycles. Sustained localized flow at the ore field scale is favored by development of long-lived, actively deforming, high-permeability structures such as fault jogs or fault intersections on high displacement faults. These structures can produce pipelike pathways linking deep reservoirs and shallower crustal levels. The generation of aftershock networks also influences fluid redistribution and discharge around the downstream ends of main-shock rupture zones. The distribution of these networks, and their repeated reactivation, is influenced by stress changes caused by main-shock rupture and by postseismic migration of fluid-pressure pulses away from the downstream ends of main-shock rupture zones.

At the deposit scale, in fracture-controlled hydrothermal systems, the highest fluid flux occurs where the apertures, densities, and connectivities of fractures are greatest. The locations and geometries of these sites are governed by fluid-driven permeability enhancement in structurally controlled sites such as jogs, bends, and terminal splays, typically in low displacement faults and shear zones, as well as by fault intersections, competence contrasts, and fold-related dilation. Permeability anisotropy in structural pathways can influence deposit-scale flow directions and shapes of ore shoots.

## Introduction

Hydrothermal ore systems comprise an upstream region, where metals and fluids are derived, and a downstream region where metals are deposited. Successful development of hydrothermal ore systems first requires an appropriate geodynamic setting to generate metal-fertile fluid reservoirs. Second, it requires the generation of permeable fluid pathways to drain fluids from potentially large-volume fluid reservoirs and

† E-mail, Stephen.Cox@anu.edu.au

transport them to volumetrically much smaller ore deposition sites (Fig. 1). The contrast between fluid/rock ratios in the upstream source region and in the downstream deposit site in hydrothermal systems commonly exceeds $10^3$ (Heinrich et al., 2000).

At depths greater than several kilometers in the continental crust, elevated confining pressures and temperatures tend to remove intergranular porosity and fracture porosity in rocks on relatively short geologic time scales, especially in regimes where reactive pore fluids are present (Cox, 1999). Accordingly, the genesis of hydrothermal ore deposits at depths greater than several kilometers is dependent on processes that generate permeability and control the distribution of fluid pathways, as well as being dependent on the availability of metal-fertile fluids.

The distribution and availability of fluids at depth in the crust is very restricted in space and time. For example, prograding and devolatilizing metamorphic regimes in the mid to deep crust could form the upstream regions of crustal-scale hydrothermal systems with potential to generate some types of ore systems (McCuaig and Kerrich, 1994; Cox, 1999). In many metamorphic belts, isotopic and petrologic evidence for rock-buffered fluid-rock reaction indicates very low fluid fluxes (Thompson, 1997). However, in other cases, fluid-buffered reactions indicate grain-scale fluid fluxes as high as $10^{-8}$ $m^3m^{-2}s^{-1}$ during collisional orogenesis (Yardley et al., 1991; Dipple and Ferry, 1992a; Ferry, 1994). By contrast, local fluid fluxes in shear zones in some greenschist to low amphibolite facies regimes can be higher than $10^{-4}$ $m^3m^{-2}s^{-1}$ (Dipple and Ferry, 1992b; Fig. 2). In ruptured fault zones in the upper, seismogenic half of the crust, much higher transitory fluid fluxes are possible (Miller et al., 2004). Accordingly, the difference in fluxes between regionally pervasive flow regimes and highly localized flow regimes during midcrustal prograde metamorphism can involve fluid focusing comparable to that necessary to generate ore systems. Despite this, the majority of metamorphic hydrothermal systems in collisional orogens have poor ore deposit endowments. This highlights the point that the production of fluid reservoirs must be complemented, not just by the development of channelized, high fluid flux regimes, but also by the availability of physical and chemical processes that can efficiently scavenge metals from fluids over very short segments of fluid pathways (Fig. 1).

To a first approximation, the crust in many geodynamically active settings comprises an upper, high-permeability, near-hydrostatic fluid-pressure regime and a deeper, lower permeability regime in which fluid pressures typically exceed hydrostatic values; transiently, at least, fluid pressures may attain near-lithostatic values at depth in the crust (Etheridge et al., 1983, 1984). The transition from hydrostatic to suprahydrostatic fluid pressures typically occurs at depths of 5 to 10 km (Sibson, 2001). Processes that foster the generation of reservoirs with different fluid pressures, and episodically breach the boundary between these fluid-pressure regimes, have potential to generate the rapid fluid redistribution and physicochemical reactions that are key factors in the genesis of hydrothermal ore deposits at depths greater than several kilometers.

This paper explores how deformation processes and physical fluid-rock interactions influence permeability evolution and the development of fluid pathways in initially low-permeability rocks. In particular, this review highlights (1) the roles of stress regimes, fluid-pressure states, and reactions in driving permeability enhancement and fluid migration; (2) the role of dynamic competition between porosity-creation

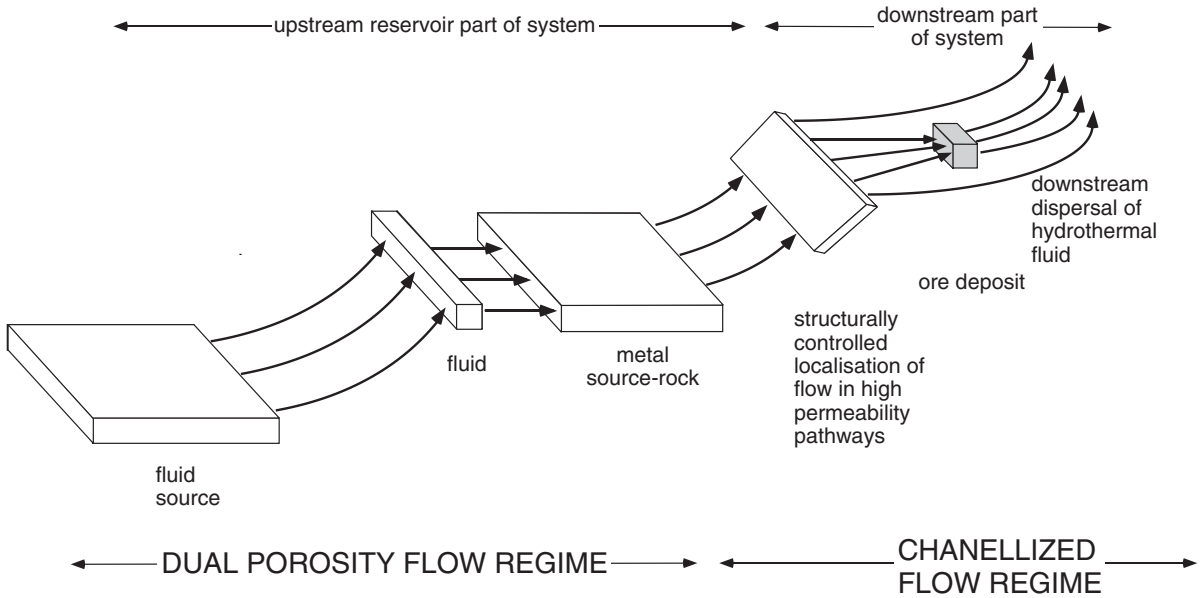


FIG. 1. Schematic overview of the basic structure of a fracture-controlled, hydrothermal ore system involving one fluid reservoir. Fluids and metals are sourced in the upstream parts of the system. Metal scavenging from source rocks in many cases involves pervasive grain-scale flow regimes. Delivery of potentially large fluid volumes to the relatively small volumes of ore deposits involves structurally controlled channelling of fluid into localized pathways such as fracture networks, faults, and shear zones. Spent fluids are dispersed downstream from ore deposits.

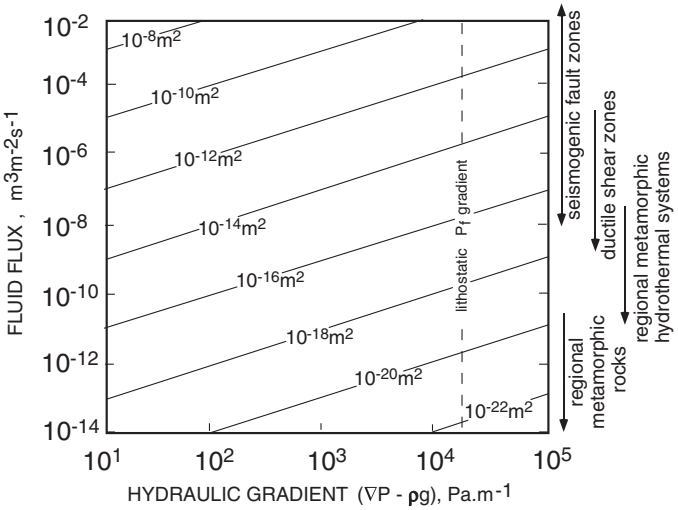


FIG. 2. The effects of vertical fluid-pressure gradients (Pascals per meter) and permeability ($m^2$) in controlling the vertical component of fluid flux ($m^3m^{-2}s^{-1}$) in hydrothermal systems. Approximate maximum flow rates are indicated for various pathways. The vertical dashed line represents a vertical lithostatic fluid-pressure gradient.

and -destruction processes in controlling temporal changes in permeability, fluid-pressure evolution, and the dynamics of fluid flow during crustal deformation; (3) the factors that influence the evolution of fluid pathways and localization of flow during progressive deformation; and (4) deposit-scale structural controls on fluid flow and lode geometries.

The focus is on processes operating in geodynamically active environments at depths greater than several kilometers in the crust, where fluid pressures are typically above hydrostatic values (i.e., overpressured fluids, used interchangeably here with suprahydrostatic). The depth of interest includes much of the continental seismogenic regime (typically the upper 10–15 km; Scholz, 1990) and the underlying aseismically deforming continental crust. Although this paper does not specifically treat flow processes in the shallow and typically near-hydrostatic-pressured crust (depths typically less than several kilometers; cf. Cathles and Adams, 2005), the principles discussed are relevant for fracture-controlled hydrothermal ore deposits formed in shallow crustal environments where high fluid fluxes and locally low permeabilities can result in the development of transient overpressuring of fluids (e.g., some intrusion-related systems; Fournier, 1999).

## Hydrothermal Ore Deposit Styles Formed at Depth in the Crust

The processes and principles discussed in this paper are applicable to many types of structurally controlled hydrothermal ore systems whose genesis involved broadly fracture-controlled flow. This group includes deposit styles related to faults, shear zones, and their associated vein systems, as well as vein-related ore deposits related to fold growth and other crustal deformation processes. These deposit styles can develop in amagmatic geodynamic settings, as well as in intrusion-related environments. The relevant deposit styles form predominantly in host rocks with low intrinsic permeability prior to fracture growth, at depths greater than several kilometers, temperatures greater than approximately 250ºC, and in suprahydrostatic fluid-pressure regimes. Many such deposits form in fault-related settings in the upper half of the crust. In this case, episodic, earthquake-producing (seismogenic) slip processes can play a key role in governing the dynamics of stress states, fluid pressures, and evolution of permeability (Sibson, 2001). In the mid to deep crust (depths of approx 15–35 km), the deformation style is predominantly aseismic, and the evolution of stress states, fluid pressures, and permeability in hydrothermal systems at these crustal levels can be expected to contrast with that in the seismogenic regime (Cox, 1999).

A major class of ore deposit that is generated by high fluid flux at depths of approximately 5 to 20 km and temperatures typically in the range 250º to 450ºC is the mesothermal (or orogenic) class of lode gold deposits. These deposits are some of the world's major gold resources (Groves et al., 1989, 2003; Cox et al., 1991; Goldfarb et al., 2001, 2005). They form from low-salinity, $H_2O$- and $CO_2$-bearing fluids (McCuaig and Kerrich, 1994) and usually develop in and around low displacement faults, shear zones, and related fracture systems that form part of larger, crustal-scale, linked shear systems (Groves et al., 1995; Cox, 1999). In many cases, the spatially related, crustal-scale faults are older structures that have been reactivated during the period of gold mineralization. Deposits are commonly clustered within small segments of fault systems (Cox and Ruming, 2004; Micklethwaite and Cox, 2004; Robert et al., 2005). The temperature range for formation, and the brittle and mixed brittle-plastic deformation styles of most mesothermal gold systems indicate that they form in a depth range that straddles the seismic-aseismic transition that typically occurs at depths of 10 to 15 km in continental crust. Lode gold deposits formed in predominantly plastic regimes at deeper crustal levels are less abundant (Barnicoat et al., 1991; Ridley et al., 2000).

The formation of lode gold deposits usually involves large fluxes of near-lithostatic pressured fluids along active faults and shear zones. Although gold-rich mesothermal systems apparently can form at all stages in the evolution of convergent accretionary and collisional orogens, they develop predominantly in the postpeak metamorphic stages of orogen evolution (Groves et al., 1989; McCuaig and Kerrich, 1994). Although fluids produced by devolatilization reactions during crustal metamorphism are implicated in the formation of many mesothermal gold systems, fluids derived from mantle sources, magmatic systems, and near-surface reservoirs provide alternative fluid sources in some cases (e.g., Kerrich and Cassidy, 1994; Ridley and Diamond, 2000).

Other types of hydrothermal ore systems that form at depth within convergent orogens include some iron oxide Cu-Au systems such as the Proterozoic Tennant Creek gold deposits and Cu-Au deposits in the Proterozoic Mount Isa inlier (Williams et al., 2005). The Mount Isa Cu deposit, which formed at midcrustal depths and temperatures of 250° to 300°C, is an example of an ore system formed in a fracture-controlled flow regime following peak metamorphism (Heinrich et al., 1995; Matthai et al., 2004). Some disseminated to massive sulfide base metal Au ore systems, such as those of the Cobar region in New South Wales (Glen, 1987; Stegman

and Pocock, 1996), also have origins related to fluid flow during regional crustal shortening in low-grade metamorphic environments. Metalliferous (Fe-Cu-Pb-Zn) quartz-carbonate-sulfide veins formed in postpeak metamorphic regimes in some orogens (e.g., Anderson et al., 2004) could also be products of giant hydrothermal systems in collisional orogens. Some unconformity-related uranium deposits, or parts of them, also involve fracture-controlled flow in metamorphic rocks, even though ore genesis involves porous flow in the overlying low-temperature sedimentary sequences as well (Wilde et al., 1989).

Fracture-controlled fluid flow in initially low-permeability host rocks is a key element in the generation of many intrusion-related ore systems. Examples include Sn-W vein deposits such as Panasqueira (Foxford et al., 2000), various other polymetallic, granite-related vein deposits (Cerny et al., 2005), gold deposits related to felsic intrusions in the Proterozoic Pine Creek inlier of the Northern Territory in Australia (Matthai et al., 1995), alkaline intrusive-related deposits such as Porgera in Papua-New Guinea (Munroe, 1995), and porphyry Cu-Au and Cu-Mo systems (Meyer et al., 1968; Heidrick and Titley, 1982; Tosdal and Richards, 2001; Seedorff et al., 2005). Many of these fracture-controlled hydrothermal systems developed in transiently suprahydrostatic fluid-pressure regimes (e.g., Redmond et al., 2004).

The formation of magmatic-related skarn systems also usually involves fracture-controlled flow, as well as flow via chemically enhanced porosity, in overpressured hydrothermal regimes (Dipple and Gerdes, 1998; Meinert et al., 2005). Fracture-controlled flow is also implicated in the formation of some Carlin-type deposits (Hofstra and Cline, 2000; Cline et al., 2005), as well as in the genesis of some precious metal systems in extensional fault complexes (Wilkins et al., 1986; Roddy et al., 1988).

## Fluid Reservoirs

### *Distribution of flow*

Transitory fluid flow is significant in a variety of active geodynamic settings, particularly in parts of accretionary and collisional orogens, but also in some extensional and strike-slip regimes (Fig. 3). Hydrothermal systems develop in both magmatically active and amagmatic environments. Hydrothermal ore deposits themselves are one of the principal indicators of high-flux fluid flow. Both in ore deposits, and in other high fluid flux environments, key indicators of intense

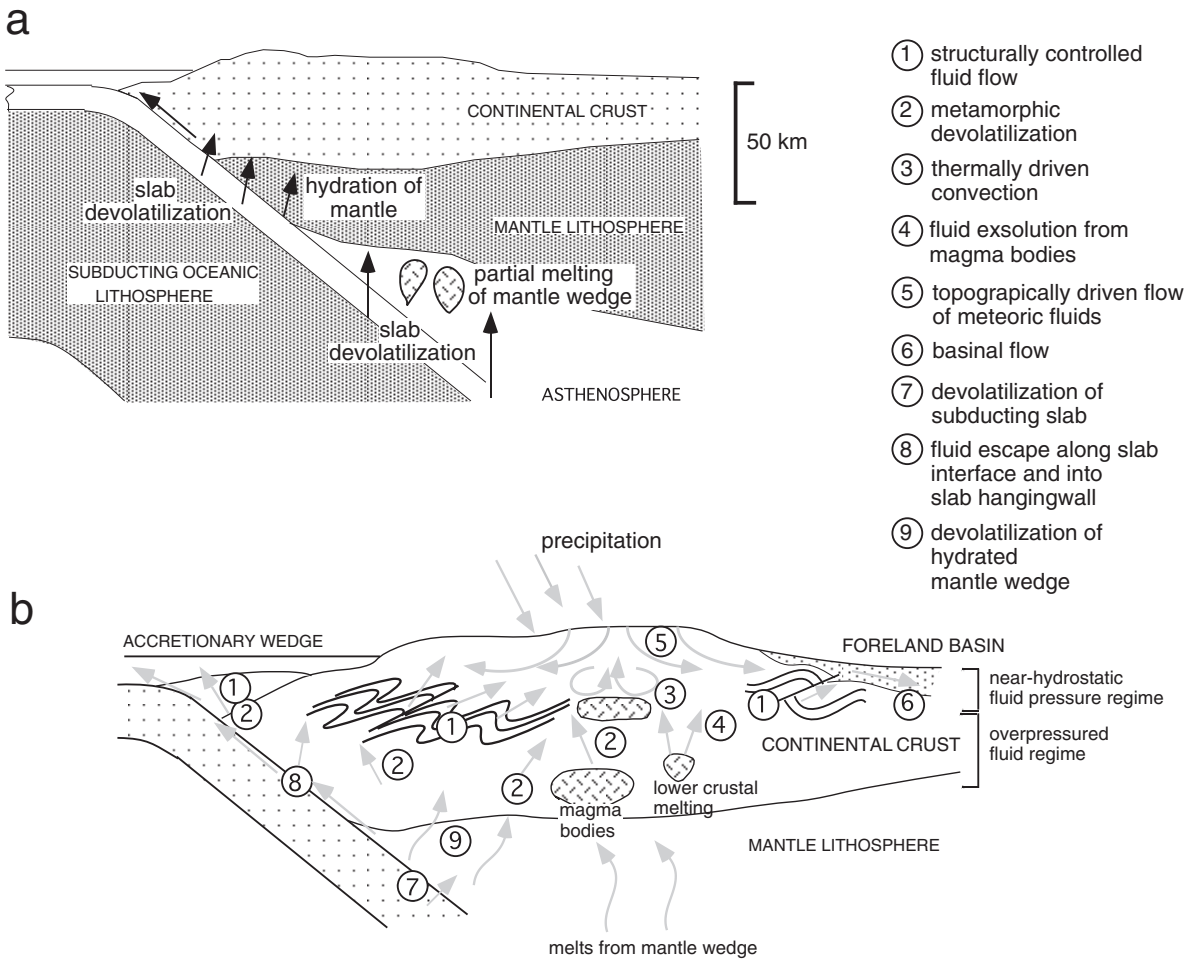


FIG. 3. a. General lithospheric-scale structure at a convergent, oceanic-continental plate boundary. b. Detail of distribution of various fluid sources and pathways.

fluid activity include abundant veins, hydrothermal alteration around veins and fracture networks, and disturbance to isotopic systems. Fluid flow and its associated effects may be regionally pervasive, occurring at the grain scale or via pervasively distributed macroscopic fracture systems. Flow may also be localized along particular high-permeability, mesoscopic to macroscopic structures such as faults, shear zones, or lithological boundaries (e.g., Oliver, 1996; Cox et al., 2001).

Permeability at depths where temperatures exceed 250ºC is normally expected to be low (e.g., Cox, 1999; Manning and Ingebritsen, 1999). Thus, in the following section, it will be shown that the high time-integrated fluid fluxes associated with hydrothermal ore genesis require substantial permeability enhancement by microscale to macroscopic fracturing, or reactions. Permeability enhancement is most effective while rocks deform at elevated pore-fluid factors (where pore-fluid factor, $\lambda_v$, is the ratio of fluid pressure $P_f$ to vertical stress $\sigma_v$). Furthermore, permeability enhancement, which is driven by deformation, high fluid pressures, or reactions, is a transient phenomenon. Sustained elevated permeability requires ongoing deformation, high pore-fluid factors, or permeability enhancing reactions.

*Types of fluid reservoirs*

Overpressured fluids that migrate at depth in the crust (typically below approx 5 km) in geodynamically active regions can be derived from a variety of reservoirs (Fig. 3). These include fluids generated by mantle sources, devolatilization reactions in prograde crustal metamorphic regimes, fluids expelled from magmatic systems, surface-derived (meteoric and seawater) fluids, and pore fluids in sedimentary basins.

*Hydrothermal systems related to prograde metamorphism:* Part of the fluid budget at convergent plate margins can be derived from prograde devolatilization reactions occurring in hydrated oceanic crust during subduction (Peacock, 1990; Phillipot and Selverstone, 1991; Manning, 2004). Typically, fluids emerging from subducting slabs at depths of 100 km or so induce partial melting in the overlying mantle wedge. However, in young, warm slabs, devolatilization at depths of 35 to 50 km can hydrate large volumes of the overlying forearc mantle wedge, producing serpentinite (Preston et al., 2003). Subsequent dehydration of the serpentinite has the potential to supply large volumes of aqueous fluids to the overlying crust. At shallower levels, permeability enhancement associated with megathrust earthquakes along the subduction interface has been implicated in fluid redistribution from the subducting plate into the overlying continental crust hanging wall (Husen and Kissling, 2001). Large strike-slip fault systems near plate boundaries also potentially provide a plumbing system that taps into mantle-derived fluids. Kennedy et al. (1997) argued for a mantle component to fluids in the San Andreas fault system in California.

Large fluid budgets are also associated with compaction and devolatilization reactions in accretionary complexes at active convergent plate margins (Vrolijk, 1987; Brantley et al., 1997; Bebout and Barton, 1989). These fluids can drain either along thrusts toward the toe of the accretionary complex or upward into the shallower parts of the complex (Fig. 3).

In active collisional orogens, fluids derived from devolatilization reactions during prograde metamorphism deep in the continental crust provide a major fluid source (Powell et al., 1991). Such reactions typically produce low-salinity $H_2O$-$CO_2$ fluids whose detailed chemistry is governed by rock buffering during progressive fluid generation, as well as by fluid-rock reaction along pathways as fluids migrate to shallower crustal levels (Greenwood, 1975; Bickle and Baker, 1990; Yardley et al., 1991; Rumble, 1994). Hydration reactions in retrograde, postpeak metamorphic regimes can increase fluid salinity (Yardley and Graham, 2002).

A significant aspect of the thermal evolution of convergent orogens is that peak metamorphism and attendant fluid evolution commonly occurs later at deep crustal levels than it does at upper crustal levels (Stüwe et al., 1993). Accordingly, deeply sourced fluids can migrate into the upper crust when that part of the crust is already on the retrograde part of its thermal history. This may be a significant control on the timing of formation of mesothermal gold systems in orogens.

Various approaches have been used to estimate fluid production rates and fluid fluxes during prograde metamorphism within the continental crust in convergent orogens. For example, Walther and Orville (1982) and Yardley (1986) estimated maximum fluid fluxes out of crustal regions undergoing devolatilization reactions as 0.3 to 0.4 kg $m^{-2}\,yr^{-1}$. Brady (1989) calculated maximum fluxes of 0.5 kg $m^{-2}\,yr^{-1}$ for complete dehydration of a 4.7-km-thick pile of pelitic metasediments during 1 m.y. Using one-dimensional numerical models of regional metamorphism, Peacock (1989) calculated maximum rates of fluid production ranging from 90 mg $m^{-3}$ $yr^{-1}$, in a discontinuous reaction model, to 6 mg $m^{-3}yr^{-1}$ in a continuous reaction model. For a 20-km-thick zone of fluid production, these rates generate fluid fluxes up to 0.1 kg $m^{-2}yr^{-1}$. This corresponds to volume flow rates of $3 \times 10^{-12}$ $m^3m^{-2}s^{-1}$, or time-integrated fluid fluxes of $10^2$ $m^3m^{-2}$ in $10^6$ yr.

A fluid flux of 0.1 kg $m^{-2}\,yr^{-1}$ is equivalent to a fluid volume of $3.5 \times 10^5$ $m^3$ flowing across a 50- × 50-$km^2$ surface area of continental crust per year. This equates to 35 $km^3$ of fluid every $10^5$ yr. Such fluid volumes are comparable to those inferred to be involved in the formation of major mesothermal gold systems (e.g., Cox, 1999).

Shear zones provide a major fluid pathway for fluids escaping from the deep crust. Isotopic and petrologic constraints on fluid fluxes in midcrustal shear zones indicate time-integrated fluid fluxes associated with alteration and vein formation in shear zones in the range $10^4$ to $10^7$ $m^3m^{-2}$ (Ferry and Dipple, 1991; Cartwright and Oliver, 2000). On the basis of volume gain due to quartz precipitation in ductile, midcrustal shear zones, Streit and Cox (1998) also estimated time-integrated fluid fluxes up to $10^6$ $m^3m^{-2}$. These estimates correspond to flow rates up to $3 \times 10^{-7}$ $m^3m^{-2}s^{-1}$ for flow over an interval of $10^6$ to $10^7$ yr. These values are substantially higher than calculated fluid fluxes of $10^3$ to $10^4$ $m^3m^{-2}$ associated with metamorphic devolatilization without flow focussing (Ferry, 1994).

High fluid flux along faults and shear zones during midcrustal metamorphism is typically associated with elevated pore fluid factors. Key evidence attesting to the development of high pore-fluid factors includes the abundance of extension

veins and fault-fill veins (Etheridge et al., 1984; Hickman et al., 1995). A number of features indicate that large pore pressure fluctuations can occur on short time scales in faults and vein swarms (e.g., Vrolijk, 1987; Wilkinson and Johnston, 1996; Brantley et al., 1997). We shall see that repeated pore fluid-pressure fluctuations are a normal response to permeability changes driven by episodic fault rupture and associated fluid redistribution from deep crustal fluid reservoirs (Sibson, 2001).

*Intrusion-related hydrothermal systems:* Overpressured fluids exsolved from crystallizing magmas provide a key fluid reservoir and metal source for a number of intrusion-related deposit types at various depths in the crust (Fournier, 1999; Redmond et al., 2004). However, other fluid reservoirs also may be involved in the generation of intrusion-related hydrothermal systems. The thermal perturbation associated with magma emplacement can generate convective flow systems (e.g., Norton and Knight, 1977; Cui et al., 2003), or lead to overpressuring of pore fluids stored in the contact aureole of the intrusion, and thereby drive fluid migration away from the intrusive body (Dutrow and Norton, 1995). Additional fluids may be generated by devolatilization reactions in the contact aureole (e.g., Ferry and Dipple, 1992).

*Surface-derived and basinal fluid reservoirs:* Porous and fractured rock in shallow crustal environments, and especially in sedimentary basins, provides major, long-lived fluid reservoirs in the upper crust (Person et al., 1996; Bjorlykke, 1997). There is substantial evidence that surface-derived fluids and basinal fluids can penetrate deep into basement underlying sedimentary basins (Forster and Smith, 1990; Taylor, 1990).

Topographically induced flow is one mechanism to achieve fluid penetration to depths of several kilometers (Forster and Smith, 1990). Earthquake ruptures, which propagate upward from the midcrust into the near-surface hydrostatic fluid-pressure regime, also provide a pathway for postseismic ingress of near-surface fluids to deeper crustal levels (McCaig, 1988). During subsequent interseismic fault healing, these fluids can be pressurized by compaction processes and expelled gradually from the fault zone (Sleep and Blanpied, 1992). The time-integrated volumes of fluids that can cycle through coseismic damage zones can be substantial. For example, a fault rupture zone with dimensions 50 km long, 20 km deep, and with a damage zone 50 m wide containing 2 percent porosity, can store 1 $km^3$ of fluid. During 100 rupture cycles, this generates a time-integrated flux of 100 $km^3$ of fluid that can be expelled from, or along, the fault zone on time scales of $10^4$ to $10^5$ yr.

Although many ore deposits form from single fluid sources, mixing and reaction between fluids derived from chemically distinct reservoirs can be an important factor in the genesis of many deposit types. Regardless of the number of fluid reservoirs involved in an ore system, necessary conditions controlling where and when a deep crustal hydrothermal ore system develops are the availability of fluids and metal-fertile reservoirs, the generation of fluid pathways, mechanisms to drive flow, and the availability of processes to efficiently precipitate metals from solution. The following sections examine processes driving fluid flow and how fluid pathways are generated during crustal deformation and metamorphism.

## Controls on Permeability Enhancement in Deep Hydrothermal Systems

### *Darcy's Law and driving forces for fluid flow*

*Pressure-driven flow:* The dependence of fluid flow in porous media on driving forces, the transport properties of the media, and the fluid properties are described by Darcy's Law. For one-dimensional horizontal flow, the dependence of fluid flux (fluid volume, Q, across cross-sectional area, A, per unit time, t) on hydraulic pressure gradients (dP/dx), is given by

$$Q/At = (k/\mu)(dP/dx). \quad (1)$$

The constants of proportionality in this relationship are the permeability (k) of the rock, and viscosity ($\mu$) of the pore fluid. Darcy's Law assumes laminar flow, which applies in porous rocks at flow rates up to about 1 $ms^{-1}$. At higher flow rates, turbulence and high inertial forces lead to breakdown of Darcy's Law (Guéguen and Palciauskas, 1994). Permeability has units of $m^2$ (1 darcy = $10^{-12}$ $m^2$) and is an intrinsic rock property that is a measure of the capacity of fluids to flow through rock. Viscosity is a measure of the viscous resistance to flow of a fluid through pore spaces.

For flow regimes with a vertical component of flow, fluid migration is driven by departures of the vertical fluid-pressure gradient from the fluid-pressure gradient that occurs in a column of connected fluid at rest. For change in depth (dz), the change in fluid pressure (dP) in a column of stationary fluid is given by

$$dP = \rho g\, dz, \quad (2)$$

where $\rho$ is the local fluid density, and g is the gravitational acceleration. The vertical fluid-pressure gradient, $\rho g$, is known as the hydrostatic fluid-pressure gradient. For vertical flow, Darcy's Law has the form:

$$Q/At = (k/\mu)(dP/dz - \rho g), \quad (3)$$

where dP/dz is the vertical component of the fluid-pressure gradient. Accordingly, where dP/dz is suprahydrostatic (i.e., $dP/dz > \rho g$), upward flow occurs, whereas for subhydrostatic vertical fluid-pressure gradients ($dP/dz < \rho g$), downward flow occurs in a fluid of uniform density.

For general flow, Darcy's Law has the form:

$$Q/At = (k/\mu)[\partial(P - \rho gz)/\partial x], \quad (4)$$

where $\partial(P - \rho gz)/\partial x$ is the hydraulic gradient for flow along the path x (Manning and Ingebritsen, 1999).

In near-lithostatic pressured regimes the vertical lithostatic driving fluid-pressure gradient is approximately19 $kPa{\cdot}m^{-1}$. Higher gradients may develop where upward migration of fluids is impeded by low-permeability domains ("seals").

For general pressure-driven flow in rocks with isotropic permeability, flow is parallel to the nonhydrostatic component of the fluid-pressure gradient. Permeability anisotropy may result in flow that is not parallel to the driving pressure gradient. For example, fluid is likely to flow along a high-permeability pathway (e.g., dilational jog in a fault or lithological contact) even if the pathway is oblique to the driving pressure gradient.

*Buoyancy-driven flow:* For fluids of nonuniform density, the $\rho g$ term in equation (3) also provides the driving force for

buoyancy-driven effects associated with spatial variations in fluid density in a porous medium. Fluid density is strongly dependent on pressure and temperature, as well as salinity. For typical crustal geothermal gradients, the rate of decrease of density of aqueous fluids, due to increase in temperature with depth, is greater than the rate of increase in density due to increasing pressure. Accordingly, aqueous fluids typically decrease in density with depth in the crust, which promotes thermal buoyancy-driven flow in permeable fluid-saturated rocks.

The change of fluid density as a function of pressure (P) and temperature (T) is given by

$$\rho(T,P) = \rho_0 + (d\rho/dT)_P \Delta T + (d\rho/dP)_T \Delta P, \quad (5)$$

and $(d\rho/dP)_T = \rho_0\beta$, $(d\rho/dT)_P = -\rho_0\alpha$, where $\beta$ is the isothermal compressibility of the fluid, $\alpha$ is the isobaric coefficient of thermal expansion, $\rho_0$ is the fluid density at a reference pressure and temperature, and $\Delta P$ and $\Delta T$ are departures from the reference pressure and temperature, respectively (Spear, 1995). In this case, Darcy's Law has the form:

$$Q/At = -(k/\mu)[dP/dz - (\rho_0 g - \rho_0 \alpha g \Delta T + \rho_0 \beta g \Delta P)]. \quad (6)$$

Where there is no pressure-driven component to the flow, Darcy's Law reduces to

$$Q/At = -(k/\mu)[\rho_0 g - \rho_0 \alpha g \Delta T + \rho_0 \beta g \Delta P] \quad (7)$$

and the terms in square brackets represent the buoyancy-induced pressure gradient that drives flow.

At midcrustal depths, the buoyancy-induced driving forces are less than 1 kPa·m$^{-1}$ or about 5 percent of the pressure-induced driving force in a system under lithostatic pressure. In overpressured hydrothermal systems, pressure-driven hydraulic gradients therefore are likely to be substantially higher than thermally induced driving forces. Accordingly, buoyancy-driven flow tends to be significant mainly in near-hydrostatic fluid-pressure regimes. However, buoyancy-driven flow can also occur in overpressured regimes but only in vertically very restricted fluid compartments where the local vertical fluid-pressure gradients have near-hydrostatic values (Etheridge et al., 1983).

Buoyancy-controlled flow drives convective flow systems that are generated either by thermally driven buoyancy differences or by chemically driven density variations, such as due to horizontal or vertical variations in fluid salinity. Sloping isotherms are particularly important in generating buoyancy-driven flows. Accordingly, convective flow regimes can be important around intrusive systems (e.g., Norton and Knight, 1977). Thermal perturbations associated with faulting also have potential to establish sloping isotherms and convective hydrothermal systems (e.g., Matthai et al., 2004).

Turcotte and Schubert (1982) discussed the conditions under which thermal convection of aqueous fluids will occur in a porous medium. The minimum vertical thermal gradient necessary to drive convection of fluid is given by

$$dT/dz = 4.2 \times 10^{-10}/kb^2, \quad (8)$$

where k is permeability and b is the length scale for convective flow. For temperature gradients greater than 20°C km$^{-1}$, and for reasonable values of the thermal expansion coefficient of aqueous fluids, porous medium convection is predicted to occur at length scales greater than several kilometers when permeabilities are greater than about $10^{-15}$ m$^2$.

Darcy's Law highlights how the geometry of fluid migration in the Earth's crust is influenced most strongly by spatial and temporal variations in (1) rock permeability, (2) gradients in fluid pressure, (3) fluid viscosity, and (4) fluid density variations. Because natural rocks have permeabilities that range over more than ten orders of magnitude (Brace, 1980; Manning and Ingebritsen, 1999), the permeability architecture of a rock mass is usually the dominant factor controlling fluid flux in most crustal-scale hydrothermal systems.

Viscosity of typical hydrothermal fluids ranges over about one order of magnitude (40–400 $\mu$Pa·s), decreasing with increasing temperature and decreasing pressure (Dudziak and Frank, 1966). Variations in viscosity therefore generally have much less impact on flow than variations in permeability. Similarly, although hydraulic gradients influence directions of flow in hydrothermal systems, the magnitude of these gradients is governed mainly by permeability variations along pathways, and by fluid-pressure states in reservoirs at the upstream and downstream ends of the system. We will see later that there can be strong feedbacks between fluid pressures, deformation processes, the evolution of permeability, and driving fluid-pressure gradients.

*Generation of hydraulic gradients:* The hydraulic gradients that govern pressure-driven fluid flow are generated in a number of ways. At shallow depths in the crust (typically less than several kilometers), topographic effects can cause marked lateral variations in fluid pressures which drive flow (Forster and Smith, 1990). Progressive changes in pore volume in deforming rocks can also drive fluid flow in deforming rock masses. For example, compaction of sedimentary sequences can be a powerful driver of flow during burial of sedimentary basins (Person et al., 1996). Dilatancy associated with crack growth and closure during inelastic deformation may generate complex hydraulic gradients during folding or shearing of rock masses (Ord and Oliver, 1997; Oliver 2001). However, the resulting fluid-pressure gradients will tend to be small for deformation at the low strain rates typical of bulk crustal deformation. The impact on fluid fluxes will be correspondingly small.

Changes in pore volumes associated with elastic deformation of intergranular pores or cracks generate transitory hydraulic gradients. Such "poroelastic" effects can be significant around active fault zones where substantial stress changes occur during the seismic cycle (Muir-Wood and King, 1993). Flow driven by poroelasticity is likely to be most prevalent where large changes in normal stress occur around areas with a high density of high aspect ratio fractures, as in the shallow crust.

At elevated temperatures in the crust (typically greater than approximately 250°C), hydraulic gradients are most strongly controlled by inelastic deformation processes and reactions that drive closure or hydrothermal sealing of pores and fractures. Porosity reduction drives pore fluid pressures toward lithostatic pressures and generates at least transiently suprahydrostatic vertical fluid-pressure gradients where fluids are present (Etheridge et al., 1984). Such fluid overpressures provide a strong upward driving force for fluid migration, especially when permeable pathways can be generated

and sustained (Fig. 4). However, the maintenance of overpressures is dependent on the relative rates of change of porosity, permeability, and rate of fluid escape (Nur and Walder, 1990). Rates of fluid production, for example, due to metamorphic devolatilization or release of magmatic-sourced hydrothermal fluids also play a fundamental role in controlling the evolution of pore fluid pressures and hydraulic gradients (Nur and Walder, 1990; Fournier, 1999).

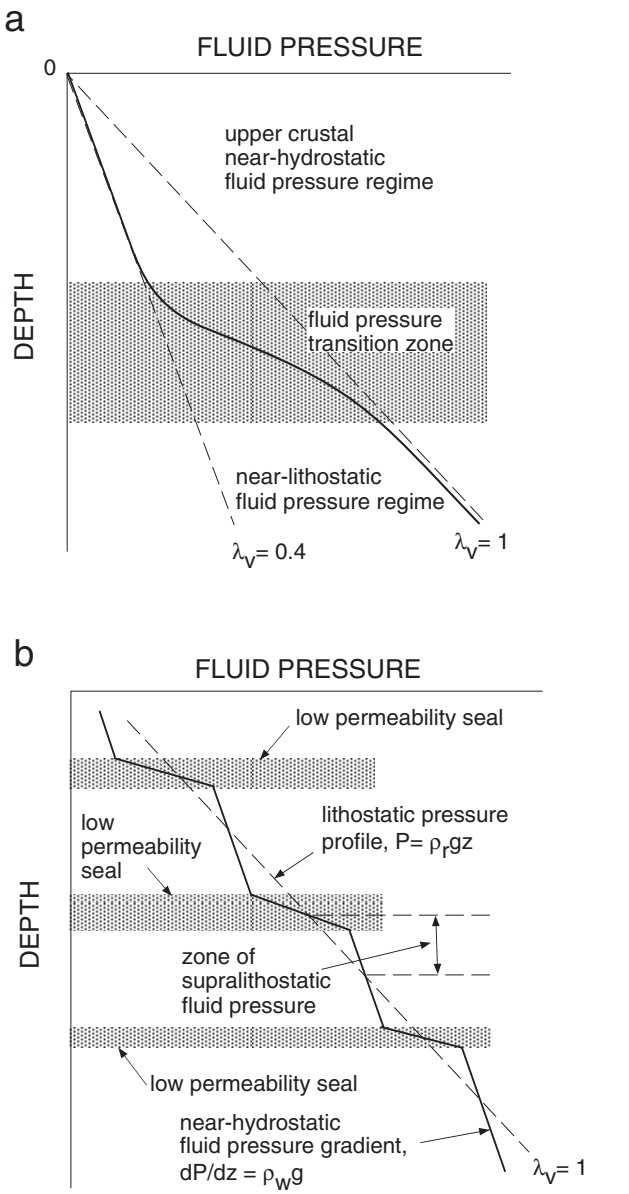


FIG. 4. a. Division of the crust into a shallow-level, near-hydrostatic fluid-pressure regime and a deeper, overpressured (suprahydrostatic) regime. The transition from the near-hydrostatic regime to suprahydrostatic regimes typically occurs at depths between 5 and 15 km. b. Compartmentalization of fluid pressure in the crust may result in a vertically stacked series of fluid-pressure cells which are separated by low-permeability regions. In fault-controlled fluid-flow regimes, seals may be either low-permeability domains or low-permeability, hydrothermally sealed parts of the faults. In fluid compartments between seals, fluid-pressure gradients can be near-hydrostatic if permeability is high enough. Suprahydrostatic fluid-pressure gradients across seals drive upward fluid flow. Near-lithostatic fluid pressures ($\lambda_v \approx 1.0$) may develop immediately underneath seals.

Fluid overpressuring is commonly observed deep in sedimentary basins (Hunt, 1990; Powley, 1990; Bjorlykke, 1997) where fluid pressurization is driven by both compaction and low-temperature dehydration reactions, and vertical fluid escape is inhibited by low-permeability rock units. Overpressured reservoirs may also have low-permeability sidewalls such as sealed fault zones (Knipe et al., 1998). In some hydrocarbon systems, vertically stacked sequences of pressurized compartments are recognized (Cathles and Adams, 2005). In the deep crust, similar fluid-pressure compartmentalization is also likely (Cox et al., 1991) but with the low-permeability boundaries of compartments being governed by competition between pore-opening and -closure processes, rather than by intrinsically low-permeability stratigraphy (Fig. 4). Compartments are likely to be transitory or migratory features in the deep crust.

Changes in rock permeability, such as occur during sudden, coseismic rupture along active faults, generate marked hydraulic gradients around faults by providing "short-circuit" pathways between fluid reservoirs with different pore pressures (Fig. 5a). This is discussed further below. Where vertical fluid-pressure gradients are less than hydrostatic values, local downflow may occur. This situation can arise, for example, where dilation associated with coseismic slip on faults causes local, sudden fluid-pressure decreases and generates transiently subhydrostatic vertical fluid-pressure gradients (Fig. 5b).

### *Evolution of intergranular permeability in isostatic stress regimes*

Grain-scale porosity usually comprises both intergranular and fracture porosity. Permeability associated with intergranular porosity is influenced by total porosity, pore diameters and shapes, diameters of pore throats between large pores, and extent of connectivity between pores. For porosity greater than about 6 to 10 percent pores are generally fully interconnected and porosity is related to permeability by

$$k \propto \Phi^n, \tag{9}$$

where $n$ is approximately 3. In this regime, permeability decrease with decreasing porosity is controlled by pore shrinkage. During compaction to lower porosities, progressive loss of connectivity between pores occurs by closure of narrow throats between the larger intergranular pores. Pores that form part of a connected network are known as the backbone porosity. Because all flow is localized along the backbone pore network, the backbone porosity controls permeability. The remaining porosity comprises two elements: isolated pores, which do not connect with the backbone porosity, even though they may form localized clusters of pores that are connected to each other; and dangling, or dead-end pores, which connect to the backbone porosity from one side only. Although they are part of the interconnected porosity and contain pore fluid, they do not contribute to the flow. At low porosities, permeability changes are directly related to progressive changes in the relative proportions of backbone, dangling, and isolated pores, as well as the total porosity of a rock.

In high-temperature isostatic stress regimes (i.e., all principal stresses equal), the relative proportions of backbone,

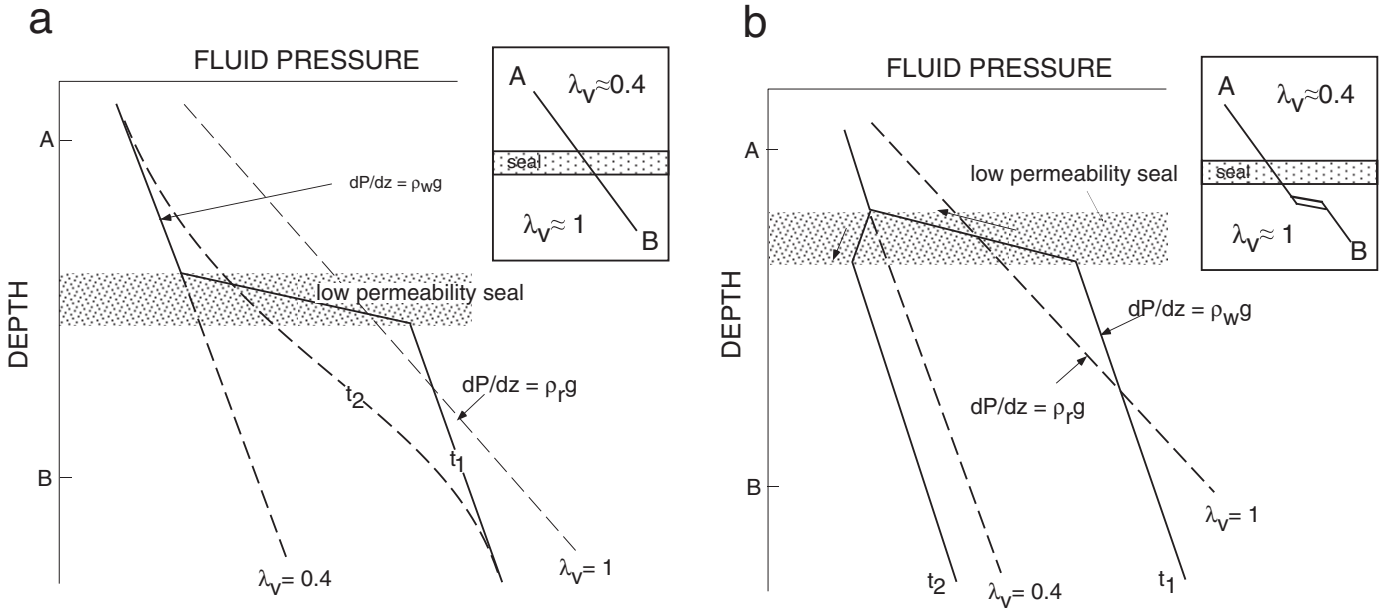


FIG. 5. a. Illustration of changes in absolute fluid pressures and fluid-pressure gradients across a low-permeability barrier between two fluid reservoirs. In this example, the upper reservoir is hydrostatically pressured and the lower reservoir is suprahydrostatically pressured. The initial depth dependence of fluid pressure is given at time $t_1$. Maximum pore-fluid factor ($\lambda_{vmax}$) occurs at base of low-permeability domain ($\lambda_{vmax} = (\sigma_3 + T)/\sigma_v$, where $\sigma_3$ is the minimum principal stress, T is the rock tensile strength, and $\sigma_v$ is the vertical stress). Rupture of the sealed barrier, e.g., by fault AB (see inset), increases permeability across the barrier. The suprahydrostatic fluid-pressure gradient drives rapid upward leakage of fluids from the lower reservoir into the upper reservoir and fluid pressures change with time (e.g., dashed line at time $t_2$). b. Change in fluid pressure with depth as a function of time along a dilatant fault zone AB (see inset), which cuts through a low-permeability seal separating two differently pressured fluid reservoirs. The seal may be either a low-permeability domain in the crust, or a low-permeability hydrothermally sealed part of the fault zone. At time $t_1$, just prior to seal breaching, an overall suprahydrostatic vertical fluid-pressure gradient between B and A drives upward fluid leakage through the low-permeability zone. If substantial dilation of the fault occurs during rupture at time $t_2$ (e.g., by coseismic dilation of jogs or dilation in a heavily fractured lateral damage zone), a transitory fluid-pressure drop occurs in that zone. Overall fluid-pressure gradients may then be transiently subhydrostatic between the dilation zone and the hydrostatically pressured regime above the ruptured seal and result in fluid drawdown, as well as fluid influx from the sidewalls of the dilatant zone. Fluid flow direction is indicated by arrows.

dangling, and isolated pores are controlled principally by total porosity and interfacial surface energy effects between minerals and pore fluids. Pores can occur at two-grain interfaces, along three-grain edges, and at grain corners (Fig. 6). For dihedral wetting angles ($\theta$) >60°, pores at two-grain interfaces tend to form isolated pockets. At low porosity, grain-edge channels pinch off to form discontinuous beads along grain edges, and pores at grain corners tend to be isolated (Fig. 6c). In contrast, at dihedral wetting angles ≤60°, connectivity between pores at grain corners may be provided to low porosities by continuous channels along grain edges (Fig. 6b). For $\theta$ >0°, the equilibrium fluid distribution on two-grain interfaces takes the form of disconnected bubbles. Only in the extreme case of $\theta = 0°$ can a continuous fluid film exist stably on two-grain interfaces.

The evolution of permeability with decreasing porosity at elevated temperatures, where surface energy effects control pore geometry, is illustrated schematically in Figure 7. The porosity-permeability relationship approximately follows the cube law (i.e., $n = 3$ in eq. 9) for porosities down to a threshold porosity ($\Phi_t$) where full connectivity between pores starts to be lost. Below this porosity, permeability is much more strongly dependent on total porosity. At a critical porosity ($\Phi_c$) pores completely lose connectivity; this is termed the percolation threshold. Below $\Phi_t$, permeability tends to obey the scaling law (Knackstedt and Cox, 1995):

$$k \propto (\Phi - \Phi_c)^2. \quad (10)$$

Experimental studies of interfacial wetting angles indicate that for a number of common mineral-fluid systems, dihedral wetting angles are typically greater than 60° (Holness, 1997). In this case, pore connectivity is lost at porosities of several percent. Accordingly, many very low porosity metamorphic fluid-rock systems are expected to be below the percolation threshold and therefore impermeable, unless deformation processes generate fracture networks.

*Grain-scale fracture permeability*

In the absence of intergranular permeability, the evolution of permeability during progressive deformation is controlled by competition between deformation-induced porosity-creation processes (fracture growth) and porosity-destruction processes (compaction, crack-healing, crack-sealing). Various experimental studies (Fischer and Paterson, 1992; Zhang et al., 1994b; Peach and Spiers, 1996) demonstrate that even small amounts of deformation can increase permeability by

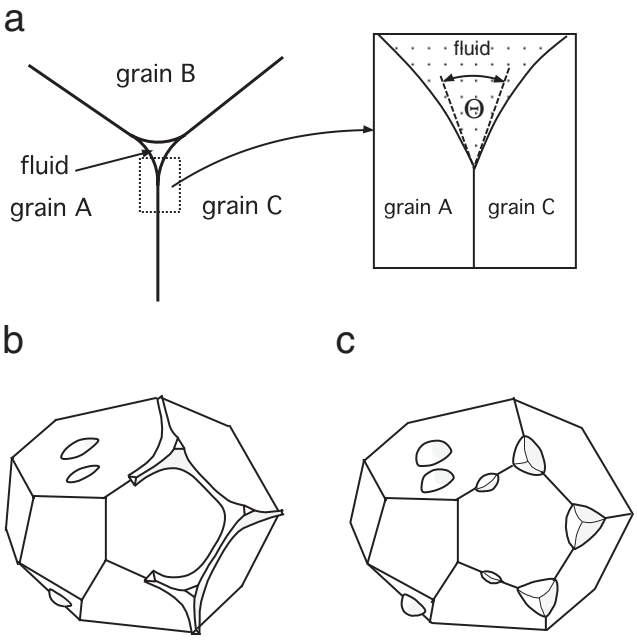


FIG. 6. Schematic illustration of pore geometries in polycrystalline grain aggregates at elevated temperatures where pore shapes are controlled by surface energy minimization. a. Cross section through a grain-edge channel. Dihedral wetting angle, $\theta$, is indicated. b. For dihedral wetting angles ≤60°, fluid forms isolated pockets on two-grain interfaces, and fluid channels along three-grain edges may connect fluid pockets at four-grain corners. c. For dihedral wetting angles >60°, fluid on two-grain interfaces, three-grain edges, and four-grain corners occurs as isolated pockets (after Watson and Brenan, 1987).

several orders of magnitude, particularly in high pore-fluid factor regimes. In the presence of nonreactive pore fluids, permeability during straining of initially low-permeability rocks evolves through four stages (Fig. 8). In the initial stage of deformation, microcracks start to nucleate and grow, but, because all cracks are isolated from each other, permeability does not change. With increasing strain, the number of microcracks, their lengths, and connectivity progressively increase and drive the system to the percolation threshold ($\varepsilon_{crit}$, stage 2). In room temperature experiments on Carrara marble at a pore-fluid factor of 0.9, the percolation threshold is reached at strains less than 3 percent (Zhang et al., 1994b). With increasing strain, rapid growth of grain-scale crack networks leads to rapid growth in connectivity (stage 3). For Carrara marble at $\lambda_v = 0.9$, a permeability increase of two orders of magnitude occurs by 3 percent shortening. Nearly total interconnectivity is achieved in the grain-scale microfracture network by 5 percent shortening, after which the rate of increase in permeability with increasing strain decreases. Further modest increases in permeability after this point (stage 4) are interpreted to reflect increases in fracture apertures, rather than increased connectivity or number of fractures.

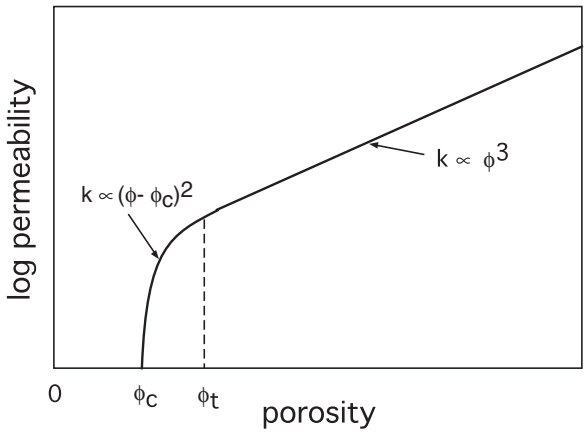


FIG. 7. Typical relationship between permeability and intergranular porosity in polycrystalline grain aggregates at high temperatures in an isostatic stress regime. At porosities greater than $\Phi_t$ all porosity is interconnected and permeability k is proportional to the cube of porosity $\Phi$. Below the percolation threshold at $\Phi_c$, all pores are isolated (modified after Zhang et al., 1994a).

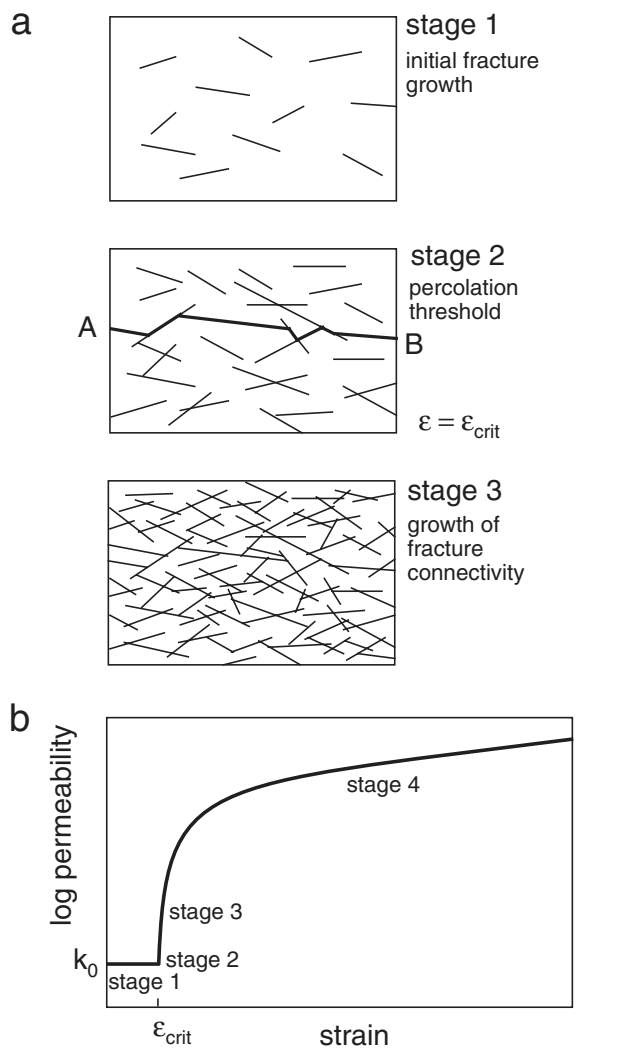


FIG. 8. Schematic illustration of evolution of two-dimensional microcrack density, connectivity, and permeability as a function of strain in rock deforming by mixed plastic and brittle deformation mechanisms. a. Growth of microcrack networks during deformation. The flow backbone at the percolation threshold is indicated by the bold line AB. b. Evolution of microcrack permeability as a function of strain in the presence of nonreactive pore fluid. Initial permeability is $k_o$. The percolation threshold is reached at $\varepsilon_{crit}$.

At elevated temperature in the midcrust, most strain is accommodated by microscopically ductile deformation mechanisms such as dislocation flow and dissolution-precipitation creep. However, deformation-induced permeability enhancement due to microcrack growth persists well into the dominantly crystal plastic deformation regime, provided pore fluid factors are high (Fischer and Paterson, 1992; Zhang et al., 1994b). As temperature increases, crack growth rates reduce, and the critical strain required for the development of a well-connected, high-permeability crack network increases. Similarly, the rate of permeability enhancement at high pore-fluid factors is higher than during deformation at low pore-fluid factors (Fig. 9a). Pore–fluid-pressure stepping experiments at constant strain (Fischer and Paterson, 1992) also indicate that rapid increases in pore-fluid factor during deformation can rapidly enhance permeability (Fig. 9b). In polymineralic rocks, grain-to-grain strain incompatibilities during deformation are expected to further enhance growth of intergranular crack networks and associated permeability enhancement.

A significant result of the experimental work is that microfracture networks develop high crack connectivity and high permeability at very low strains, provided pore fluid factors are high, even in regimes that favor macroscopically ductile deformation. Accordingly, low-strain deformation can have a major impact on crustal permeability enhancement.

Evidence for grain-scale dilatancy and related permeability enhancement being associated with natural deformation is commonly well preserved in low-grade metamorphic environments where deformation-related microfabrics are not overprinted by progressive recrystallization of mineral assemblages. For example, Cox and Etheridge (1989) described grain-scale intergranular and intragranular microfractures filled by fibrous to equigranular mineral precipitates. Similar grain-scale dilatancy is widespread in shear zones formed in low greenschist-facies environments (e.g., Guermani and Pennachioni, 1998). The importance of ductile shear zones as sites of enhanced permeability and fluid flow is supported by isotopic and petrologic studies (e.g., Kerrich et al., 1977; Dipple and Ferry, 1992b; McCaig, 1997; Streit and Cox, 1998).

Stress control on the orientations of grain-scale microcracks can lead to permeability anisotropy in deforming rocks (Fig. 10). For example, during approximately coaxial plane strain, microfractures form at high angles to the direction of maximum stretch and will have best connectivity in a direction parallel to the intermediate strain axis (Fig. 10b). For approximately simple shear deformation, the permeability anisotropy will be parallel to the foliation in a direction perpendicular to the stretching lineation; this is also the Y-axis of the finite strain ellipsoid (Fig. 10c).

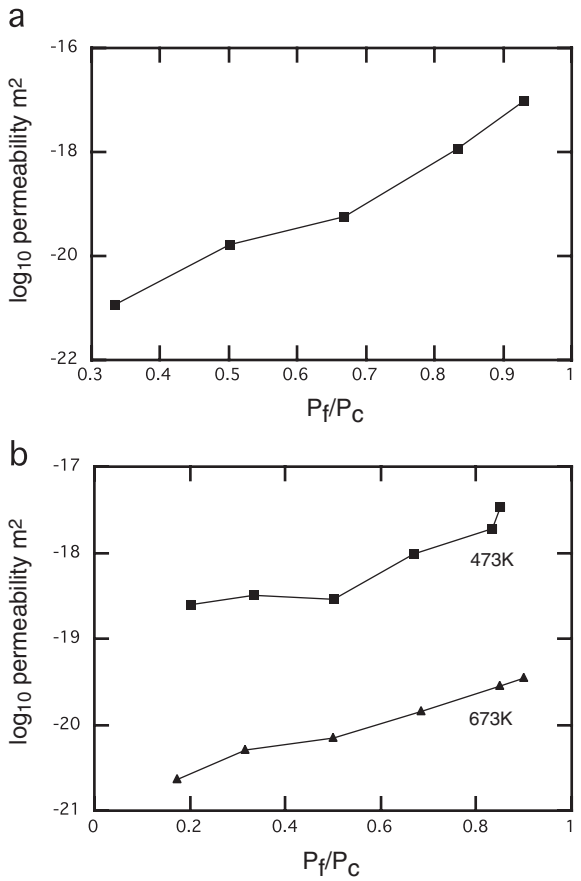


FIG. 9. a. Dependence of permeability on pore-fluid factor (ratio of pore fluid pressure $P_f$ to confining pressure $P_c$) at a strain of 10% shortening during room temperature deformation at constant pore-fluid factor. Modified after Zhang et al. (1994b). b. Change of permeability at constant strain when fluid pressure is increased. Modified after Fischer and Paterson (1992).

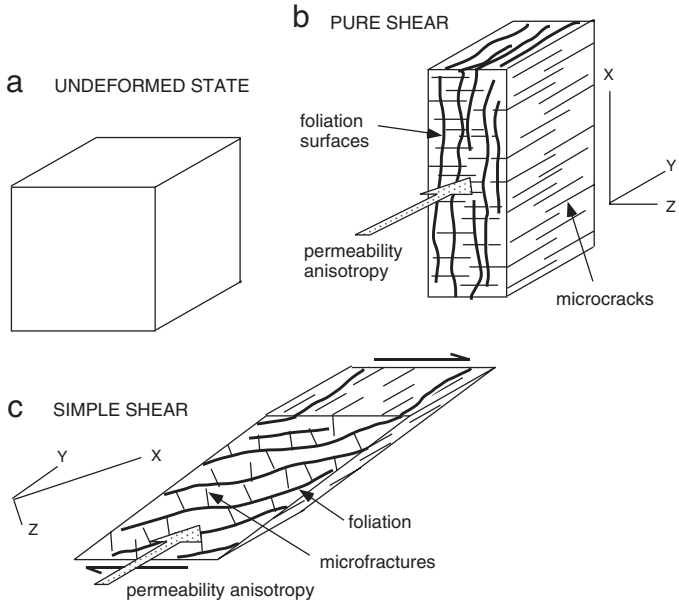


FIG. 10. Anisotropy of permeability associated with grain-scale microfracturing and foliation development in metamorphic rocks. Microfractures enhance permeability. Foliation surfaces impede flow at high angles to foliation. a. Starting strain state. b. For plane strain coaxial deformation, maximum stretch occurs along the X-axis, maximum shortening parallel to the Z-axis, and there is no change in length parallel to the Y-axis. Microfracturing on the ZY plane and foliation development along the XY plane results in highest permeability along the Y-axis during deformation. c. During simple shear, microfractures nucleate perpendicular to the direction of instantaneous maximum stretch (i.e., the $\sigma_3$ orientation). With progressive simple shear, the foliation and microfractures rotate clockwise. Maximum crack connectivity is along the Y-axis of the strain ellipsoid.

Anisotropy of permeability during approximately simple shear deformation has been experimentally studied by Zhang et al. (1999). Permeability anisotropies up to one and a half orders of magnitude develop in quartz-feldspar-mica aggregates at room temperatures. More substantial anisotropy is expected at elevated temperatures in conjunction with foliation development.

*Competition between grain-scale crack production and crack healing and/or sealing processes*

At elevated temperatures in hydrothermal systems, porosity-destruction processes, such as intergranular cementation, compaction, and both healing and sealing of fractures, drive permeability reduction. Permeability evolution is therefore controlled by competition between deformation-induced porosity-creation processes and various porosity-destruction processes.

At conditions typical of mid- to deep crustal environments, microstructural and experimental evidence indicates that high-permeability microcrack pathways are healed on geologically short time scales (Brantley et al., 1990). Accordingly, deformation is crucial to sustain high permeability during the operation of a hydrothermal system.

Quantitative insights about how permeability destruction processes influence permeability evolution in deforming rocks are provided by the crack healing experiments of Zhang et al. (2001). In this study, marble was experimentally deformed and subsequently heat treated isostatically at effective confining pressures between 50 and 150 MPa at temperatures up to 700°C in the presence of nonreactive argon pore fluid. Both connected porosity and permeability progressively decrease with time as cracks heal and lose connectivity (Fig. 11). During crack healing, permeability is proportional to the cube of connected porosity.

Similarly, compaction and pore sealing in gouges and breccias in fault zones rapidly destroy pore connectivity produced by slip events (Angevine et al., 1982; Cox and Paterson 1991; Kanagawa et al., 2000; Tenthorey et al., 2003), such that fault zones lose grain-scale permeability during interseismic intervals if reactive pore fluid is present. Little is known about rates of crack sealing (i.e., fracture closure due to mineral precipitation) in fault zones, but the process will be strongly influenced by levels of mineral supersaturation, flow rates, and temperatures (Streit and Cox, 2000; Hilgers et al., 2004). Observed rates of sealing in geothermal systems indicate that microfractures probably have very short lifetimes relative to the lifetimes of hydrothermal systems (e.g., Lowell et al., 1993). In summary, for flow to continue, high rates of permeability destruction in hydrothermal systems require continuous regeneration of permeability by deformation processes.

*Reaction-enhanced permeability*

Transitory porosity enhancement is associated with volume changes during metamorphic reactions at elevated temperatures and pressures (Rumble et al., 1982; Ferry, 1994; Zhang et al., 2000; Tenthorey and Cox, 2003). Reaction-enhanced porosity change can be important in controlling grain-scale fluid infiltration in regional metamorphic environments (especially at the upstream end of crustal-scale hydrothermal systems). It may also be significant at the downstream part of hydrothermal systems, for example, in skarn environments and in zones of pervasive hydrothermal alteration associated with fluid discharge from fracture-controlled fluid pathways into intrinsically low-permeability wall rocks.

Devolatilization reactions are particularly important in driving reaction-enhanced permeability. Most such reactions involve overall decrease in the volume of the solid reaction products relative to the reactants, and pore space is transiently generated during fluid production. For example, during dehydration of fully dense serpentinite, breakdown of antigorite to olivine + talc + $H_2O$ is associated with rapid permeability increase by three to four orders of magnitude (Fig. 12; Tenthorey and Cox, 2003). A further example of permeability enhancement during devolatilization is provided by the reaction

$$\text{quartz} + \text{calcite} = \text{wollastonite} + CO_2. \qquad (11)$$

Zhang et al. (2000) demonstrated that at a confining pressure of 200MPa and pore water pressure of 175 MPa ($\lambda_v$ = 0.88), the reaction proceeds to completion on time scales of less than 40 h at temperatures between 650° and 700°C.

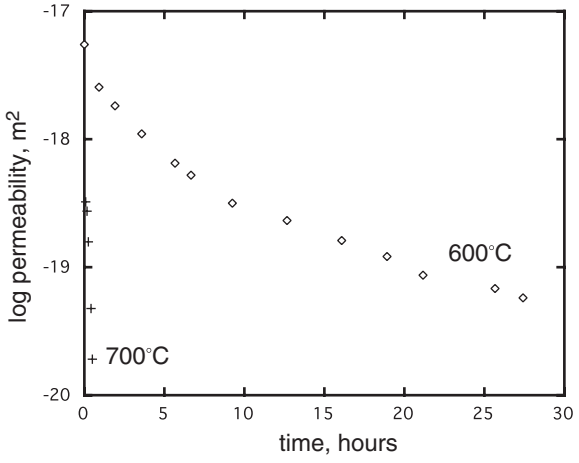


FIG. 11. Evolution of permeability in cracked Carrara marble during isothermal crack healing at 600° and 700°C, 300MPa confining pressure, and 250 MPa pore-fluid pressure. After Zhang et al. (2001).

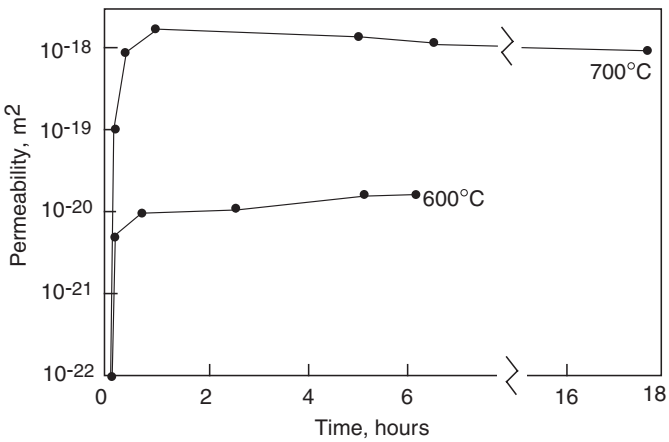


FIG. 12. Permeability enhancement associated with devolatilization reaction in serpentinite. After Tenthorey and Cox (2003).

Permeabilities as high as $10^{-16.5}$ m$^2$ were maintained during incomplete decarbonation reaction at 600°C. However, at 700ºC permeability reduced from $10^{-16.5}$ m$^2$ to $10^{-19}$ m$^2$ as the reaction proceeded toward completion. In contrast, at a pore-fluid factor of 0.5, rapid compaction of the reactants and reaction products was stimulated by the high effective confining pressure and reduced the permeability to less than $10^{-19}$ m$^2$. This inhibited $H_2O$ infiltration and severely limited reaction progress. Accordingly, at low pore-fluid factors, reaction can be shut down if the rate of permeability creation due to the devolatilization reaction is exceeded by the rate of permeability destruction due to pressure-driven compaction of pore spaces. Pore-fluid factors thus play a key role in controlling reaction progress and permeability evolution during metamorphic reactions. Reaction-enhanced permeability during devolatilization reactions is expected to provide an important mechanism by which deep-seated fluids become mobile during crustal metamorphism (Ferry, 1994).

*Macroscopic fracture-controlled permeability*

*Failure modes:* Fluid transport is governed by the development of macroscopic fracture networks, as well as by grain-scale permeability. Three types of fractures are important in controlling macrocopic fracture permeability; these are extension fractures, shear fractures (or faults), and hybrid extensional shear fractures (Fig. 13). Extension fractures develop at scales ranging from microscopic to macroscopic (greater than tens of meters long), whereas low-displacement shear failures, typical of faults which host lode gold deposits, can extend for up to thousands of meters. The fractures can be hydraulically linked to much larger, crustal-scale faults and their associated fracture arrays, which together comprise a flow network that has a high permeability when faulting is active. High-permeability rupture zones generated by large earthquakes are tens to hundreds of kilometers long and tens of kilometers deep (Sibson, 2001). Importantly, macroscopic fracture systems can develop not only in the brittle upper crust (typically depths less than 10–15 km) but also in the more ductile deeper crust, provided pore-fluid factors are high enough.

Pure extension fractures form perpendicular to the minimum principal stress ($\sigma_3$) and open perpendicular to the fracture wall (Fig. 13a). In intact, isotropic rock, shear fractures typically form at angles between 25° and 35° to the orientation of the maximum principal stress ($\sigma_1$); the fault plane contains the orientation of the intermediate stress ($\sigma_2$) (Fig. 13b). Two conjugate sets of shear fractures can form in isotropic rocks and produce a meshlike permeable network. Where developed, their intersection is subparallel to $\sigma_2$. Hybrid extensional shear fractures have components of displacement both parallel, and perpendicular, to the fracture plane. They form at angles between 0° and approximately 25° to the $\sigma_1$ direction (Fig. 13c).

*Stress- and fluid-pressure–driven failure:* Changes in both fluid pressure and stress states can drive macroscopic fracture growth and permeability enhancement in hydrothermal systems. Pure extension failure occurs only at relatively small stress differences, typically less than approximately 4T, where T is the tensile strength of the rock. For $4T < (\sigma_1 - \sigma_3) < 5.7T$, failure occurs in extensional shear mode. Shear failure occurs at stress differences greater than approximately 5.7T. Because rock tensile strengths are typically less (sometimes substantially less) than about 10 MPa, the occurrence of pure extension veins in hydrothermal systems indicates stress differences less than 40 MPa during vein opening (Etheridge, 1983).

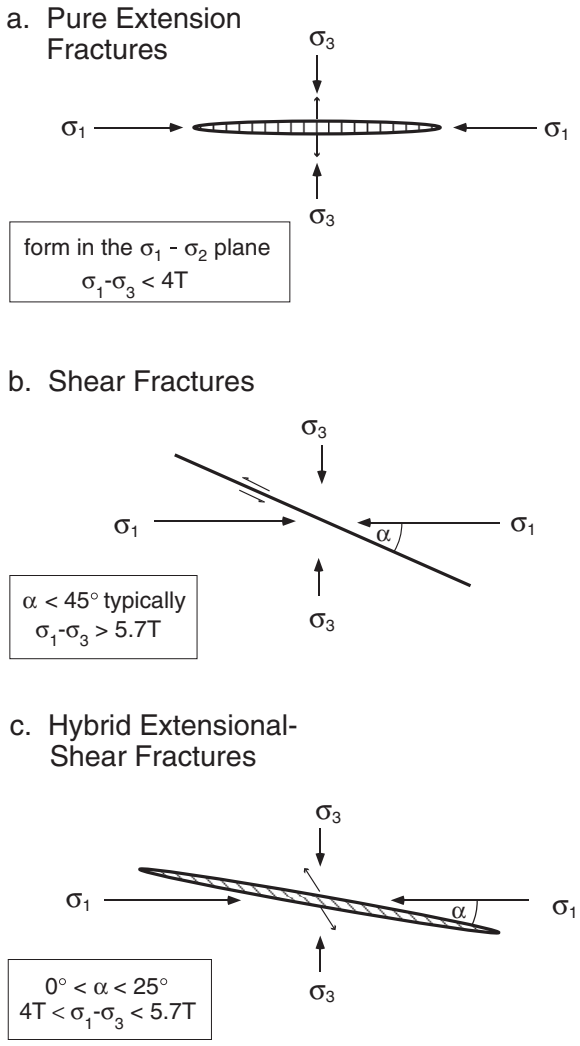


FIG. 13. Orientation relationships between stress fields and (a) extension fractures, (b) shear fractures, and (c) hybrid extensional shear fractures. The variable T in the figure refers to the tensile strength of the rock.

The combined role of changes in stresses and/or fluid-pressure states can be illustrated using failure mode diagrams that plot failure envelopes as a function of pore-fluid factor and stress difference ($\sigma_1$–$\sigma_3$). For example, in Figure 14, the pore-fluid factors and stress differences leading to failure in extensional, extensional shear, and shear modes are plotted for a thrust regime at a depth of 12 km. From some ambient stress and fluid-pressure states, failure can be induced either by increasing the pore-fluid factor along trajectories such as *x*, without changing the absolute stress state (an example of purely fluid-driven failure), or by maintaining a constant pore-fluid factor and increasing the stress difference (e.g., trajectory *z*), or some combination of both stress and fluid-pressure increase (e.g., trajectory *y*).

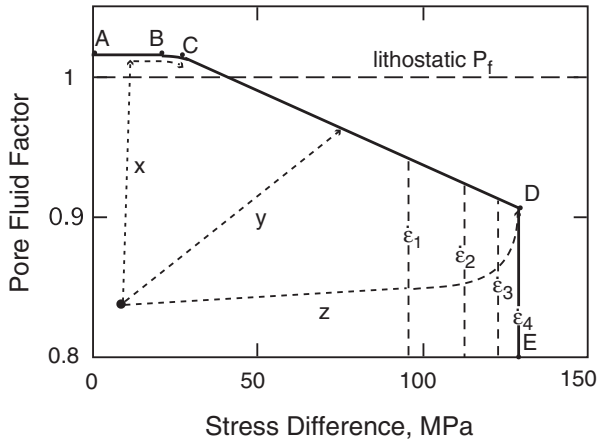


FIG. 14. Failure-mode diagram illustrating brittle and plastic failure envelopes as a function of pore-fluid factor and stress difference. The diagram is constructed for optimally oriented reverse faulting at a depth of 12 km in rock with a cohesive strength of 10 MPa, tensile strength of 5 MPa, and friction coefficient of 0.75. The failure envelope is indicated by the curve ABCDE. Hydraulic extension failure occurs in the interval AB; extensional shear occurs between B and C; brittle shear failure occurs between C and D. Strain-rate–dependent ductile shear failure envelopes are shown qualitatively for various strainrates ($\varepsilon_1 < \varepsilon_2 < \varepsilon_3 < \varepsilon_4$). At a high rate of increase of pore-fluid factor relative to stress change (path x), failure may first occur by extension fracture, followed by extensional shear failure at B, then by shear failure at C. For increase in both pore-fluid factor and stress difference along path y, brittle shear failure is induced. For rapid increase in shear stress relative to the rate of increase of pore-fluid factor (path z), failure may first occur by ductile creep at increasing strain rates, until brittle shear failure occurs at D.

At low stress differences, macroscopic extension failure requires an increase in pore-fluid factor at rates more rapid than increase in stress difference. This type of fluid-driven extension fracturing is known as hydraulic extension fracture. The only mechanism by which hydraulic extension fractures can form at depth is if

$$P_f = \sigma_3 + T. \quad (12)$$

This relationship is known as the hydraulic fracture criterion. The abundance of mineral-filled extension fractures in many epigenetic ore deposits indicates that fluid pressures greater than $\sigma_3$ are common in hydrothermal systems. The opening of hydraulic extension fractures limits the maximum fluid pressures that may develop in hydrothermal systems.

Higher rates of increase of stress difference relative to increase in pore-fluid factor lead to permeability enhancement by brittle shear failure (trajectory *y*, Fig. 14). At elevated temperatures, as stress difference increases, ductile creep at increasing strain rates may precede brittle shear failure (trajectory *z*, Fig. 14).

A significant aspect of fluid-driven fracturing is that, even without changes in the stresses acting on a previously nondeforming rock medium, infiltration of high-pressure fluids can drive the growth of fractures. The orientations of these fractures are controlled by the orientation of the principal stresses, magnitudes of the stress differences, and geometry of any preexisting mechanical anisotropies in the rock mass (Cox et al., 2001). The stress and fluid-pressure states required for fracture generation as a function of depth in contractional, extensional, and strike-slip settings are discussed by Sibson (2001).

*Permeability of fracture networks:* For steady-state, laminar flow in a parallel-sided fracture, the effective permeability is given by

$$k = a^2/12, \quad (13)$$

where *a* is the fracture aperture. In reality, relationships between fracture apertures and flow rates are more complicated because fracture roughness leads to aperture changes along fractures; consequently flow paths through irregular fractures are tortuous (Witherspoon et al., 1980; Taylor et al., 1999). However, the equation (13) relationship highlights the critical role of fracture aperture in controlling fluid flux. If the aperture is doubled, the permeability increases by a factor of 4. Accordingly, dilatant sites on fault surfaces (e.g., bends, jogs, or other irregularities) where aperture is higher than elsewhere in the structure will localize flow to those sites.

For networks of randomly distributed fractures that are not fully interconnected, bulk permeability is given by

$$k = (\pi/120) \cdot f\, a^3 r^2/l^3, \quad (14)$$

where *a* is the mean fracture aperture, *r* is the mean fracture length, *l* is the mean fracture spacing, and connectivity *f* is $0 \leq f \leq 1$ (Guéguen and Dienes, 1989). Although fracture orientations are seldom random, this relationship provides insights about magnitudes of fracture-controlled permeability in hydrothermal systems. For example, for fracture apertures of 100 $\mu$m, mean length of 4 m, mean separation of 5 m, and connectivity of only 0.1, macroscopic permeability is predicted to be $3 \times 10^{-16}$ m$^2$.

Permeability in cracked materials is very sensitive to changes in both stress state and fluid pressure (e.g., Brace et al, 1968). For a fluid-filled fracture at fluid pressure $P_f$ with normal stress, $\sigma_n$, acting perpendicular to the fracture, the effective normal stress, $\sigma_n'$, is defined as the difference between $\sigma_n$ and $P_f$. A simple approximation for the dependence of permeability on effective normal stress is provided by the relationship

$$k = k_0 \exp(-\sigma_n'/\sigma_0), \quad (15)$$

where $k_0$ is permeability at zero effective stress, and $\sigma_0$ is a constant (Rice, 1992). Accordingly, decreases in normal stress and increases in fluid pressure in fractured rocks can be key factors driving episodes of permeability enhancement.

In summary, for flow in fracture-controlled hydrothermal systems, the highest flux will occur where and when (1) fracture apertures are highest, (2) fracture density is highest, and (3) fracture connectivity is highest. These three factors provide fundamental controls on the localization of fluid flow in hydrothermal ore systems. Additionally, fracture growth is maximized where pore-fluid factors are highest. Although fracture networks can be highly dilatant, their formation generally involves very low strain. Accordingly, major permeability enhancement by macroscopic fracturing does not require high strains.

As is the case for grain-scale fracture-controlled permeability, the permeability of macroscopic fracture networks is controlled by competition between crack growth and crack closure processes. At elevated temperatures, mineral deposition

rates typically compete with fracture dilation to rapidly destroy fracture permeability. For example, in hydrothermal upflow zones, millimeter-wide fractures have been modeled as being sealed by quartz precipitation on time scales of decades at 300°C (Lowell et al., 1993). Consequently, in deforming hydrothermal environments, fracture apertures and connectivities will be dynamically evolving parameters, with permeability being dependent on rates of fluid- and stress-driven fracture growth and on rates of crack sealing.

*Steady-state permeability versus episodic permeability enhancement during crustal deformation*

As permeability in high-temperature hydrothermal regimes is governed by competition between growth of grain-scale to macroscopic crack networks and thermally or fluid-activated crack closure processes, the time dependence of permeability will be sensitive to styles of deformation and fluid-pressure history.

In the seismogenic regime, typically in the upper 10 to 15 km of the continental crust, slip tends to occur episodically within faults for periods up to several tens of seconds. During the interseismic periods in this regime, there is little or no deformation. Coseismic slip rapidly generates high permeabilities in fault damage zones, whereas interseismic periods will be dominated by pore collapse, crack closure, and permeability reduction (Fig. 15). Flow therefore will tend to be episodic in the seismogenic regime but more continuous in the deeper, aseismic parts of the crust (Cox, 1999).

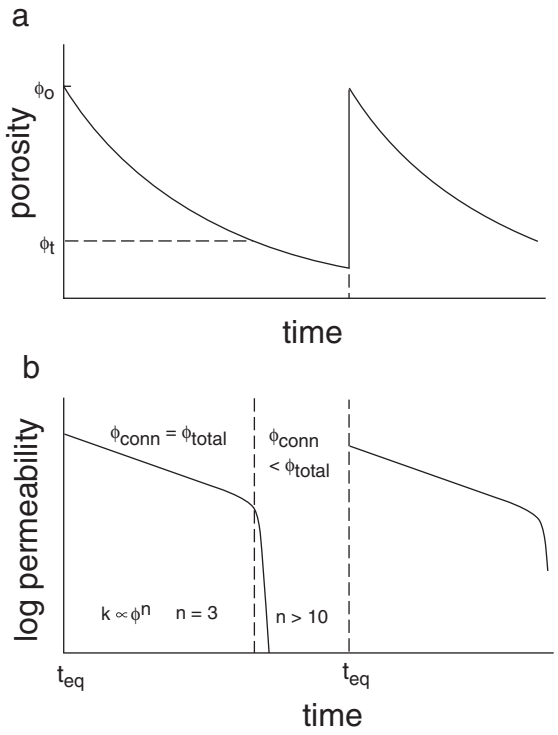


FIG. 15. Schematic illustration of evolution of (a) porosity and (b) permeability as a function of time in an episodically slipping fault zone. $\Phi_t$ is the threshold porosity below which the connected porosity ($\Phi_{conn}$) becomes less than the total porosity ($\Phi_{total}$). Fault rupture and coseismic permeability enhancement occurs at $t_{eq}$.

## Evolution of Fluid Pathways during Progressive Deformation

*General aspects related to growth of percolation networks*

We have seen that fluid migration at depth in the crust can involve flow through pervasive, grain-scale pores, as well as being localized along macroscopic fracture systems. In many situations this dual porosity is likely to be important. Short-range flow and intense fluid-rock reaction involve pervasive flow at the grain scale. Flow on this scale is important for sourcing metals in the upstream parts of hydrothermal systems. It is also critical for chemical fluid-rock interaction at ore deposition sites. In the mid- to deep crust, modest grain-scale permeability severely limits length scales for pervasive flow. Effective extraction of fluid from grain-scale pathways and transport on length scales greater than tens of meters is much more effective via macroscopic, fracture-controlled permeability. Enhanced, structurally controlled permeability is typically related to features such as faults, shear zones, associated damage zones, and other fracture networks whose distribution is related to folding and actively deforming lithologic contacts across which there is competence contrast. In many metamorphic settings, there is evidence for fracture-controlled fluid pathways being separated typically by distances less than approximately 1,000 m (Cox et al., 1987; Ferry and Gerdes, 1998; Oliver, 2001).

The significance of active faults, shear zones, and other fracture networks in controlling fluid migration is illustrated by analytic solutions and numerical modeling studies of flow patterns around high-permeability zones embedded in a less permeable matrix (Phillips, 1991; Matthai and Roberts, 1997; Taylor et al., 1999; Braun et al., 2003). For permeable structures inclined at low angles to the regional gradient in hydraulic head, fluid focusing occurs around the higher pressure (upstream) parts of fracture networks, whereas fluid discharge occurs in the lower pressure (downstream) parts of fracture networks (Fig. 16). The dimensions of potential fluid-charge regions are comparable to the dimensions of the high-permeability segments of faults and shear zones. High-permeability pathways inclined at high angles to the regional hydraulic gradient are much less effective at focussing fluid flow.

Fracture- and/or shear-controlled hydrothermal systems develop where and when linked permeable structures develop sufficient connectivity to create networks that link fluid source rocks, fluid reservoirs, and ore deposition sites. Percolation theory (Sahimi, 1994) provides useful insights about the evolution of hydraulic connectivity and partitioning of flow among elements of a network of permeable structures in an otherwise low-permeability medium (Guéguen et al., 1991; Berkowitz, 1995; Cox et al., 2001).

As for grain-scale pore networks, macroscopic percolation networks (comprising faults, fractures, and shear zones) can be described in terms of three types of elements: backbone, dangling, and isolated elements. Backbone elements provide a direct connection from one side of the system to the other (e.g., metal-source reservoir to ore deposit) and carry the bulk of the fluid flux. Dangling elements branch from the flow backbone and act as fluid feeders to the backbone in the upstream part of the system or as distributary or discharge

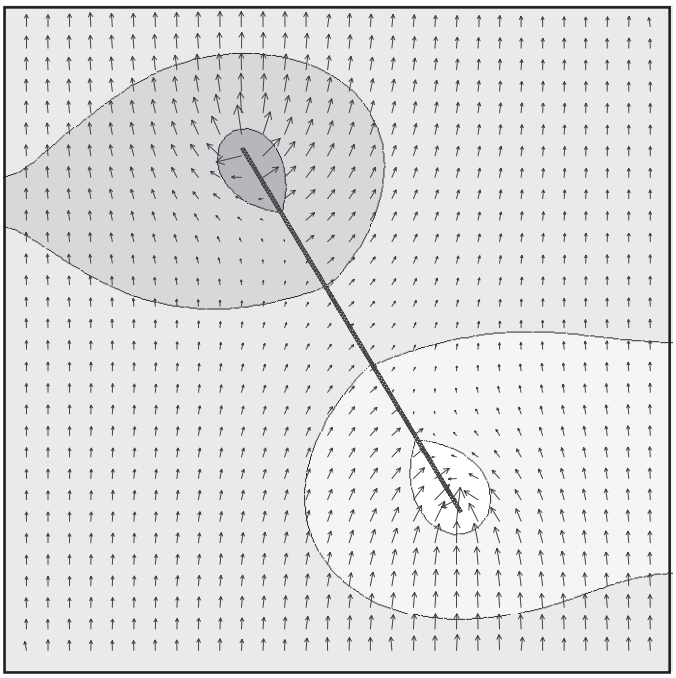

FIG. 16. Finite element model simulating steady-state, pressure-driven fluid-flow pattern in a vertical plane around a permeable fault or shear zone embedded in a less permeable rock. A vertical lithostatic fluid-pressure gradient is maintained in the medium away from the fault. Length of flow vectors corresponds to flow velocity. Flow vectors within the fault are not shown. Contours indicate departures of fluid pressure from lithostatic values. Light areas are below lithostatic pressures, dark areas are above lithostatic. The fault permeability is $10^3$ times that of the surrounding host-rock matrix. Note that flow is focussed at the upstream (lower) part of the structure, and fluid discharge occurs around the downstream (upper) part of the structure. After Cox et al. (2001).

structures in the downstream part of the system. Isolated elements are disconnected from both the backbone and dangling elements in the network and are therefore low-flux structures not connected to fluid reservoirs. Two end-member scenarios for growth of percolation networks are recognized; these are ordinary percolation and invasion percolation (Sahimi, 1994).

*Ordinary percolation*

The growth of fracture-controlled flow networks occurs by ordinary percolation when fracture growth is controlled largely by stress states. In this case fractures nucleate and grow in approximately random locations throughout a deforming, uniform rock mass (Fig. 17a). At very low bulk crustal strains most of the faults or shears in a deforming domain will be short, isolated structures. With increasing deformation, active faults and shears increase in length and surface area; new structures also nucleate and grow such that fracture connectivity increases with strain. At the percolation threshold, enough fractures connect to allow a sudden onset of flow across the fracture system. The point at which the percolation threshold is reached is dependent on several factors, including strain accommodated by growth of permeable faults, fractures, and shear zones. Fracture geometries and relative rates of fracture growth and nucleation are also important (Zhang and Sanderson, 1994; An and Sammis, 1996; Odling, 1997).

Partitioning of flow among elements of a fracture and/or shear network is dependent on the relative proportions of backbone, dangling, and isolated elements (Cox et al., 2001). Just above the percolation threshold, even though the flow backbone is a very small fraction of the total network, most of the flow is localized along this part of the system (Fig. 17a). At higher strains the proportion of elements that are part of the backbone progressively increases, so that flow becomes progressively more evenly distributed across the system as more faults, fractures, or shears become connected to each other and to fluid reservoirs and sinks.

The percolation threshold is reached when approximately 30 percent of the sites are occupied. For permeable meshes of conjugate faults, with typical length and/or displacement scaling relationships (Scholz, 1990), the percolation threshold is reached at bulk strains of only a few percent (Cox et al., 2001).

*Invasion percolation*

The ordinary percolation model described above assumes that, although elements of a percolation network nucleate randomly, all elements grow at the same rate. If fracture systems connect to an overpressured fluid reservoir, invasion of high-pressure fluids along fluid-accessing faults and fractures in the network may greatly enhance their growth rates relative to elements isolated from fluid reservoirs. In this scenario, formation of fluid-driven percolation networks will be dominated by preferential growth of those parts of the network that connect directly to high pore-fluid factor reservoirs. In this case, the network is dominated by backbone and dangling fractures (Fig. 17b).

The fluid-driven growth, or "self-generation" (Sibson, 1996), of percolation networks in response to invasion of overpressured fluid provides a positive feedback between fluid access and fracture growth rate. This is likely to localize repeated slip on the flow backbone that formed at the percolation threshold, allowing that part of the fracture system to repeatedly tap into fluid reservoirs. Fluid-driven growth of invasion percolation networks could lead hydrothermal systems to self-organize near the percolation threshold.

Several points emerge from percolation modeling. First, as the percolation threshold is reached at bulk strains of only a few percent, fracture-controlled hydrothermal systems and associated ore deposits can be expected to develop at very low strains. Second, for networks just above the percolation threshold, where the backbone is a very small proportion of the total fracture population, flow is localized on relatively few structures that link fluid sources and sinks. This situation maximizes the potential for generation of giant ore deposits. In contrast, for hydrothermal systems well above the percolation threshold, fluid flow is distributed over a larger proportion of the fracture population. This more dispersed flow is likely to produce more distributed, potentially smaller mineral deposits.

*Percolation in a seismogenic framework*

The basic percolation models, described above, are particularly relevant to evolution of flow networks in the mid- to

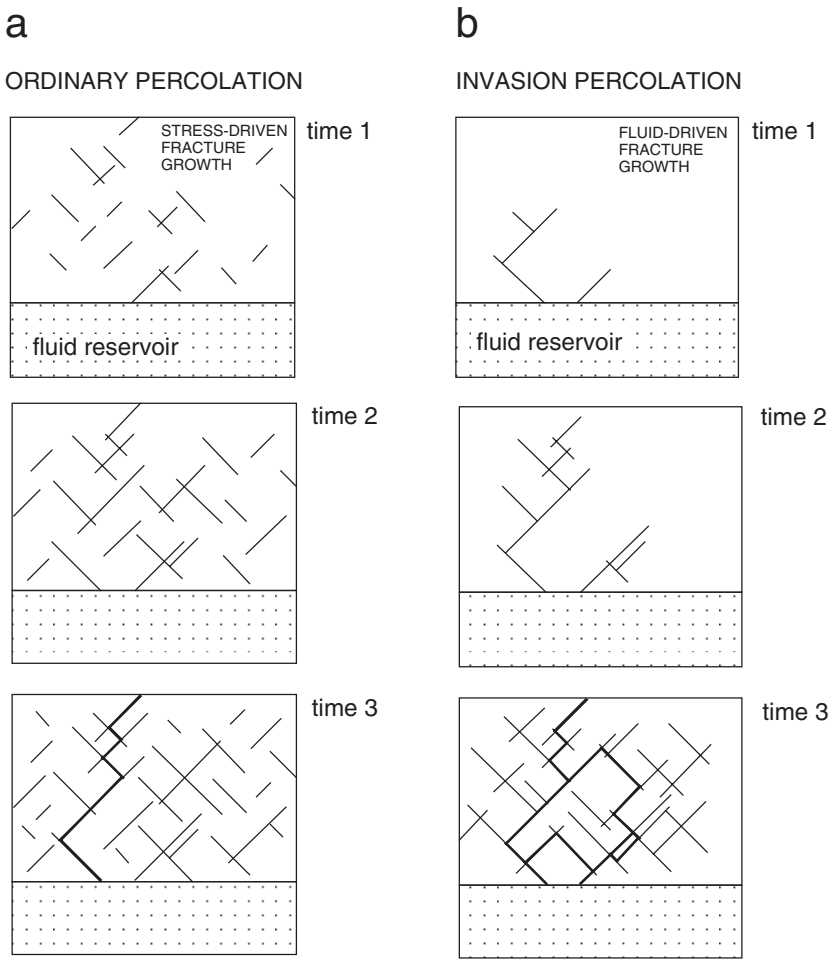


FIG. 17. Progressive evolution of connectivity in a growing fault network. a. An "ordinary" percolation model in which fault growth is stress driven and faults nucleate randomly throughout the rock mass, increasing in surface area with time. b. An "invasion" percolation model in which fault nucleation and growth is fluid driven. Here, only faults that connect to a high pore-fluid factor reservoir nucleate and grow. The percolation threshold is reached at time 3; the backbone pathway is indicated by bold lines.

deep crustal parts of actively deforming shear systems where approximately steady-state deformation generates near steady-state permeability. However, deformation typically migrates with time through the crust, so that connectivity of the network to reservoirs is expected to change with time. Therefore, the locus of highest fluid flux should migrate with time. For example, during the propagation of thrust systems the locus of deformation typically moves toward the foreland with time (Boyer and Elliot, 1982). Accordingly, the locus of high fluid flux activity will also migrate toward the foreland, provided the active thrusts continue to tap into fluid reservoirs.

In the seismogenic regime, at any stage in the growth of fault-controlled permeability networks, flow paths will be controlled by competition between coseismic permeability enhancement on ruptured fault segments and interseismic fault sealing which destroys permeability. As successive rupture events migrate around an active fault system, the distribution of high-permeability pathways is expected to evolve in complex ways. Additionally, rapid changes in permeability in fault networks on time scales of seismic slip recurrence (i.e., approximately decades to centuries) could cause sudden changes in the location and structure of the flow backbone.

*Self-organization of flow in fault-controlled flow networks*

The mechanical evolution of linked fault systems involves nucleation and growth of individual fault segments and development of mechanical connectivity between segments as total displacement increases (Ellis and Dunlap, 1988; Cowie and Scholz, 1992; Cowie, 1998). With increasing deformation, through-going faults eventually develop and form a mechanical backbone in the fault system. Most displacement subsequently localizes along the backbone faults, and they evolve into the highest displacement faults. The mechanically isolated and dangling faults accumulate less displacement than the backbone faults (Cowie and Scholz, 1992).

The generation of fluid pathways in active fault systems is closely linked to the mechanical evolution of the system. When major slip events localize along through-going backbone faults, then permeability enhancement and fluid flow will also localize along these structures and their associated

damage zones. Accordingly, the flow network will stay near the fluid percolation threshold. At seismogenic depths, repeated slip and interseismic fault sealing will repeatedly switch fluid flow on and off (see also next section). If interseismic permeability loss in the flow backbone is rapid on time scales of rupture recurrence, then the flow system will be driven back below the percolation threshold during interseismic healing. This sort of feedback process, which causes the flow network to oscillate about the percolation threshold, is an example of "self-organized criticality" (Bak, 1997).

## Flow Regimes in the Aseismic and Seismogenic Parts of the Crust

### *Pervasive flow in the deep crustal aseismic regime*

Fluid migration from deep crustal fluid reservoirs into shallower hydrothermal systems must occur within an hierarchical network of pathways in which regional hydraulic gradients drive flow from the upstream to downstream parts of the network. Initial flow must occur via transitory grain-scale pores (e.g., during devolatilization reactions) or repeatedly regenerated microcrack networks in deforming, high pore fluid factor regimes. More permeable pathways are likely to be provided by networks of macroscopic fractures pervasively distributed through the rock mass but not necessarily spatially associated with faults or shear zones. These structures serve to drain fluids from grain-scale porosity. Vein swarms, which may mark such drainage pathways, are common in some metamorphic regimes (e.g., Fisher and Brantley 1992). The vein swarms, in turn, provide high-permeability channelways, which direct fluid migration into the upstream parts of larger scale networks of active faults, shear zones, or other transiently permeable structures. From these, fluids are delivered to downstream structural levels.

In the deep, aseismic crust, flow is initiated usually by fluid production events. Miller and Nur (2000) discussed how rise in fluid pressure can dramatically enhance permeability. They proposed a "toggle switch" model in which fluid-pressure pulses self-generate permeable flow networks and propagate fluid-pressure fronts through the crust. Other models indicate that, even in the deep crust during continuous fluid production, flow can self-organize into repeated pulses of upward-migrating fluid.

*Porosity waves:* Connolly and Podlachikov (1998) discussed how a fluid-pressure perturbation to an initial steady-state flow regime can initiate surges in flow or episodic waves of fluid-filled porosity, known as porosity waves or fluid-pressure waves. Pressure waves could be particularly important in establishing flow during mid-to deep crustal metamorphic devolatilization episodes.

The detailed nature of porosity waves is predicted to depend on whether the rock deforms by elastic or viscous processes. Fluid flow in the viscous regions of the mid- to lower crust can be accomplished by self-propagation of isolated domains of fluid-filled porosity with transitory permeability enhancement. In metamorphic environments undergoing devolatilization the fluids are expected to be pervasively distributed within grain-scale microcrack networks or fracture arrays. The low-permeability carapaces around migrating pressure waves have potential to generate domains, immediately below the carapace, where fluid pressure exceeds $\sigma_3$ and permeability is greatly enhanced (Connolly, 1997). Crack-seal textures in veins that are pervasively distributed through large volumes of some metamorphic belts (e.g., Ramsay, 1980; Fisher and Brantley, 1992) could be a record of fluid-pressure fluctuations associated with episodic migration of porosity waves through the midcrust.

Upward propagation of fluid-pressure pulses associated with porosity waves provides a potential trigger for fault rupture near the base of the seismogenic regime. Futhermore, if large fault ruptures propagate down into midcrustal porosity waves, they have potential to drain fluid from pressure waves and generate episodic high fluid-flux events downstream in the shallower hydrostatic regime. The fluid-flux events would be recorded as periods of anomalous high fluid pressures. Permeable shear zones that intersect migrating pressure waves could similarly drain these migrating reservoirs but on longer time scales. In this scenario, as networks of shear zones become hydraulically connected to successive porosity waves, they should experience repeated episodes in which high fluid pressures, fluid fluxes, and transitory permeability enhancement propagate upward through the shear-zone network. Crack-seal microstructures in extension veins spatially associated with ductile shear zones in some cases could be a record of the drainage of fluid-pressure waves via active and permeable shear systems.

Numerical modeling by Connolly (1997) indicated that upward strengthening of the crust increases the wavelength and amplitude of fluid-pressure waves. Order-of-magnitude strength contrasts may even arrest wave propagation and control the distribution of overpressured fluid reservoirs in the crust.

Pervasive flow of fluid through actively deforming crust may therefore involve steady-state flow or episodic migration of fluids via porosity waves. Pervasive flow is expected to be modulated by the effects of strain or displacement localization that generates local permeability enhancement. This will be especially important around shear zones, faults, and other high-permeability sites. Structures with enhanced permeability relative to the surrounding bulk crust provide sinks into which dispersed fluid migrates. Pervasive to localized fluid migration in near-lithostatic fluid-pressure regimes in the mid- to lower crust provides a dynamic reservoir of overpressured fluids that can drive brittle failure and self-generate pathways, allowing these deep reservoirs to drain into fault networks in the upper crust.

An example of the potential role of major fault rupture events driving permeability enhancement and transitory fluid migration deep in a modern convergent orogen is provided by the $M_w = 8$ subduction zone earthquake near Antofagasta, Chile, on 30 July, 1995. After the rupture event a seismic wavespeed anomaly developed deep in the fore-arc region of the Andean continental crust, above the subducting slab (Husen and Kissling, 2001; Koerner et al., 2004). The anomaly is interpreted to have been associated with a large flux of fluid migrating out of the downgoing slab, across the newly ruptured slab interface, and into the continental crust hanging wall. The earthquake ruptured at least a 30-km-downdip segment of the subduction interface. Over a period of 59 days, a fluid-pressure pulse is interpreted to have migrated

approximately 15 km into the fault hanging wall, changing the ratio of compressional wave velocity to shear wave velocity. Rapid propagation of the velocity anomaly requires that pervasive, fluid-pressure–driven fracture growth increased the permeability of the deep continental crust to values as high as $10^{-13}$ m$^2$.

The presence of a contemporary fluid reservoir deep in a metamorphic pile is also suggested by magnetotelluric data in the New Zealand Southern Alps (Wannamaker et al., 2002). A broad, U-shaped conductivity anomaly in the mid- to deep crust of this currently active collisional orogen is interpreted as a domain of interconnected, deeply sourced fluid generated by devolatilization reactions.

*The role of coseismic permeability enhancement in influencing flow*

In regimes where coseismic slip on faults suddenly increases their permeability and interseismic hydrothermal sealing progressively reduces permeability, fluid flow will be episodic and dominated by immediate postseismic transient flow regimes, rather than by steady-state flow regimes.

Numerical modeling of the evolution of fluid-flow regimes in and around faults following rupture has been described by Matthai and Fischer (1997), Matthai and Roberts (1997), Taylor et al. (1999), and Braun et al. (2003). For a fault embedded in a less permeable medium, flow and the associated fluid-pressure field evolve through three stages following coseismic permeability enhancement (Braun et al., 2003). In the first stage, the fluid-pressure gradient that existed prior to rupture is relaxed as fluid rapidly flows through the fault, driven by the initial hydraulic head gradient between the upstream and downstream ends of the rupture. In the second stage, fluid flow in the fault leads to rapid fluid-pressure changes in the rock around the upstream and downstream ends of the fault. Fluid is rapidly expelled from the downstream end of the fault and extracted from the rocks surrounding the upstream end of the fault. This leads to a reduction in the fluid-pressure gradient between the extremities of the fault. By the third phase, fluid flow in the rock matrix adapts to the new fault permeability and a steady-state pressure field develops around the fault (Fig. 16).

The three stages in the evolution of flow regimes initiated by fault rupture events are illustrated by the time evolution of fluid velocity at the center of the fault (Fig. 18). In stage 1 of the evolution, normalized fluid velocity remains constant until time $\tau_f$, when the flow velocity starts to decrease at the beginning of the transient flow in the stage 2 flow regime. The timescale $\tau_f$ is the time required for the fluid to travel the length of the fault and is therefore a function of the fault length and the fault permeability. $\tau_f$ decreases with increasing contrast in permeability between the fault and the surrounding rock mass. In contrast, the time $\tau_F$ required to reach the start of the steady-state flow regime is controlled by the permeability of the rock mass and decreases with decreasing fault length.

For realistic permeability contrasts between ruptured faults and their surrounding, less permeable rock mass, the flow rate in the steady-state flow regime is a small fraction of the flow rate in the initial and transient phases of flow (Fig. 18; Braun et al., 2003). In particular, because the fluid velocity

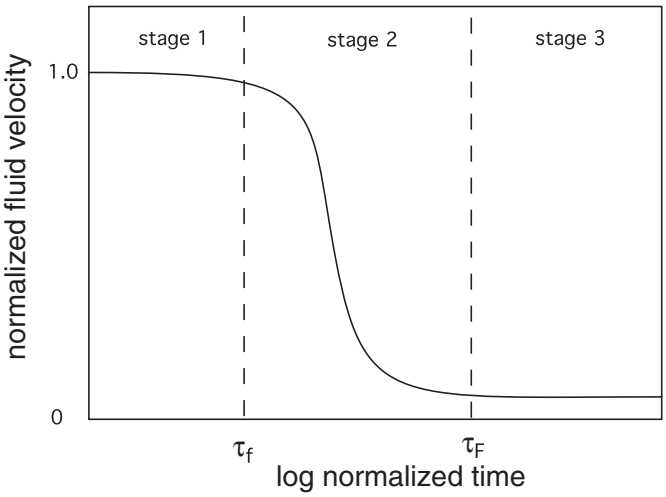


FIG. 18. Evolution of fluid velocity within a fault following rupture-driven permeability enhancement. $\tau_f$ is the time required for fluid to migrate from the upstream to downstream end of the fault immediately after rupture. $\tau_F$ is the time required for the system to attain a steady-state flow regime. Modified after Braun et al. (2003).

inside the fault is constant during the first stage of flow, the total amount of fluid Q (volume per unit length of fault) flowing through the fault during the first stage ($0 < t < \tau_f$) is given by

$$Q = \Phi S l^2 W \psi_0 / L, \quad (16)$$

where $\Phi$ is the fault porosity, S the specific storage, $l$ the fault length, W the fault thickness, $\psi_0$/L the hydraulic head gradient in the system remote from the fault, and L the dimension of the modeled rock mass. $l^2$W is the fault volume. For dipping faults embedded in a vertical hydraulic gradient, the fluid velocity and fluid flux will scale with cos$\alpha$, where $\alpha$ is the fault dip (Braun et al., 2003).

The quantity of fluid that percolates through the fault during this period of maximum fluid flow is independent of the fault permeability. Taking $l$ = 0.5L, W = 0.0005$l$, S = 0.01 m$^{-1}$, $\Phi$ = 0.05, and $\psi_0$/L = 0.5, for a 1-km-long fault, the total fluid flux Q in stage 1 is $2.5 \times 10^5$ m$^3$ every failure cycle. For 1,000 slip events, the total fluid flux will be 0.31 km$^3$. For a slip history involving 1,000 slip events on a 10-km-long rupture surface, total fluid flux is predicted to be $3.1 \times 10^2$ km$^3$. This fluid volume is comparable to that involved in the formation of large hydrothermal mineral systems (Cox, 1999).

Braun et al. (2003) estimated that the time required to reach stage 2 conditions, after a rupture event, varies between 30 and 300,000 yr. This depends on the permeability of the fault and surrounding rock mass. In contrast, the time to reach steady-state flow conditions, $\tau_F$, is calculated to be between 3 and $3 \times 10^4$ m.y. The fastest time scales relate to wall rocks with permeabilities in the range $10^{-12}$ to $10^{-16}$ m$^2$. This corresponds to permeabilities typical of pervasively fractured igneous and metamorphic rocks. The larger time scales are relevant for relatively unfractured wall rocks with permeabilities of $10^{-18}$ to $10^{-22}$ m$^2$. The duration of the stage 1 flow regime, for moderate- to high-permeability host rocks, is of the same order of magnitude as earthquake recurrence times

and indicates that kilometer-scale faults are unlikely to attain steady-state flow regimes during interseismic intervals. This result is consistent with independent modeling by Matthai and Fischer (1996) and Matthai and Roberts (1997). Although the modeling assumes constant interseismic permeability, interseismic fault sealing is likely to cause reductions in flow rates during the stage 1 flow regime.

Where faults drain fluids from the surrounding rock medium, rapid, transitory flows after slip events have a major influence on total volumes of fluid involved in the mineralization process. Furthermore, steady-state flow models grossly underestimate the actual volume of fluids flowing through faults. Fault-controlled hydrothermal systems, such as those involved in the formation of mesothermal gold deposits, require fluid transport over distances of many kilometers. The modeling indicates that time scales are likely to be insufficient for ore fluids to percolate large distances through essentially intact host rocks, when driven by transient fluid-pressure gradients around the kilometer-scale faults that usually host these deposits. Instead, the effective transport of hydrothermal fluids from metal source areas to sites of ore deposition is dependent on the growth of networks of high-permeability structures (e.g., faults, shear zones, and associated damage zones), which can drain fluids from large crustal volumes and provide fast transport paths to ore deposition sites. Significantly, if faults are to effectively drain large fluid reservoirs, then the reservoirs themselves must have high permeability. As the grain-scale permeability of texturally equilibrated mid- to deep crustal metamorphic rocks is typically less than $10^{-18}$ m$^2$ (Manning and Ingebritsen, 1999), effective drainage of crustal-scale reservoirs at depth requires substantial permeability enhancement by generation of deformation-induced and/or fluid-pressure–driven high-permeability pathways throughout the reservoirs.

### *Rupturing of overpressured reservoirs—high fluid flux fault-valve processes*

Episodic flow regimes associated with fault ruptures which tap into overpressured fluid reservoirs have been described qualitatively by "fault-valve" models which have been applied particularly to mesothermal gold systems (Sibson et al., 1988; Boullier and Robert, 1992; Cox, 1995; Robert and Poulsen, 2001; Sibson, 2001). A contemporary example of probable fault-valve behavior is provided by postseismic fluid migration associated with the 1997 Umbria Marche earthquake sequence in the Apennines, Italy (Miller et al., 2004).

The fluid reservoirs that drive fault-valve behavior can be broad domains of fluid-saturated crust or more restricted domains, such as hydraulically linked damage zones around fault and/or shear networks. The enhanced microfracture porosity in ductile shear zones deforming at high pore fluid factors provides potentially large fluid reservoirs that can leak into shallower level brittle fault systems. Fluid-saturated shear zones would be tapped most efficiently when large earthquake ruptures propagate down into their ductile roots from the seismogenic regime.

The most extreme episodic flow regimes are likely to be associated with rupturing of low-permeability seal domains which separate moderate- to high-permeability, near-lithostatic fluid-pressured compartments, from shallow crustal, near-hydrostatic regions. Fault-valve behavior could also occur in intrusive-related hydrothermal systems where hydrothermally sealed carapaces around intrusions separate inner, high-temperature, overpressured parts of the system from cooler, outer, lower fluid-pressure parts of the system (Fournier, 1999).

The major feature of fault-valve behavior is that fault rupture events cause sudden permeability enhancement and connectivity to lower pressure reservoirs. This initiates fluid discharge up the fault zone from overpressured reservoirs (Fig. 19). Rapid fluid discharge is followed by gradual hydrothermal resealing of the fault and subsequent fluid-pressure recovery in the upstream part of the rupture zone. The cycle is repeated at each rupture event. Accordingly, fault-valve processes result in episodic migration of fluid batches through fault-controlled hydrothermal systems.

*Upstream ends of fault ruptures*: In overpressured hydrothermal systems, the prefailure stage of the fault-valve cycle is characterized by increasing fluid pressure in the upstream area of the system below sealed zones (Fig. 20). If fluid pressure reaches $\sigma_3$ + T before shear failure (Fig. 20b), then hydraulic extension fractures nucleate and grow prior to shear failure. The ubiquitous extension vein arrays associated with fault-related mesothermal gold deposits probably form at this stage of the fault-valve cycle (Cox, 1995). Opening and propagation of extension fractures limits the maximum fluid pressures that can be attained when stress differences are low (<4T). At higher stress differences, maximum sustainable pore fluid pressures are less than $\sigma_3$ + T and extension fractures cannot form (Sibson, 2001).

Extension veins formed adjacent to the upstream parts of rupture zones should contain fluid inclusions trapped at the maximum fluid pressures prior to failure. However, fluid inclusions trapped when open, fluid-filled veins collapse during the coseismic fluid-pressure decrease, record much lower pressures (Boullier and Robert, 1992; Wilkinson and Johnston, 1996).

Prior to rupture events, fluid-pressure buildup below seals can lead also to fluid discharge from this part of the fault zone. Prefailure fluid discharge is important in the formation of disseminated ore in wall rocks where ore deposition is controlled by fluid-rock interaction.

At failure, both seal breaching and dilation within the fault zone are associated with rapid fluid-pressure drop in the upstream parts of the rupture zone (Fig. 20). Around dilatant zones, such as jogs or damage zones near rupture terminations, coseismic fluid-pressure drop may be sufficient to transiently drive fluids into the dilatant zones from the adjacent wall rocks. Mixing between fault fluids and externally derived fluids, which are in equilibrium with wall rocks, can provide a powerful control on localization of ore deposition in fault-fill veins. Postrupture mixing between fault fluids and fluids which had discharged from the fault zone prior to rupture and reacted with wall rock may influence ore deposition (Cox et al., 1995). Similarly, coseismic fluid-pressure drop that occurs throughout the upstream part of the fault zone, and especially in dilatant jogs, can drive phase separation and related ore deposition processes in fault-fill veins (e.g., Sibson et al., 1988; Cox et al., 1995). Fluid inclusions in fault-fill

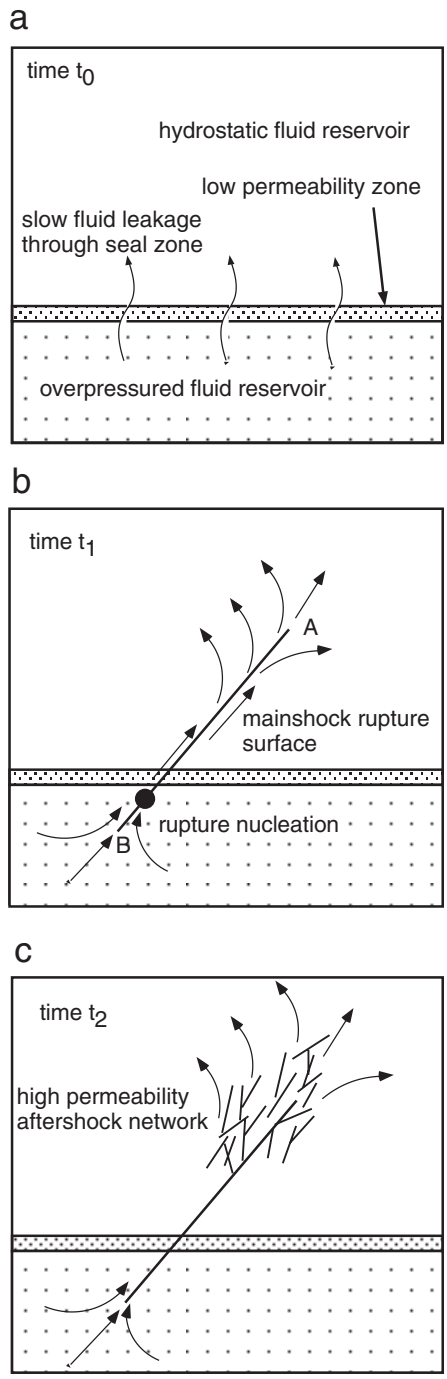


FIG. 19. Fault-valve behavior and postseismic fluid redistribution around a fault zone that has tapped a deep, overpressured fluid reservoir. a. Two reservoirs are separated by a low-permeability domain across which there is slow fluid leakage. b. Fault rupture breaches the seal domain, leading to rapid fluid drainage up fault AB. c. As the fluid pressure pulse migrates outward from the main-shock rupture near its downstream end, rising fluid pressure can trigger aftershocks. Permeability enhancement along aftershock ruptures facilitates more rapid drainage of fluids from the deep reservoir via the main-shock zone. The aftershock ruptures form a hydraulically connected distributary flow network.

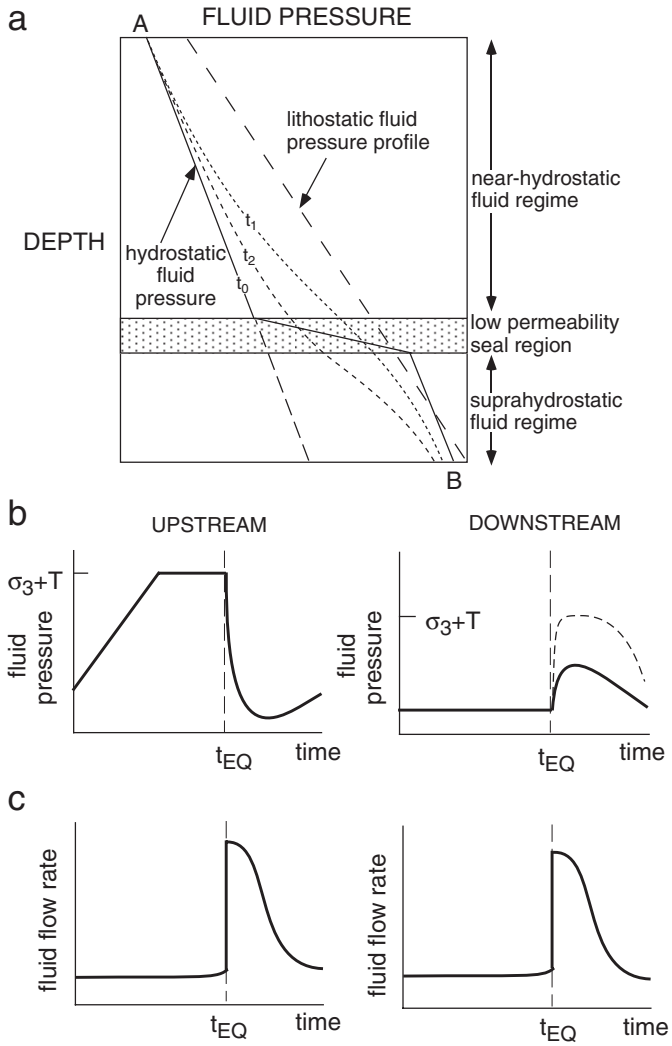


FIG. 20. Evolution of fluid-pressure regimes associated with fault rupture and breaching of a low-permeability seal separating a suprahydrostatic from a near-hydrostatic fluid-pressure compartment. a. Variations of fluid pressure with depth. The solid line AB is the fluid pressure along the fault AB in Figure 19b at time $t_0$ immediately prior to main-shock rupture. The fluid-pressure gradient above the seal is hydrostatic. Although the vertical fluid-pressure gradient below the seal is near-hydrostatic, the absolute fluid pressure is suprahydrostatic. Following main-shock rupture, the establishment of hydraulic connectivity between A and B leads to rapid migration of a fluid-pressure pulse upward along the fault, together with a decrease in fluid pressure below the breached seal and an increase in fluid pressure above the breached seal (e.g., time $t_1$). Fluids migrate into the rupture zone at its lower (upstream) end and discharge from the fault near its upward (downstream) end. The fluid-pressure profile evolves with time (e.g., time $t_2$) as the supply of overpressured fluid around the upstream end of the fault is depleted. b. Variation of fluid pressure with time at the up- and downstream ends of the rupture. Fault rupture occurs at $t_{EQ}$. Near-lithostatic fluid pressure may be attained transiently in the downstream part of the system after rupture (dashed line). c. Variation in fluid flux with time.

veins, especially in dilatant jogs, should record trapping predominantly in the low fluid-pressure regime immediately after fault rupture.

*Downstream ends of fault ruptures:* In contrast to the fluid-pressure evolution in the upstream part of a fault rupture zone, the highest fluid pressures develop in the downstream

part of the rupture after slip events (Fig. 20). Extension veins will only form in the downstream region after mainshock rupture if the migrating, post-rupture fluid-pressure pulse reaches the local value of $\sigma_3$ + T (dashed line in downstream fluid-pressure evolution in Fig. 20b).

*Suction pump models in near-hydrostatic systems*

Sibson (1987, 2001) has discussed fluid redistribution around seismically active faults in near-hydrostatic regimes. The major effect of episodic fault rupture is that coseismic dilation in the fault zone results in a localized, coseismic fluid-pressure drop. This "suction pump" behavior draws fluids in toward the ruptured zone and leads to a gradual, postseismic recovery of fluid pressure (Fig. 21). The coseismic fluid-pressure drop may be important in driving both phase separation and fluid mixing in near-hydrostatic–pressured hydrothermal systems, such as some epithermal systems.

*Stress-driven fluid migration—the poroelastic response*

Fluid redistribution processes driven by fault-valve and suction pump behavior are associated with large, inelastic deformations and permeability change within fault zones. However, changes in stress and fluid-pressure states associated with the seismic cycle can also drive elastic deformations of fluid-containing pores and fracture networks. These so-called poroelastic effects may play a role in moving fluids around fault systems (Muir-Wood and King, 1993). In the mid- to deep crust, stress- and fluid-pressure–driven elastic deformation of high aspect ratio fractures will cause a greater poroelastic response than elastic deformation of more equant intergranular pores. Poroelastic behavior in fracture-controlled reservoirs is most sensitive to changes in normal stress acting on the fractures. If fractures formed in the ambient stress regime that drives faulting, the normal stress will be $\sigma_3$.

As an example, let us consider the poroelastic behavior of approximately vertical fractures produced in a damage zone around a normal fault. Normal faults are characterized by a stress regime in which $\sigma_3$ is subhorizontal and $\sigma_1$ is subvertical. In the prefailure phase, $\sigma_3$ progressively decreases with time and $\sigma_1$ stays approximately constant. In this case, and assuming nearly constant fluid pressures, fractures will elastically dilate in the lead-up to rupture events and suddenly decrease aperture during coseismic recovery of $\sigma_3$ (Fig. 22). If fracture density is highest adjacent to active faults, prefailure poroelastic dilatancy draws fluids laterally in toward the fault zone. Coseismic increase in $\sigma_3$ will then decrease fracture porosity, driving fluid migration either into the ruptured fault or laterally away from the fault zone.

For reverse fault environments, where $\sigma_3$ (vertical stress, normal to fractures) changes tend to be small, poroelastic effects will be negligible compared to those for normal faults. The effects for strike-slip faults will be intermediate between those for normal and reverse faults.

In hydrothermal systems involving fault-valve behavior (e.g., most mesothermal gold systems), high fluid fluxes associated with breaching of overpressured reservoirs is likely to overwhelm any fluid flow and hydraulic gradients related to poroelastic effects.

*Convective fluid flow within fault rupture planes*

Inplane convective flow within fault damage zones may occur transiently after rupture events provided that the slip-generated permeability in the rupture surface and the associated damage zone is high enough, and the damage zone is fluid saturated and has a near-hydrostatic vertical fluid-pressure gradient. Onset of convection and the patterns of convection are controlled by the thermal properties of the rock and the fluid, the vertical temperature gradient, and the

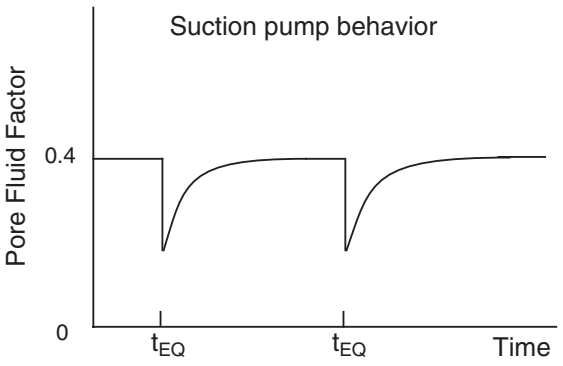


FIG. 21. Suction-pump model for flow around an episodically slipping fault zone in a near-hydrostatic fluid-pressure regime. Coseismic dilatancy in the fault zone causes sudden fluid-pressure decrease at times $t_{EQ}$. Postseismic fluid flow into the damage zone immediately after rupture events allows fluid pressures to recover to prefailure levels. Modified after Sibson (2001).

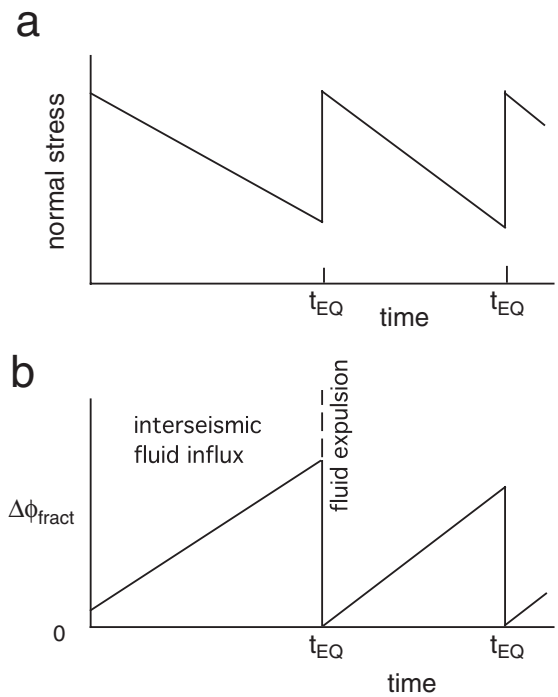


FIG. 22. Poroelastic effects on fluid redistribution in a damage zone around an active normal fault in a near-hydrostatic regime. a. With decreasing $\sigma_3$ prior to fault rupture, normal stress ($\sigma_n$) on steep fractures decreases. Upon fault rupture (at times $t_{EQ}$), there is a sudden recovery in normal stress. b. Poroelastic change in fracture porosity ($\Delta\Phi_{fract}$) as a function of time. With decreasing normal stress in the interseismic period, fractures dilate and draw fluid into the fault damage zone. Sudden increase in normal stress at fault rupture causes a decrease in fracture apertures and drives fluid out of the damage zone.

permeability of the fault zone (Murphy, 1979; Zhao et al., 2004). High fault permeability and low wall-rock permeability favor highly localized convective flow within the rupture zone.

### Localization of Fluid Flow at Regional Scales

*The role of irregularities in fault geometry in crustal-scale fault systems*

It has been shown that large changes in fluid-flow rates can occur during the seismic cycle in crustal-scale fault systems. Fluid fluxes are also spatially very variable along the length of fault networks. This irregular distribution of flow provides a fundamental control on where potentially mineralizing hydrothermal systems can develop within fault systems. Importantly, to form well-endowed ore systems, high-permeability areas need to be long-lived features during the evolution of active fault networks.

Localization of flow within small segments of fault networks during postseismic fluid redistribution appears to be influenced largely by geometric irregularities. These irregularities play a key role in controlling the magnitude of permeability enhancement, not just during major rupture events but also during subsequent evolution of the system as aftershocks propagate and enhance permeability up to many kilometers away from main shock ruptures.

Geometric irregularities in fault systems have their origins in the way fault networks grow (Sibson, 2001). Large throughgoing faults grow by linkage between initially disconnected, shorter fault segments. Linkage occurs via the formation of bends, jogs, or relay structures, so that large faults usually consist of nearly planar, structurally simple fault segments, linked by shorter zones having greater structural complexity. Similarly, at the ends of high displacement faults, decreasing net slip on the principal displacement surface is commonly taken up by distributed strain around the ends of the structure. These strains are accommodated by the formation of various types of extensional or contractional splay structures. These are also sites of marked structural complexity compared to the more planar segments of fault systems. Bends, jogs, relays, and terminal splay structures on high displacement faults are sites of the most intense damage within crustal-scale fault systems (e.g., Kim et al., 2004) and are typically associated with higher densities of low displacement faults and related fractures than elsewhere in fault systems. Accordingly, they tend to be the high-permeability sites in fault systems.

Structurally complex damage zones are expected to be most active and most permeable in immature fault systems while they are actively developing linkages between segments. As fault systems accumulate displacement, there is a general decrease in frequency of geometric irregularities that provide barriers to propagation of large ruptures (Wesnousky, 1988). Accordingly, with increasing finite displacement on crustal-scale faults, geometric barriers are eventually short circuited and deactivated by diversion of principal slip surfaces around them. Overall permeability of fault systems is therefore expected to decrease with increasing maturity (Sibson, 2001). In particular, deactivated lateral and terminal damage zones will lose their permeability and cease to influence the distribution of flow in hydrothermal systems.

Damage zones associated with fault linkages and terminations give rise to a fundamental permeability anisotropy in fault systems. Linkage structures in strike-slip systems have strong vertical connectivity, whereas in reverse and normal fault systems they have high horizontal connectivity (Fig. 23). Both contractional linkages and dilatant linkages are enhanced permeability sites after rupture events. Even though they are sites of shortening, contractional linkages have very high densities of low displacement faults and related fractures. The Victory Complex in the St. Ives goldfield, 80 km south of Kalgoorlie, Western Australia, provides an example of a major mesothermal gold system which is developed in a kilometer-scale contractional jog within a large strike-slip fault system (Cox and Ruming, 2004).

Because fault segments between linkage and terminal damage zones are more planar and structurally less complex, they probably have lower bulk permeability than damage zones. Additionally, the less damaged planar segments of faults can be sealed faster than the high aperture, high fracture density sites provided by fault linkage and terminal damage zones. Accordingly, flow is predicted to persist longer in the interseismic period in the complex damage zones than in intervening less complex planar fault segments (Micklethwaite and Cox, 2004).

*Localization of flow in aftershock networks*

There are two intriguing aspects about the distribution of mesothermal gold deposits in crustal-scale fault networks that may help to understand controls on large-scale distribution of flow in fault-controlled hydrothermal systems. First, these deposits tend to form predominantly within low displacement faults and shear zones adjacent to much larger crustal scale shears, rather than in the kinematically related, high displacement structures. The ore-hosting structures can be several kilometers from the high displacement faults. Second, mesothermal gold deposits have a very clustered distribution within crustal-scale fault networks. They tend to occur in goldfields with dimensions up to around 10 km in diameter and typically along small segments of much more extensive crustal scale shear systems (Robert et al., 2005). For example, in the Kalgoorlie region of the Eastern Goldfields province of the Archean Yilgarn craton in Western Australia, the majority of gold deposits are spatially related to the Boulder-Lefroy fault system (Cox and Ruming, 2004). Deposits exhibit a strong clustering, with significant Au endowments being present in the Paddington, Kalgoorlie-Boulder, New Celebration, and St Ives goldfields. These goldfields are spaced approximately 30 km apart along the Boulder-Lefroy fault system.

*The role of coseismic stress transfer:* Insights about the distribution of fluid pathways in fault systems are provided by the behavior of modern seismogenic fault systems. The highest displacement faults repeatedly rupture in magnitude 6 to 8 events and are expected to exert most control on fluid redistribution during repeated seismic cycles. The low displacement faults form part of a much broader damage zone around crustal-scale faults and may be hydraulically linked to the high displacement ruptures. In this case, the low displacement faults can form fluid feeder zones, delivering fluid to the high displacement structures in their upstream regions.

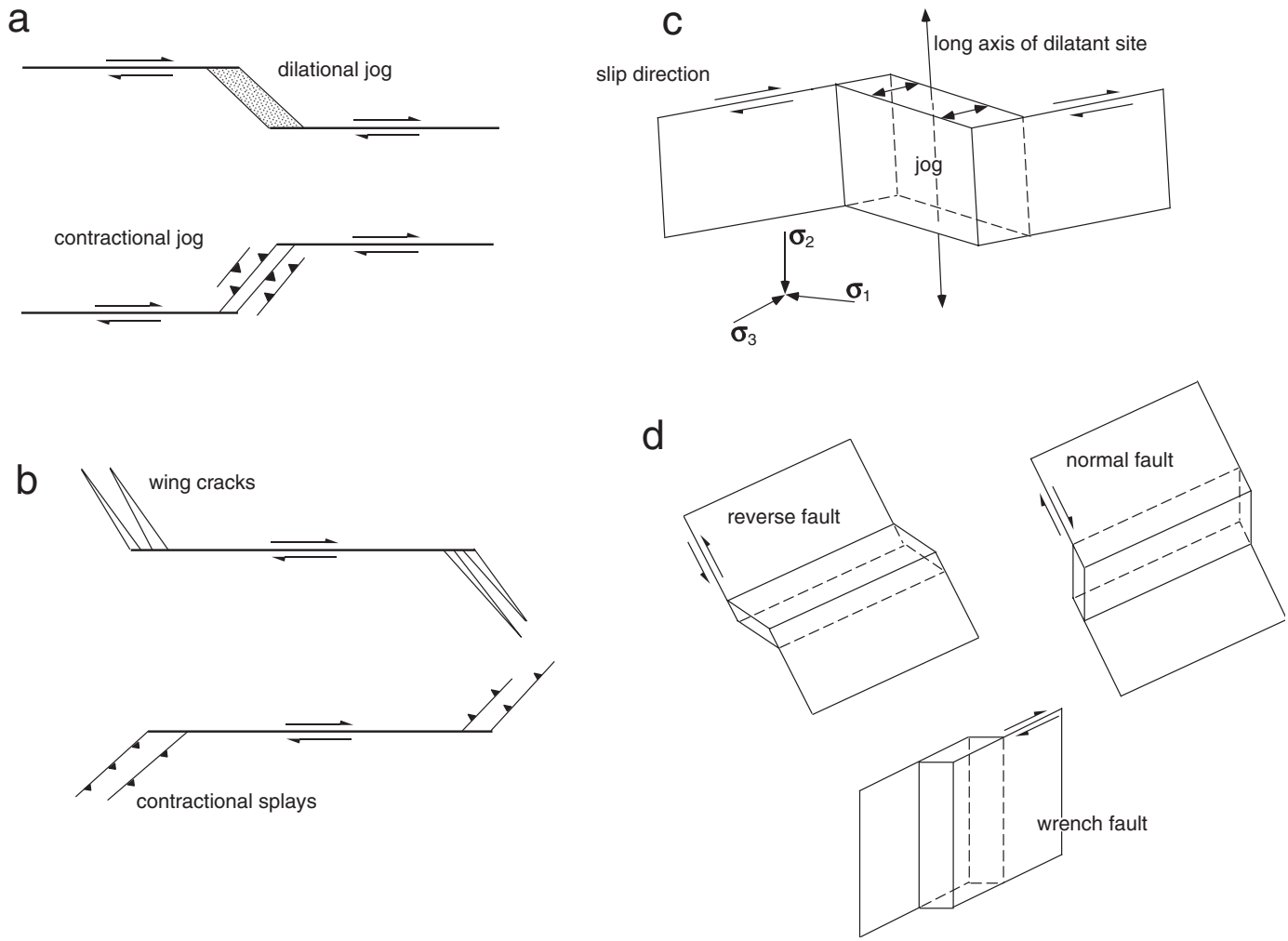


FIG. 23. a. Geometry of contractional and dilational jogs. b. Wing-cracks and contractional splays developed around fault terminations. c. Geometry of a dilational jog relative to fault-slip direction. d. Orientations of jogs in contractional, extensional, and wrench tectonic regimes. High fracture density, aperture, and connectivity along jogs favors high fluid flux along the jog axis. After Cox et al. (2001).

In contrast, in the downstream part of these systems, the low displacement damage zone provides distributary structures that facilitate fluid discharge from high displacement fault zones (Fig. 19). Most slip on low displacement faults occurs during aftershock sequences that follow main shocks on the large displacement structures. Interestingly, most aftershocks are not randomly distributed around mainshock ruptures but typically concentrate in particular areas around mainshock rupture zones (Stein, 1999).

Modeling of coseismic static stress change in modern seismogenic systems is having much success in explaining the nonrandom distribution of aftershocks (King et al., 1994; Stein, 1999). The probability of aftershock activity is interpreted to increase where the difference between shear strength, $\tau_s$ and imposed shear stress, $\tau$, decreases as a result of mainshock–driven changes to stress and fluid-pressure states. The difference between shear stress and shear strength is known as the Coulomb failure stress. The rupture-driven change in Coulomb failure stress, ΔCFS, therefore measures change in the proximity of the shear stress and fluid-pressure state to failure conditions in a rock mass and is given by

$$\Delta CFS = \Delta\tau - \Delta\tau_s, \tag{17}$$

where $\Delta\tau$ and $\Delta\tau_s$ are the change in shear stress and shear strength, respectively. Shear strength is given by

$$\tau_s = C + (\mu\sigma_n - P_f), \tag{18}$$

where C is the cohesive strength, $\mu$ is the friction coefficient, $\sigma_n$ is the normal stress, and $P_f$ is the pore fluid pressure. Accordingly,

$$\Delta CFS = \Delta\tau - \mu(\Delta\sigma_n - \Delta P_f) \tag{19}$$

can be calculated by elastic-frictional modeling of fault slip (e.g., King et al., 1994). Domains of positive ΔCFS have a higher probability of producing aftershocks than areas of negative ΔCFS. The locations of lobes of positive ΔCFS are influenced by the locations of mainshock rupture arrest, fault kinematics, slip magnitude, and the orientation of the regional stress field. The modeling approach usually assumes an

undrained pore-fluid condition in which sudden, coseismic changes in stress states drive changes in fluid pressure via poroelastic effects only (Stein, 1999).

By analogy with active seismogenic systems, the low displacement faults and brittle-ductile shear zones that host mesothermal gold deposits are interpreted as being repeatedly reactivated as aftershocks following major rupture events on nearby high displacement faults (Cox and Ruming, 2004). Application of stress-transfer modeling in fault-controlled hydrothermal systems is providing insights about controls on the distribution of mineralization in fault systems (Cox and Ruming, 2004; Micklethwaite and Cox, 2004). The present work suggests that major contractional or dilational jogs on high displacement faults play a key role in localizing mainshock rupture arrest. For example, the distribution of low displacement faults containing gold deposits in the St. Ives goldfield is consistent with rupture arrest and coseismic static stress change being controlled by the presence of a large contractional jog in a regional fault system (Fig. 24). Although major mineralization occurs in an imbricate thrust array in the jog, substantial mineralization also occurs in low displacement faults up to 10 km from the jog, within areas where modeled coseismic static stress change favored aftershock activity. Similarly in the Mount Pleasant goldfield, 50 km northwest of Kalgoorlie, the distribution of fault-hosted gold mineralization correlates well with modeled areas of positive ΔCFS associated with rupture arrest on a regional-scale dilational jog on a high displacement fault (Micklethwaite and Cox, 2004).

Accordingly, large jogs on high displacement faults not only provide major conduits for fluid redistribution in fault networks but may also control mainshock rupture arrest and thereby influence coseismic stress changes and the distribution of domains where aftershocks occur. Aftershock networks potentially enhance crustal permeability for many kilometers away from jogs and are interpreted to provide distributary percolation networks along which fluids discharge from jogs or other high-permeability arrest points on high displacement faults. During the life of an active fault system, aftershock domains are expected to be reactivated hundreds to thousands of times, with new batches of hydrothermal fluid percolating though them after each mainshock rupture.

Whether aftershock networks become mineralized will depend first on whether the network taps into appropriate

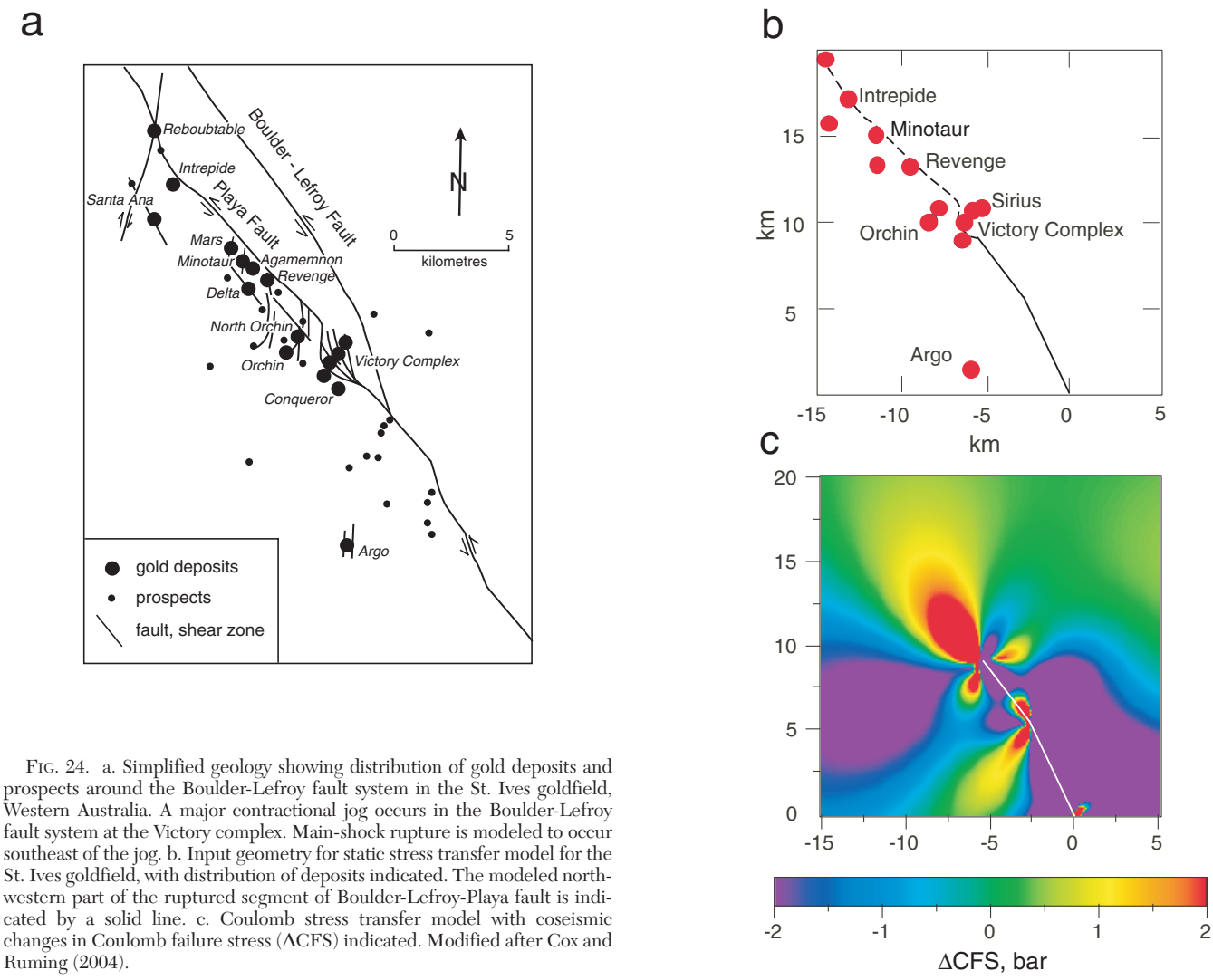


FIG. 24. a. Simplified geology showing distribution of gold deposits and prospects around the Boulder-Lefroy fault system in the St. Ives goldfield, Western Australia. A major contractional jog occurs in the Boulder-Lefroy fault system at the Victory complex. Main-shock rupture is modeled to occur southeast of the jog. b. Input geometry for static stress transfer model for the St. Ives goldfield, with distribution of deposits indicated. The modeled northwestern part of the ruptured segment of Boulder-Lefroy-Playa fault is indicated by a solid line. c. Coulomb stress transfer model with coseismic changes in Coulomb failure stress (ΔCFS) indicated. Modified after Cox and Ruming (2004).

reservoirs. Second, mineralization will depend on whether the network is repeatedly reactivated long enough for a significant metal endowment to accumulate. This requires mainshock rupture propagation to be repeatedly arrested by long-lived asperities in fault systems. Third, appropriate physical and chemical processes must operate to scavenge metals from fluids along the fluid pathways.

*Fluid-triggered aftershocks:* Rapid postseismic fluid redistribution and consequent changes in the fluid-pressure field should occur when mainshock ruptures penetrate overpressured fluid reservoirs. In this situation, changes in Coulomb failure stress and consequent aftershock triggering may be substantially influenced by postseismic fluid-pressure changes (Nur and Booker, 1972; Bosl and Nur, 2002), as well as by the effects of coseismic static stress transfer (see eq. 19).

A contemporary example of probable fluid triggering of aftershocks is described by Miller et al. (2004). They demonstrate that the distribution of aftershocks associated with the 1997 Umbria Marche earthquake sequence in the northern Apennines, Italy, is not well-explained by coseismic static stress transfer. The Umbria Marche mainshock nucleated at a depth of approximately 6 km and ruptured a moderately dipping normal fault. The earthquake sequence commenced with two earthquakes of magnitude 5.7 and 6, nine h apart. These were followed by thousands of events over several months. The aftershocks migrated through a region measuring 40 km in length and 15 km in width over a 30-day period.

A large proportion of aftershocks in the Umbria Marche sequence occurred in the hanging wall of the mainshock rupture. Miller et al. (2004) argued that the spatial distribution of aftershocks and the time-dependent migration of aftershock activity can be explained by a model in which mainshock rupture breached a seal between a deep, overpressured, $CO_2$-rich reservoir and the shallower, near-hydrostatic–pressured regime. Seal breaching caused discharge of fluids from the deep fluid reservoir and propagation of a fluid pressure-pulse upward and outward from the main shock rupture surface (Fig. 19c). Rising fluid pressure in the surrounding crust is interpreted to have triggered slip on low displacement faults, causing aftershocks. The modeled fluid-driven, postseismic changes in Coulomb failure stress are calculated to be two orders of magnitude greater than typical coseismic static stress changes of 0.1 to 0.2 MPa.

The rate of migration of the inferred postseismic fluid-pressure pulse (approx 1 km/d) indicates that the large-scale permeability in the mainshock-aftershock zone was approximately $4 \times 10^{-11}$ m$^2$ (Miller et al., 2004) during the aftershock sequence. This extreme permeability enhancement corresponds to highly fractured rock.

The interpretations of Miller et al. (2004) have important implications for understanding fluid pathways in fault-controlled hydrothermal ore systems. The work first highlights the role of earthquakes in generating episodic hydraulic connectivity between deep, overpressured fluid reservoirs and shallower crustal regimes. Second, it highlights how postseismic fluid redistribution is not only influenced by coseismic permeability enhancement along mainshock rupture zones. Postseismic propagation of fluid-pressure pulses away from the mainshock zone can also drive permeability enhancement within a broad domain around the mainshock zone by promoting fluid-driven failure on aftershock ruptures. The aftershock ruptures form a fluid-driven, invasion percolation network that progressively drains fluids from the deeper level, breached reservoir via the mainshock rupture zone.

The fluid-triggered aftershock model predicts that, after each mainshock, the network of hydraulically linked aftershock ruptures grows progressively outward from the mainshock zone. Because aftershock networks can extend many kilometers from the main shock rupture surface, ore potential may develop well away from the high displacement mainshock structures that drain deeper crustal, metal-fertile fluid reservoirs.

The spatial distribution of aftershocks that are triggered by migrating fluid-pressure pulses can be different from that predicted by coseismic static stress transfer. In particular, fluid-triggered aftershock permeability enhancement is expected to be highest around the upper parts of mainshock rupture zones (Fig. 19c). In moderately dipping rupture zones, fluid discharge occurs preferentially into the hanging wall of the rupture surface. Note, however, that fluid-triggered aftershocks and aftershocks triggered by coseismic static stress changes represent two end-member situations. In many seismogenic fault systems, both driving processes are likely to influence the distribution of aftershocks and hence the distribution of fluid pathways that can drain fluid reservoirs.

The seismic activity around the Umbria Marche rupture zone indicates that individual pulses of postseismic fluid redistribution can occur on time scales of months. Migration of aftershocks following the 1992 Landers earthquake sequence in California is also interpreted to have been influenced by fracture-controlled fluid redistribution on similar time scales (Bosl and Nur, 2002).

## Deposit-Scale Controls on Flow in Hydrothermal Systems

### *Permeable damage zones related to faults and shear zones*

As on the regional scale, faults and associated fracture arrays exhibit heterogeneous distributions of fracture apertures and fracture densities at deposit scales. Areas with the highest apertures and/or fracture densities produce the highest permeability sites that localize the highest fluid fluxes. High fracture apertures and densities are typically associated with deposit-scale fault bends, step-over regions, or jogs which link approximately planar segments of faults and shear zones (e.g., Hulin, 1929; Bateman, 1959; Sibson, 2001; Fig. 23).

Both deposit-scale contractional and dilational jogs provide sites with high fracture density that localize fluid flow and ore deposition. The orientation relationships between faults, jogs, and slip directions result in the long axis of jogs developing approximately parallel to the $\sigma_2$ orientation (Fig. 23c). This produces a permeability anisotropy favoring flow parallel to the jog axis. For reverse and normal faulting regimes, extensional and contactional jogs have subhorizontal plunges (Fig. 23d). This provides good horizontal fracture connectivity and permeability within faults and may cause ore shoots to have gentle plunges (e.g., Cox et al., 1995). In contrast, strike-slip regimes produce jogs with good vertical connectivity, which can control the geometry of steeply plunging ore shoots (Fig. 23d).

In both the Ballarat and Castlemaine goldfields in central Victoria, gently plunging dilational jogs on low displacement reverse faults provide a major control on lode location and geometry (Cox et al., 1991). As noted earlier, the Victory Complex of gold deposits in the St. Ives goldfield is localized within a contractional jog on a regional sinistral fault system. Individual lodes are localized within faults that form an imbricate thrust array within the jog zone (Cox and Ruming, 2004). Mineralization also occurs in heavily fractured competent units in the jog zone. The less steeply dipping segments of thrusts tend to be more dilatant than steeply dipping fault segments and are associated with fault-fill vein mineralization.

High fracture permeability is also localized around fault termination zones, where fault splays, wing cracks, or brecciated regions develop (Fig. 23b). An outstanding example of wing crack or horsetail structures controlling the distribution of mineralization occurred in the Leonard mine at Butte, Montana (Bateman, 1959; Fig. 25). Here, mineralized, northwest-trending, steeply dipping wing cracks have propagated up to 100 m away from the tips of northeast-trending dextral strike-slip fault veins. The array of wing cracks forms a high-density, mineralized fracture array, presumably with greatly enhanced vertical permeability during mineralization, over an area of 650 × 150 m and at least 1,000 m in vertical extent (Meyer et al., 1968).

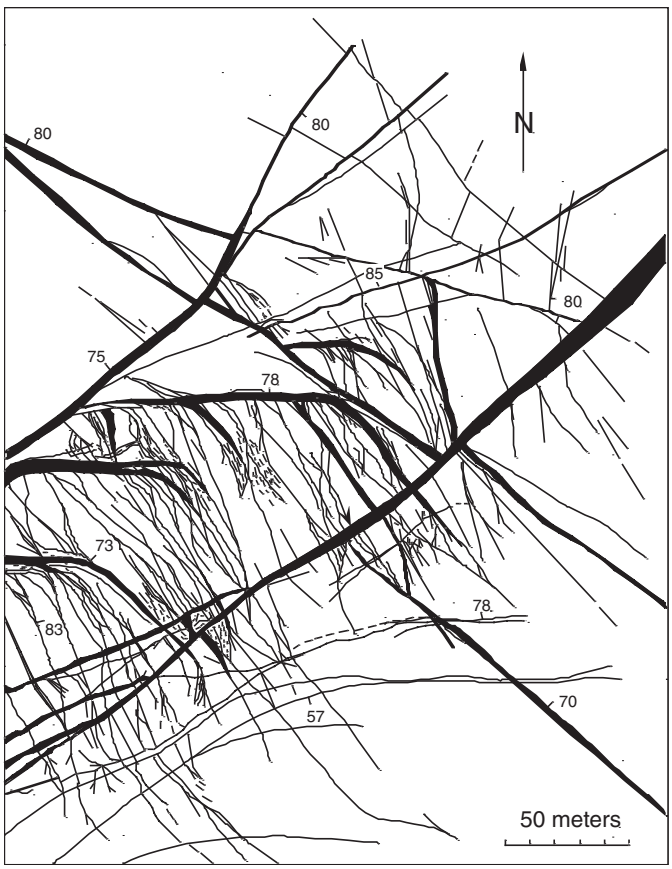


FIG. 25. Fault-related wing-crack arrays associated with fault-controlled mineralization in the Leonard mine, Butte, Montana. Modified after Bateman (1959).

Although much mineralization in fault-related ore systems occurs in fault-fill lodes, or disseminated mineralization adjacent to faults and shear zones, further mineralization is also usually associated with arrays of extension veins which can extend for many meters away from faults (e.g., Fig. 25). Fault-related extension veins provide distributary networks for fluid discharge from faults into reactive wall rocks.

*Effects of competence contrast on fluid pathways*

Where competent rock layers are embedded in a less competent matrix, more rapid deformation of the matrix generates strain compatibility problems between the competent layer and the matrix. During shortening at high angles to layer interfaces, one way for strain compatibility to be maintained along the competent interface is for the competent layer to stretch by fracture or boudinage. Fracture may produce arrays of extension veins localized within the competent layer, at high angles to the boundary of the competent layer. Extension of competent layers may also be achieved by production of hybrid extensional shear fractures or faults. Fracture arrays associated with low strain, layer-parallel extension of competent layers provide an important structural control on fluid migration and ore localization in many mesothermal lode gold systems. Examples include the Walhalla-Woods Point deposits in Victoria (Clappison, 1954; Edwards, 1954), the syenite-hosted Wallaby deposit in the Eastern Goldfields of Western Australia (Salier et al., 2004), and stacked faults at Lamaque, Quebec (Robert and Poulsen, 2001). Although vertical stretching during the formation of each of these vein-related lode systems should lead to marked subhorizontal permeability anisotropy, good vertical connectivity was also provided by the intersecting mesh of mineralized fractures.

The distribution of lode-hosting structures at the Golden Mile (low displacement faults and shear zones) and Mount Charlotte (extension and extensional-shear veins) deposits at Kalgoorlie also reflects competence contrasts (Clout et al., 1990). In both these cases, permeability enhancement due to fracturing and lode formation was localized in a thick, competent dolerite sill that is embedded in more ductile stratigraphy. Fracture formation occurred particularly within a coarse-grained granophyric zone in the sill.

At high strains, complete pull-apart of competent layers forms boudins. The separation zones between boudins provide high-permeability fluid pathways. An example is discussed by Oliver et al. (2001) where intense alteration, veining, and minor mineralization in the Mary Kathleen fold belt, Queensland, is localized around the ends of boudins in amphibolites.

During approximately plane strain, where extension occurs predominantly in one direction, the permeability anisotropy associated with boudin separation leads to highest permeability along a direction parallel to the boudin long axis. The geometry of ore shoots can reflect this permeability anisotropy. Boudins are particularly well developed where competent units are incorporated in high-strain ductile shear zones, as well as on fold limbs in areas with tight folding. In flattening strain regimes, boudin separation zones can form in any direction within the flattening plane (XY plane of the strain ellipsoid), so there need not be a preferred permeability anisotropy in any particular direction within the layering.

Where strain compatibility is not maintained at an interface between competent and incompetent layers, mechanical decoupling localizes along the boundary. In low-temperature or high pore-fluid factor environments, this nucleates a brittle fault along the interface. In ductile regimes, a shear strain gradient can develop at the interface. This may nucleate a shear zone that can grow to dimensions much larger than the competence contrast that initiated it. Both brittle and plastic decoupling at mechanical interfaces enhance permeability and may localize flow and ore deposition.

The presence of competent layers may also influence localization of permeability enhancement in other ways. In particular, dilatant jogs can be localized where faults obliquely cut though competent layers.

*Fold-related fluid pathways*

Three basic buckle-folding mechanisms control the initial phases of fold growth during layer parallel shortening; these are flexural slip, flexural flow, and tangential longitudinal strain (Ramsay and Huber, 1987). Which mechanism operates is influenced by the strength of mechanical coupling between layers, the mechanical behavior of layers, and competence contrasts between layers. Each mechanism produces distinctive strain and displacement distributions around buckled layers and is associated with distinctive fracture styles that influence permeability enhancement, vein formation, and ore localization during folding.

*Tangential longitudinal strain:* Tangential longitudinal strain is a term used to describe one way in which strain can be distributed in fold hinge zones during folding (Ramsay, 1967). It is particularly relevant for folding of competent layers in low- to moderate-temperature environments. During the early stages of fold growth by tangential longitudinal strain, the outer arcs of competent layers are stretched parallel to bedding in fold hinges, whereas the inner arcs are shortened parallel to bedding. If pore-fluid factors are high enough for fluid pressure to exceed the near-field minimum principal stress, outer-arc stretching is associated with formation of extension veins at high angles to bedding in fold hinges on the outer arc of individual competent rock layers or packages of competent layers (Fig. 26a). Normal faults can also form in this area. Inner-arc shortening can be associated with growth of reverse faults and associated veins, as well as intensification of foliation development.

Ramsay (1974) noted that late during fold tightening, the strain states in fold hinges may change. In this case, the outer arcs of fold hinges in competent layers may undergo late extension at high angles to bedding, producing bedding-parallel veins near the outer arcs of competent layers. Similarly, late extension fractures at high angles to layering can open on the inner arcs of competent layers.

*Flexural flow folding:* Flexural flow folding involves approximately layer-parallel simple-shear deformation on fold limbs. Such behavior typically occurs in relatively incompetent materials such as slate. As layers maintain approximately constant bed length on fold limbs during simple shear, there is no stretching or shortening of layers during this process. In high pore-fluid factor regimes, a component of layer-parallel shear on fold limbs can be accommodated by the formation of en echelon extension veins (Fig. 26b). Localized, layer-parallel fluid flow is expected to be associated with grain-scale permeability enhancement in layers undergoing flexural flow.

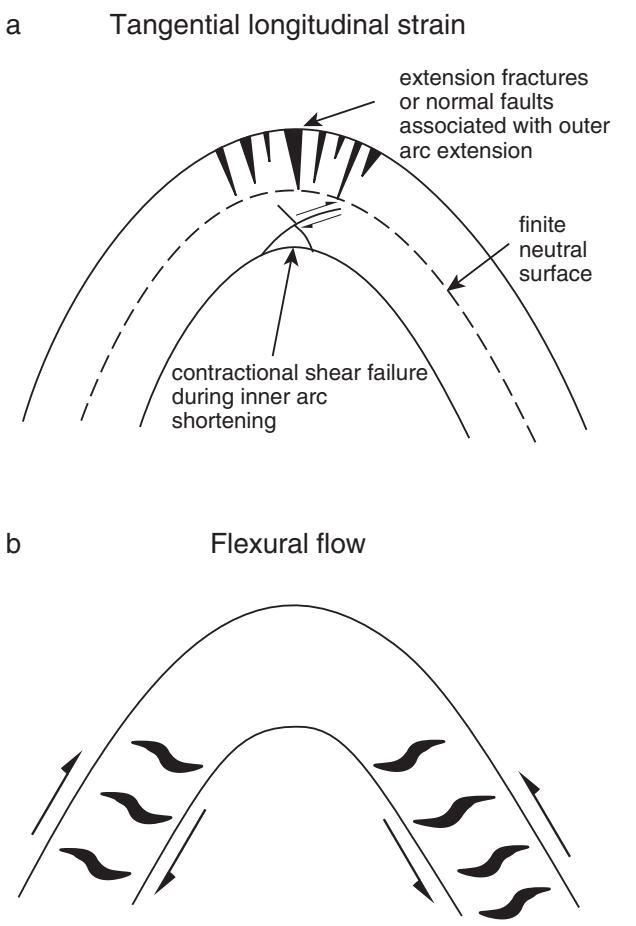


FIG. 26. a. Fracture distributions and permeability enhancement associated with tangential longitudinal strain in fold hinge zones. b. En echelon fracture arrays associated with flexural flow in relatively incompetent layers on fold limbs.

*Flexural slip and related kink and chevron folding:* In multilayered sequences where mechanical decoupling can occur along bedding interfaces, fold growth may involve slip along bedding in a direction perpendicular to fold hinges (Fig. 27a). This behavior is common during the growth of chevron folds in fairly regularly layered sedimentary rock sequences.

In high pore-fluid factor regimes, bedding-parallel flexural slip is associated with the formation of massive to laminated veins along bedding (Fig. 27b). Bedding-parallel veins host a substantial part of the vein-hosted gold mineralization in turbidite-hosted gold deposits such as the Bendigo, Victoria (Hulin, 1929; Chace, 1947; Cox et al., 1991; Schaubs and Wilson, 2002) and the Meguma, Nova Scotia, deposits (Kontak et al., 1990). Bedding-parallel veins can be active at all stages of fold growth, from early layer-parallel shortening, through to shortening after fold lock-up. Bedding-parallel slip is particularly well developed during chevron folding of interlayered competent and incompetent units, such as sandstone-siltstone-slate sequences typical of turbidite packages (Ramsay, 1974).

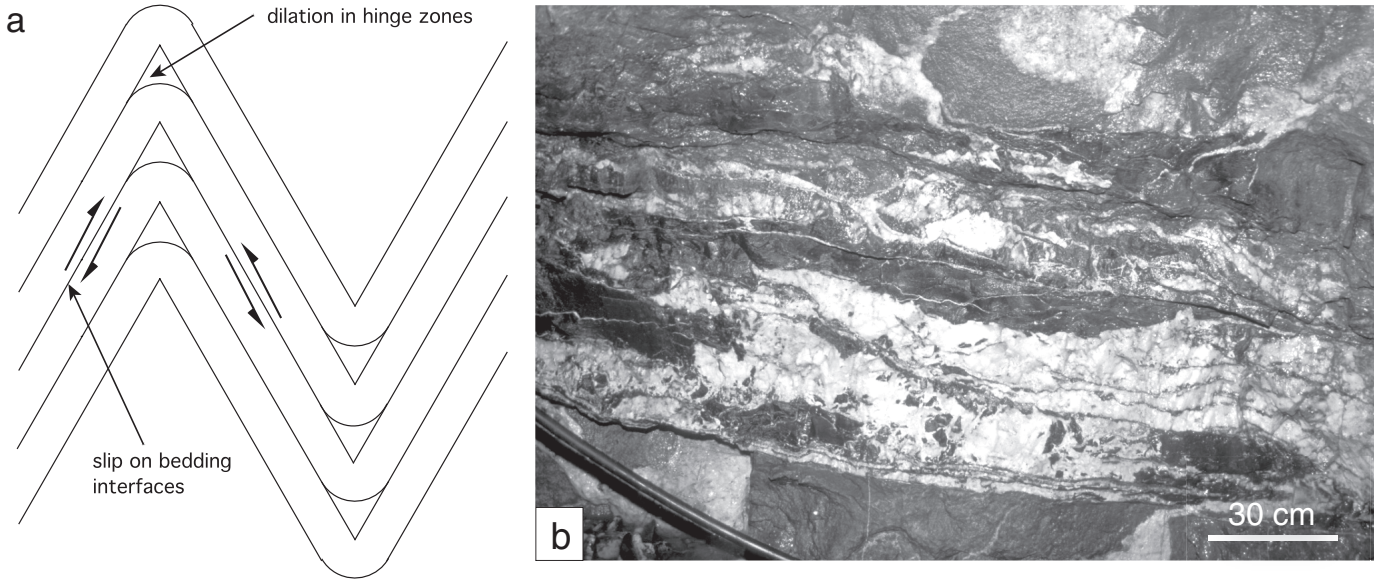


FIG. 27. a. Flexural slip in a multilayered sequence produces bedding-parallel slip and hinge dilation. b. Bedding-parallel gold-bearing quartz lode associated with bedding-parallel slip during fold growth. Sheepshead anticline, Bendigo, Victoria, Australia.

A geometric consequence of fold growth by flexural slip is that, if pore-fluid factors are high enough, dilation and saddle reef formation can occur at fold hinges (Fig. 27a). Saddle reefs and related structures provide high-permeability parallel to fold hinges during their formation. Chevron folding of interlayered competent and incompetent rock sequences is particularly associated with the formation of saddle reefs and related structures (Ramsay, 1974). Dilation at fold hinges is favored by a high ratio of thickness of competent to incompetent packages (Fig. 28). Hinge dilation tends to occur in the incompetent packages adjacent to competent sequences. The dilational zones may open to produce simple saddle reef veins or much more complex vein stockworks (Fig. 29). The presence of anomalously thick competent layer packages, embedded in a succession of more thinly layered competent and incompetent units, tends to localize major dilation both above and below the thick competent package, as well as generating dip misfits along the fold limbs. These space problems can be accommodated by formation of saddle reefs and the generation of limb thrusts that break across the fold hinge adjacent to the thick competent layer (Fig. 30a, b). Note that unless pore-fluid factors are high in fold hinges, dilation cannot occur; hinge collapse and the formation of bulbous fold hinges occurs instead.

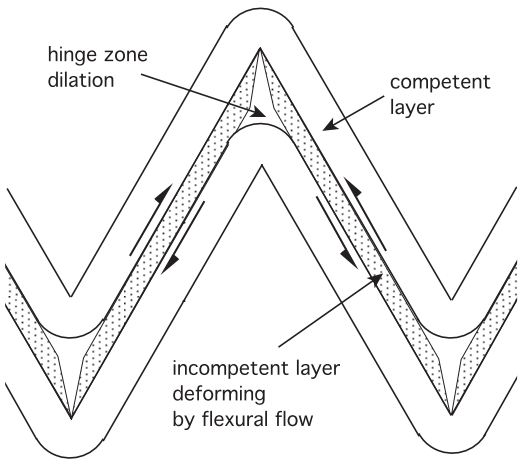


FIG. 28. Formation of hinge dilation zones associated with chevron folding of interlayered competent and incompetent units. Strain in the incompetent layer is approximately simple shear (i.e., flexural flow) on the fold limbs. The competent layer is essentially unstrained on the fold limbs, whereas in the fold hinge zone, strain can approximate tangential longitudinal strain. Modified after Ramsay (1974).

The presence of anomalously thin competent layers in a generally more thickly layered sequence also generates space problems during chevron folding. The thin competent layer usually accommodates the strain in the thickly bedded package by layer-parallel stretching on fold limbs. This involves formation of veins approximately perpendicular to bedding in the competent units (Figs. 29c, 30c).

Many saddle reef structures in the Bendigo goldfield are modified by the presence of mineralized limb thrusts that break through the hinge area to form bedding-discordant faults. Where they are bedding-discordant, the limb thrusts usually are spatially associated with arrays of extension veins in both their footwall and hanging wall. In contrast, the bedding-parallel veins on fold limbs seldom have associated extension veins until they are close to the hinge zone. Where partial hinge collapse occurs around anomalously thick competent packages, vertically elongate to cuspate saddle reef structures are developed. Some of these structures are tens of meters high.

The presence of dilational zones in fold hinges, associated limb thrusts, fault- and fold-related extension veins, and limb stretching, all establish a strong permeability anisotropy that favors fluid flow parallel to fold hinges during growth of chevron folds.

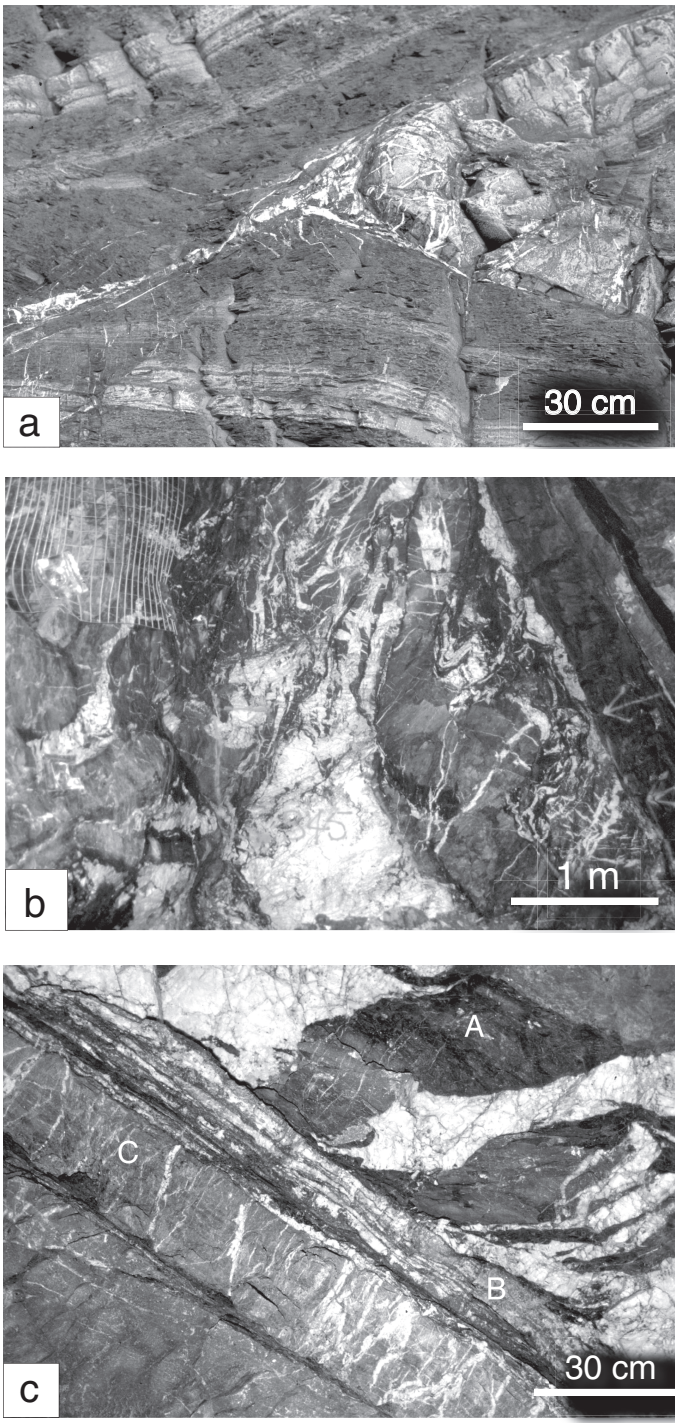


FIG. 29. Vein development near hinge zones of chevron folded sequences. a. Complex quartz veining (white) associated with hinge dilation and associated limb faulting in the hinge of a recumbent fold, Millook Haven, UK. b. Development of complex vein arrays in an anticlinal hinge zone, Sheepshead anticline, Bendigo. Bedding on right side of image dips steeply to the right; bedding on left side of image dips moderately to the left. c. Vein formation and related fracture-controlled permeability in an interbedded sequence of sandstone and slate, near the hinge zone of the Sheepshead anticline. In incompetent slate layer A, vein formation is associated with flexural flow during fold growth. Bedding-parallel flexural slip and dilation at B has produced a bedding-parallel laminated vein. Layer-parallel stretching has produced arrays of extension veins at high angles to bedding in competent sandstone layer C.

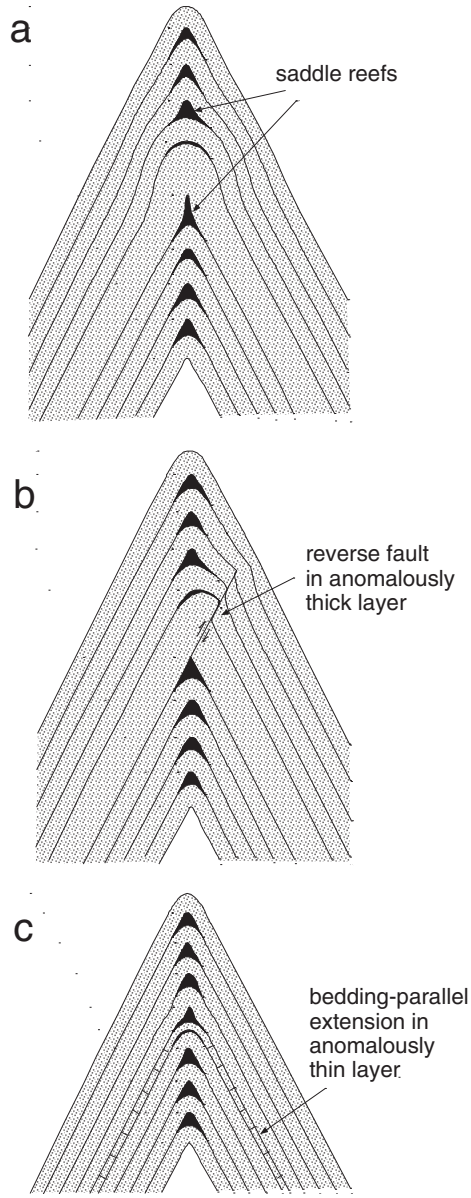


FIG. 30. Effects of variable layer thicknesses on distribution of dilational sites, faults, and fractures during chevron folding. a. Bulbous hinge structure in an anomalously thick folded layer. b. Limb thrust developed due to presence of an anomalously thick layer. c. Layer-parallel stretching and fracturing in an anomalously thin competent layer. Modified after Ramsay (1974).

In the Bendigo goldfield, saddle reefs and related structures are developed predominantly in anticlinal hinge zones. Very few synclines, other than small parasitic ones in major anticlinal zones, have substantial vein development (Cox et al., 1991). This relationship is interpreted to indicate that pore-fluid factors in synclinal domains did not reach sufficiently high levels to promote fracture growth. This is understandable if anticlinal zones acted as low-permeability stratigraphic and/or structural traps and pressure-driven flow forced fluids broadly upward along high-permeability pathways (e.g., active bedding-parallel faults) until flow was impeded at anticlinal hinges. During opening of saddle reefs

and related structures, permeability anisotropy favors subsequent fluid migration up plunge along anticlinal hinge zones. Skelton et al. (1995) have also described evidence for flow localization at the hinges of regional antiforms during regional folding, foliation development, and prograde metamorphism in the Scottish Highlands.

At Bendigo, the major vein-hosted mineralization is developed in the culmination zones (i.e., the structurally highest positions associated with fold plunge reversal) in about ten doubly plunging anticlines, over an area of 50 km$^2$. This supports an interpretation that fluid-pressure gradients along high-permeability anticlinal hinge zones drove flow up plunge toward regional anticlinal fold culminations. The highest pore-fluid factors are interpreted to have developed beneath low-permeability, unfractured carapaces in the culmination of each anticline. Vein-hosted lode formation in these areas was probably promoted by fluid-driven failure and progressive propagation of fluid-pressure pulses to successively higher stratigraphic levels in culmination zones.

At the Ballarat and Castlemaine goldfields in central Victoria, bedding-parallel faults continued to be active after fold lock-up. In these goldfields, unlike Bendigo, bedding-parallel slip zones generally are not associated with saddle reefs at fold hinges but instead generate limb thrusts where they intersect fold hinges. Limb thrusts cut across the adjacent fold limb as less steeply dipping, bedding-discordant faults (Cox et al., 1991; Cox, 1995). Where they intersect the next fold hinge, they again become bedding-parallel and more steeply dipping. This geometry forms a dilatant jog that is elongate parallel to the fold hinge and would promote a strong component of fluid migration parallel to fold hinges within the jog (Fig. 31). Permeability enhancement associated with slip on the steeply dipping bounding faults is interpreted to have provided strong vertical hydraulic connectivity.

Where flexural slip operates in multilayered sequences, the early stages of folding tend to produce kinklike and box folds prior to the pervasive development of chevron folds at higher bulk shortening (Paterson and Weiss, 1966). The general geometry of kink folds is illustrated in Figure 32. If the kink-band boundary is not the bisector of the two limbs of a kink fold, dilation, or contraction across the layering may occur in the kinked zone (Anderson, 1964; Ramsay, 1967). Where the angle between the kink-band boundary and the layering outside the kink band ($\alpha_1$) is less than the angle between the kink-band boundary and the layering within the kink band ($\alpha_2$), dilation normal to layering occurs (Ramsay, 1967; Ramsay and Huber, 1987). During development of macroscopic folds, these dilatant sites provide potentially important fluid pathways. Dilation at layer interfaces localizes especially where there is a competence contrast. This process is likely to have been a factor controlling fluid pathways, as well as initiation of some gold-bearing, layer-parallel veins, during the early stages of folding at Bendigo and other turbidite-hosted goldfields. More extensive discussion of controls on bedding-parallel vein formation during the transition from kink folding, at low bulk strain, to chevron folding at higher strain, is provided by Fowler and Winsor (1996).

*Superimposed homogeneous strain during folding:* During buckle folding in low-temperature metamorphic regimes, folds tend to frictionally lock-up when interlimb angles reach

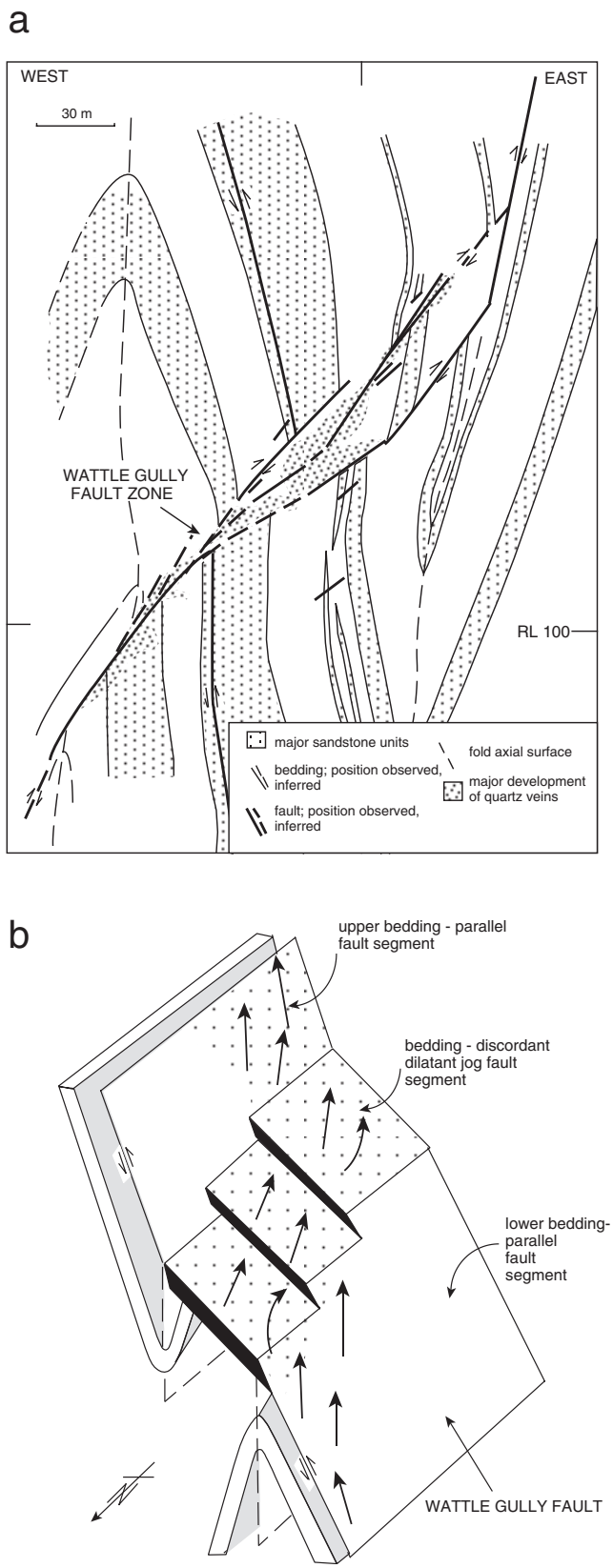


FIG. 31. a. Fold-related dilatant jog, Wattle Gully gold deposit, Victoria. b. Schematic three-dimensional illustration of the fold-related dilatant jog, Wattle Gully fault zone. Inferred fluid-flow directions indicated. Modified after Cox (1995) and Cox et al. (1995).

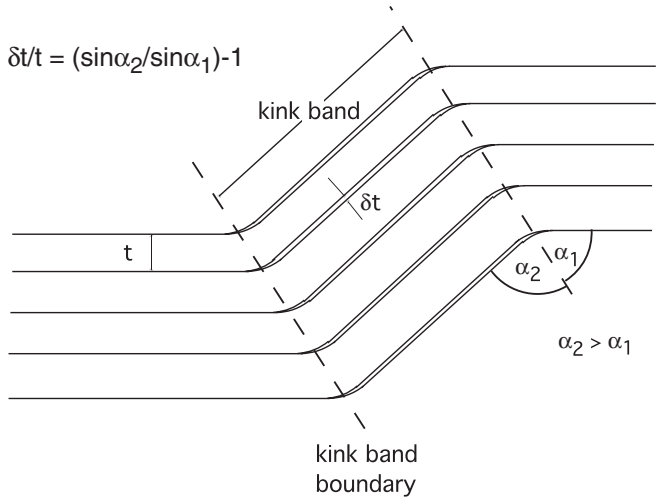


FIG. 32. Dilation along layer boundaries associated with formation of a kink fold. Dilation is localized within the kink band when $\alpha_2 > \alpha_1$. $\delta t/t$ provides a measure of dilation in the kink band, where t is the bed thickness. Modified after Ramsay (1967).

approximately 55°. Further bulk shortening then involves penetrative deformation of layers, as well as faulting. As folds tighten, competent layers on fold limbs become stretched and boudinaged. During approximately plane strain deformation, boudins pull apart typically in a direction at a high angle to the fold axis. This generates permeability anisotropy with good connectivity along the direction of fold axis. In other cases, where the superimposed deformation approximates flattening strain, shortening perpendicular to the axial plane results in stretching both perpendicular and parallel to the fold axis, producing so-called "chocolate tablet" boudinage. Pull-apart of competent layers in this way leads to good connectivity in all directions that are parallel to layering within the stretched competent layer.

Extension of folds parallel to the fold axis may also produce fractures and veins that cut across fold axial surfaces at high angles. These fractures tend to host mineralization formed late during folding.

*Fault-bend folding and fault-propagation folding:* Fault-bend folding and fault-propagation folding are important processes during crustal shortening, especially in foreland fold and thrust regimes. An important aspect of fault-related folding is that, as thrust sheets move across fault ramps, fold hinges and related fracture damage zones migrate through thrust sheets. Experimental simulation of fault-related folding (Chester et al., 1991) provides fascinating insights into the development of permeability in thrust systems (Fig. 33). For the boundary conditions of their experiments, intense fracturing and associated permeability enhancement occurred in the leading hinge area of the ramp anticline, as well as in the hanging wall of the fault ramp. The fracture swarm in the fault ramp nucleates at the trailing edge of the ramp and then passively migrates in the direction of thrust sheet transport. Fault propagation folding is also associated with growth of fracture networks in the hinge of the propagating fold and in both the hanging wall and footwall of the thrust near the trailing edge of the ramp. Note that these fracture networks will

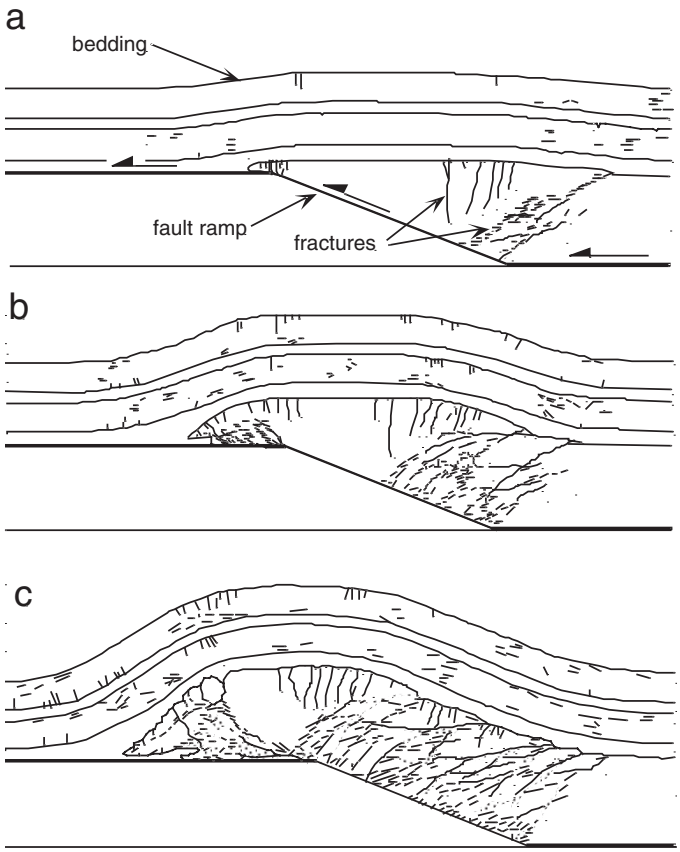


FIG. 33. Distribution of fracture permeability associated with progressive growth of an experimentally produced, fault-related fold. Thin black lines and stipple represent fractured areas. Modified after Chester et al. (1991).

only be permeable while the fractures are dilating; that is, while they are moving through fault bend zones.

## Concluding Remarks

Dominant influences on the development of crustal-scale hydrothermal systems at depths greater than several kilometers in the crust include the following:

1. Fluid redistribution is driven largely by hydraulic gradients between fluid reservoirs and the downstream ends of percolation networks.
2. Deformation processes and high pore-fluid factors play a fundamental role in driving permeability enhancement.
3. Competition between permeability-creation and permeability-destruction processes leads to rapid destruction of permeability in fracture-controlled hydrothermal systems unless ongoing deformation and/or high pore-fluid factors repeatedly regenerate permeability.
4. Localization of deformation leads to localization of flow.
5. In aseismic deformation regimes, steady-state deformation is expected to be associated with steady-state flow regimes. However, the spontaneous development of porosity waves may generate episodic fluid flow.
6. In the upper-crustal seismogenic regime, fault slip and associated permeability enhancement in the rupture zone can initiate fluid-flow events. Interseismic hydrothermal sealing

of faults and draining of the hydraulically accessible parts of fluid reservoirs progressively shuts down flow. Accordingly, fault-related flow is typically episodic in the seismogenic regime.

7. Active faults and shear zones play a key role in draining overpressured fluid reservoirs and establishing high fluid flux systems that generate epigenetic ore systems.

8. Elevated pore-fluid factors play a key role in driving growth of percolation networks through invasion percolation. The greatest localization of flow may occur when networks of faults and shear zones are close to their percolation threshold. Cyclic failure and fault sealing during the seismic cycle may maintain permeability of fault systems near the percolation threshold.

9. Localization of flow within volumetrically small parts of high displacement fault and/or shear networks can be controlled by the distribution of jogs and relay structures that provide pipelike connectivity to deep, overpressured reservoirs.

10. Many epigenetic ore deposits are spatially associated with low displacement faults and shear zones in larger, crustal-scale fault networks. The low displacement structures are interpreted as members of aftershock networks that are repeatedly reactivated after mainshocks on high displacement faults. The location of aftershock networks is strongly influenced by the distribution of mainshock arrest points on high displacement faults, by coseismic stress transfer and by fluid-driven growth of percolation networks by invasion of high-pressure fluid pulses away from high-permeability sites at the downstream end of mainshock ruptures.

11. Deposit-scale localization of fluid flow is strongly influenced by fluid-driven growth of fracture permeability in structurally controlled sites. Permeability enhancement is associated particularly with jogs and other irregularities on faults and shear zones, fault intersections, various fold-related dilation sites, and fracture growth related to effects of competence contrasts in deforming layered media. Understanding how fracture permeability may develop in different geologic situations can help to predict the location of fluid pathways and thus the location of potential ore zones.

## Acknowledgments

This work was greatly stimulated by interactions with a number of people. I particularly acknowledge discussions with J. Braun, M. Knackstedt, S. Micklethwaite, S. Miller, M. Paterson, R. Sibson, and E. Tenthorey. The ideas in this paper have also been stimulated by discussions and field trips with many members of the mining and minerals exploration communities. They have been very generous with their time and providing opportunities to work in a variety of deposit types. I especially thank the geological teams at the St. Ives Gold Mining Company, the Porgera gold deposit, the Placer Dome operations in Western Australia, and Bendigo Mining. This work was supported by the Australian Research Council. M. Etheridge and H. Poulsen are thanked for very constructive reviews. J.P. Richards and J.W. Hedenquist provided excellent editorial advice.

## REFERENCES

An, L.-J., and Sammis, C.G., 1996, A cellular automaton for development of crustal shear zones: Tectonophysics, v. 253, p. 247–270.

Anderson, R., Graham, C.M., Boyce, A.J., and Fallick, A.E., 2004, Metamorphic and basin fluids in quartz-carbonate-sulphide veins in the SW Scottish Highlands: A stable isotope and fluid inclusion study: Geofluids, v. 4, p. 169–185.

Anderson, T.B., 1964, Kink bands and related geological structures: Nature, v. 202, p. 272–274.

Angevine, C.L., Turcotte, D.L., and Furnish, M.D., 1982, Pressure solution lithification as a mechanism for stick-slip behavior of faults: Tectonics, v. 1, p. 151–160.

Bak, P., 1997, How nature works—the science of self-organized criticality: Oxford, Oxford University Press, 212 p.

Barnicoat, A.C., Fare, R.J., Groves, D.I., and McNaughton, N.J., 1991, Synmetamorphic lode gold deposits in high-grade Archean settings: Geology, v. 19, p. 921–924.

Bateman, A.M., 1959, Economic mineral deposits, 2nd ed.: New York, John Wiley and Sons, 916 p.

Bebout, G.E., and Barton, M.D., 1989, Fluid flow and metasomatism in a subduction zone hydrothermal system: Catalina schist terrane, California: Geology, v. 17, p. 976–980.

Berkowitz, B., 1995, Analysis of fracture network connectivity using percolation theory: Mathematical Geology, v. 27, p. 467–483.

Bickle, M.J., and Baker, J., 1990, Advective-diffusive transport of isotopic fronts: An example from Naxos, Greece: Earth and Planetary Science Letters, v. 97, p. 79–93.

Bjorlykke, K., 1997, Lithological control on fluid flow in sedimentary basins, *in* Jamtveit, B., and Yardley, B.W.D., eds., Fluid flow and transport in rocks—mechanisms and effects: London, New York, Chapman and Hall, p. 15–34.

Bosl, W.J., and Nur, A., 2002, Aftershocks and pore fluid diffusion following the1992 Landers earthquake: Journal of Geophysical Research, v. 107, doi: 10.1029/2001JB000155.

Boullier, A.-M., and Robert, F., 1992, Palaeoseismic events recorded in Archaean gold-quartz vein networks, Val d'Or, Quebec, Canada: Journal of Structural Geology, v. 14, p. 161–180.

Boyer, S.E., and Elliot, D., 1982, Thrust systems: American Association of Petroleum Geologists Bulletin, v. 66, p. 1196–1230.

Brace, W.F., 1980, Permeability of crystalline and argillaceous rocks: International Journal of Rock Mechanics, Mining Science and Geomechanics Abstracts, v. 17, p. 241–251.

Brace, W.F., Walsh, J.B., and Frangos, W.T., 1968, Permeability of granite under high pressure: Journal of Geophysical Research, v. 73, p. 2225–2236.

Brady, J. B., 1989, The role of volatiles in the thermal history of metamorphic terranes: Journal of Petrology, v. 29, p. 1187–1213.

Brantley, S.L., Evans, B., Hickman, S.H., and Crerar, D.A., 1990, Healing of microcracks in quartz—implications for fluid flow: Geology, v. 18, p. 136–139.

Brantley, S.L., Fisher, D.M., Deines, P., Clark, M.B., and Myers, G., 1997, Segregation veins: Evidence for deformation and dewatering of a low grade metapelite, *in* Holness, M.B., ed., Deformation-enhanced fluid transport in the Earth's crust and mantle: London, Chapman and Hall, p. 267–288.

Braun, J., Munroe, S., and Cox, S.F., 2003, Transient fluid flow in and around a fault: Geofluids, v. 3, p. 81–87.

Cartwright, I., and Oliver, N.H.S., 2000, Metamorphic fluids and their relationship to the formation of metamorphosed and metamorphogenic ore deposits: Reviews in Economic Geology, v. 11, p. 81–96.

Cathles, L.M., III, and Adams, J.J., 2005, Fluid flow and petroleum and mineral resources in the upper (<20-km) continental crust:Economic Geology 100th Anniversary Volume, p. 77–110.

Černý, P., Blevin, P.L., Cuney, M., and London, D., 2005, Granite-related ore deposits: Economic Geology 100th Anniversary Volume, p. 337–370.

Chace, F.M., 1947, Origin of Bendigo saddle reefs with comments on the formation of ribbon quartz: Economic Geology, v. 44, p. 561–597.

Chester, J.S., Logan, J.M., and Spang, J.H., 1991, Influence of layering and boundary conditions on fault-bend and fault-propagation folding: Geological Society of America Bulletin, v. 103, p. 1059–1072.

Clappison, R.J.S., 1954, The Morning Star mine, Wood's Point, *in* Edwards, A.B., ed., Geology of Australian ore deposits: Melbourne, Australasian Institute of Mining and Metallurgy, p. 1077–1082.

Cline, J.S., Hofstra, A.H., Muntean, J.L., Tosdal, R.M., and Hickey, K.A., 2005, Carlin-type gold deposits in Nevada: Critical geologic characteristics and viable models: Economic Geology 100th Anniversary Volume, p. 451–483.

Clout, J.M.F., Cleghorn, J.H., and Eaton, P.C., 1990, Geology of the Kalgoorlie goldfield, *in* Hughes, F.E., ed., Geology of the mineral deposits of Australia and Papua New Guinea: Australasian Institute of Mining and Metallurgy Monograph Series, v. 14, p. 411–431.

Connolly, J.A.D., 1997, Devolatilization-generated fluid pressure and deformation-propagated fluid flow during prograde regional metamorphism: Journal of Geophysical Research, v. 102, p. 18,149–18,173.

Connolly, J., and Podlachikov, Y.Y., 1998, Compaction-driven flow in viscoelastic rock: Geodynamica Acta, v. 11, p. 55–84.

Cowie, P.A., 1998, A healing-reloading feedback control on the growth rate of faults: Journal of Structural Geology, v. 20, p. 1075–1087.

Cowie, P.A., and Scholz, C.H., 1992, Growth of faults by accumulation of seismic slip: Journal of Geophysical Research, v. 97, p. 11085–11095.

Cox, S.F., 1995, Faulting processes at high fluid pressures: An example of fault-valve behavior from the Wattle Gully fault, Victoria, Australia: Journal of Geophysical Research, v. 100, p. 841–859.

——1999, Deformational controls on the dynamics of fluid flow in mesothermal gold systems: Geological Society of London Special Publications, v. 155, p. 123–139.

Cox, S.F., and Etheridge, M.A., 1989, Coupled grain-scale dilatancy and mass transfer during deformation at high fluid pressures, Mt Lyell area, Tasmania: Journal of Structural Geology, v. 11, p. 147–162.

Cox, S.F., and Paterson, M.S., 1991, Experimental dissolution-precipitation creep in quartz aggregates at high temperatures: Geophysical Research Letters, v. 18, p. 1401–1404.

Cox, S.F., and Ruming, K., 2004, The St Ives mesothermal gold system, Western Australia—a case of golden aftershocks?: Journal of Structural Geology, v. 26, p. 1109–1125.

Cox, S.F., Etheridge, M.A., and Wall, V.J., 1987, The role of fluids in syntectonic mass transport, and the localization of metamorphic vein-type ore deposits: Ore Geology Reviews, v. 2, p. 65–86.

Cox, S.F., Sun, S.-S., Etheridge, M.A., Wall, V.J. and Potter, T.F., 1995, Structural and geochemical controls on the development of turbidite-hosted gold-quartz vein deposits, Wattle Gully mine, central Victoria, Australia: Economic Geology, v. 90, p. 1722–1746.

Cox, S.F., Braun, J., and Knackstedt, M.A., 2001, Principles of structural control on permeability and fluid flow in hydrothermal systems: Reviews in Economic Geology, v. 14, p. 1–24.

Cui, X., Nabelek, P.I., and Liu, M., 2003, Reactive flow of mixed $CO_2$-$H_2O$ fluid and progress of calc-silicate reactions in contact metamorphic aureoles: Insights from two-dimensional modeling: Journal of Metamorphic Geology, v. 21, p. 663–684.

Dipple, G.M., and Ferry, J.M., 1992a, Metasomatism and fluid flow in ductile shear zones: Contributions to Mineralogy and Petrology, v. 112, p. 149–164.

——1992b, Fluid flow and stable isotope alteration in rocks at elevated temperatures with applications to metamorphism: Geochimica et Cosmochimica Acta, v. 56, p. 3539–3550.

Dipple, G.M., and Gerdes, M.L., 1998, Reaction-infiltration feedback and hydrodynamics at the skarn front: Mineralogical Association of Canada Short Course Series, v. 26, p. 71–97.

Dudziak, K.H., and Frank, E.U., 1966, Messung der viscositaet des wassers bis 560° und 3500 bar: Berichte Bunsenges Physikalisches Chemie, v. 70, p. 1120–1128.

Dutrow, B., and Norton, D., 1995, Evolution of fluid pressure and fracture propagation during contact metamorphism: Journal of Metamorphic Geology, v. 13, p. 677–686.

Edwards, A.B., 1954, Mines of the Walhalla-Wood's Point auriferous belt, *in* Edwards, A.B., ed., Geology of Australian ore deposits: Melbourne: Australasian Institute of Mining and Metallurgy, p. 1061–1076.

Ellis, D., and Dunlap, J., 1988, Displacement distribution on faults as they link up: Journal of Structural Geology, v. 10, p. 183–192.

Etheridge, M.A., 1983, Differential stress magnitudes during regional deformation and metamorphism: Upper bound imposed by tensile fracturing: Geology, v. 11, p. 231–234.

Etheridge, M.A., Wall, V.J., and Vernon, R.H., 1983, The role of the fluid phase during regional metamorphism: Journal of Metamorphic Geology, v. 1, p. 205–226.

Etheridge, M.A., Wall, V.J., Cox, S.F., and Vernon, R.H., 1984, High fluid pressures during regional metamorphism and deformation—implications for mass transport and deformation mechanisms: Journal of Geophysical Research, v. 89, p. 4344–4358.

Ferry, J.M., 1994, An historical review of metamorphic fluid flow: Journal of Geophysical Research, v. 99, p. 15,487–15,498.

Ferry, J.M., and Dipple, G.M., 1991, Fluid flow, mineral reactions and metasomatism: Geology, v. 19, p. 211–214.

——1992, Models for coupled fluid flow, mineral reaction and isotopic alteration during contact metamorphism: The Notch Peak aureole, Utah: American Mineralogist, v. 77, p. 577–591.

Ferry, J.M., and Gerdes, M.L., 1998, Chemically reactive fluid flow during metamorphism: Annual Review of Earth and Planetary Sciences, v. 26, p. 255–287.

Fischer, G.J., and Paterson, M.S., 1992, Measurements of permeability and storage capacity in rocks during deformation at high temperature and pressure, *in* Evans, B., and Wong, T.-F., eds., Fault mechanics and transport properties of rocks: San Diego, Academic Press, p. 213–252.

Fisher, D.M., and Brantley, S.L., 1992, Models of quartz overgrowth and vein formation: Deformation and fluid flow in an ancient subduction zone: Journal of Geophysical Research, v. 97, p. 20,043–20,061.

Forster, C., and Smith, L., 1990, Fluid flow in tectonic regimes, *in* Nesbitt, B.E., ed., Mineralogical Association of Canada Short Course on "Crustal Fluids" Handbook, v. 18, p. 1–47.

Fournier, R.O., 1999, Hydrothermal processes related to movement of fluid from plastic into brittle rock in the magmatic-epithermal environment: Economic Geology, v. 94, p. 1193–1212.

Fowler, T.J., and Winsor, C.N., 1996, Evolution of chevron folds by profile shape changes: Comparison between multiplayer deformation experiments and folds of the Bendigo-Castlemaine goldfields, Australia: Tectonophysics, v. 258, p. 125–150.

Foxford, K.A., Nicholson, R., Polya, D.A., and Hebblethwaite, R.P.B., 2000, Extensional failure and hydraulic valving at Minas da Panasqueira, Portugal—evidence from vein spatial distributions, displacements and geometries: Journal of Structural Geology, v. 22, p. 1065–1086.

Glen, R.A., 1987, Copper and gold deposits in deformed turbidites at Cober, Australia: Their structural control and hydrothermal origin: Economic Geology, v. 82, p. 124–140.

Goldfarb, R.J., Groves, D.I., and Gardoll, S., 2001, Orogenic gold and geologic time: A global synthesis: Ore Geology Reviews, v. 18, p. 1–75.

Goldfarb, R.J., Baker,T., Dubé, B. Groves, D.I., Hart,C.J.R., and Gosselin, P., 2005, Distribution, character, and genesis of gold deposits in metamorphic terranes: Economic Geology 100th Anniversary Volume, p. 407–450.

Greenwood, H.J., 1975, Buffering of pore fluids by metamorphic reactions: American Journal of Science, v. 275, p. 573–593.

Groves, D.I., Barley, M.E., and Ho, S.E., 1989, Nature, genesis and tectonic setting of mesothermal gold mineralization in the Yilgarn block, Western Australia: Economic Geology Monograph 6, p. 71–85.

Groves, D.I., Goldfarb, R.J., Robert, F., and Hart, C.J.R., 2003, Gold deposits in metamorphic belts: Overview of current understanding, outstanding problems, future research, and exploration significance: Economic Geology, v. 98, p. 1–29.

Groves, D.I., Ridley, J.R., Bloem, E.M.J., Gebre-Meriam, M., Hagemann, S.G., Hronsky, J.M.A., Knight, J.T., McNaughton, N.J., Ojala, J., Vielreicher, R.M., McCuaig, T.C., and Holyland, P.W., 1995, Lode-gold deposits of the Yilgarn block: Products of late-Archaean crustal-scale overpressured hydrothermal systems: Geological Society of London Special Publications, v. 95, p. 155–172.

Guéguen, Y., and Dienes, J., 1989, Transport properties of rocks from statistics and percolation: Mathematical Geology, v. 21, p. 1–13.

Guéguen, Y., and Palciauskas, V., 1994, Introduction to the physics of rocks: Princeton, Princeton University Press, 294 p.

Guéguen, Y., David, C., and Gavrilenko, P., 1991, Percolation networks and fluid transport in the crust: Geophysical Research Letters, v. 18, p. 931–934.

Guermani, A., and Pennachioni, G., 1998, Brittle precursors of plastic deformation in a granite: An example from the Mont Blanc massif (Helvetic, western Alps): Journal of Structural Geology, v. 20, p. 135–148.

Heidrick, T.L., and Titley, S.R., 1982, Fracture and dike patterns in Laramide plutons and their structural and tectonic implications: American Southwest, *in* Titley, S.R., ed., Advances in geology of the porphyry copper deposits: Southwestern North America: Tucson, AZ, University of Arizona Press, p. 73–91.

Heinrich, C.A., Bain, J.H.C, Mernagh, T.P., Wyborn, L.A.I., Andrerw, A.S., and Waring, C.L., 1995, Fluid and mass transfer during metabasalt alteration and copper mineralization at Mount Isa: Economic Geology, v. 90, p. 705–730.

Heinrich, C.A., Andrew, A.S., and Knill, M.D., 2000, Regional metamorphism and ore formation: Evidence from stable isotopes and other fluid tracers: Reviews in Economic Geology, v. 11, p. 97–117.

Hickman, S., Sibson, R., and Bruhn, R., 1995, Introduction to special issue: Mechanical involvement of fluids in faulting: Journal of Geophysical Research, v. 100, p. 12,831–12,840.
Hilgers, C., Dilg-Gruschinski, K., and Urai, J.L., 2004, Microstructural evolution of syntaxial veins formed by advective flow: Geology, v. 32, p. 261–264.
Hofstra, A.H., and Cline, J.S., 2000, Characteristics and models for Carlin-type gold deposits: Reviews in Economic Geology, v. 13, p. 163–220.
Holness, M.B., 1997, The permeability of non-deforming rock, *in* Holness, M.B., ed., Deformation-enhanced fluid transport in the Earth's crust and mantle: The Mineralogical Society Series, v. 8: London, Chapman and Hall, p. 9–39.
Hulin, C.D., 1929, Structural control of ore deposition: Economic Geology, v. 24, p. 15–49.
Hunt, I.M., 1990, Generation and migration of petroleum from abnormally pressured compartments: American Association of Petroleum Geologists Bulletin, v. 74, p. 1–12.
Husen, S., and Kissling, E., 2001, Post-seimsic fluid flow after the large subduction zone earthquake of Antofagasta, Chile: Geology, v. 29, p. 847–850.
Kanagawa, K., Cox, S.F., and Zhang, S., 2000, Effects of dissolution-precipitation processes on the strength and mechanical behavior of quartz gouge at high-temperature hydrothermal conditions: Journal of Geophysical Research, v. 105, p. 11,115–11,126.
Kennedy, B.M., Kharaka, Y.K., Evans, W.C., Ellwood, A., DePaolo, D.J., Thordsen, J., Ambats, G., and Mariner, R.H., 1997. Mantle fluids in the San Andreas fault system, California: Science, v. 278, p. 1278–1281.
Kerrich, R., and Cassidy, K.F., 1994, Temporal relationships of lode gold mineralization to accretion, magmatism, metamorphism and deformation—Archaean to present: A review: Ore Geology Reviews, v. 9, p. 263–310.
Kerrich, R., Fyfe, W.S., Gorman, B.E., and Allison, I., 1977, Local modification of rock chemistry by deformation: Contributions to Mineralogy and Petrology, v. 65, 183–190.
Kim, Y.-S., Peacock, D.C.P., and Sanderson, D.J., 2004, Fault damage zones: Journal of Structural Geology, v. 26, p. 503–518.
King, G.C.P., Stein, R.S., and Lin, J., 1994, Static stress changes and the triggering of earthquakes: Bulletin of the Seismological Society of America, v. 84, p. 935–953.
Knackstedt, M., and Cox, S.F., 1995, Percolation and pore geometry of crustal rocks: Physical Reviews, series E, v. 51, p. R5181–R5184.
Knipe, R.J., Jones, G., and Fisher, Q.J., 1998, Faulting, fault sealing and fluid flow in hydrocarbon reservoirs—an introduction: Geological Society of London Special Publications, v. 147, p. vii-xxi.
Koerner, A., Kissling, E., and Miller, S.A., 2004, A model of deep crustal fluid flow following the $M_w$ = 8.0 Antofagasta, Chile earthquake: Journal of GeophysIcal Research, v. 109, B06307, DOI: 10.1029/2003JB002816.
Kontak, D.J., Smith, P.K., Kerrich, R., and Williams, P.F., 1990, Integrated model for Meguma Group gold deposits, Nova Scotia, Canada: Geology, v. 18, p. 238–242.
Lowell, R.P., Van Capellan, P., and Germanovich, L.N., 1993. Silica precipitation in fractures and the evolution of permeability in hydrothermal upflow zones: Science, v. 260, p. 192–194.
Manning, C.E., 2004, The chemistry of subduction-zone fluids: Earth and Planetary Science Letters, v. 223, p. 1–16.
Manning, C.E., and Ingebritsen, S.E., 1999, Permeability of the continental crust—the implications of geothermal data and metamorphic systems: Reviews in Geophysics, v. 37, p. 127–150.
Matthai, S.K., and Fischer, G., 1996, Quantitative modeling of fault-fluid-discharge and fault-dilation-induced fluid-pressure variations in the seismogenic regime: Geology, v. 24, p. 183–186.
Matthai, S.K., and Roberts, S.G., 1997, Transient versus continuous fluid flow in seismically active faults: An investigation by electric analogue and numerical modeling, *in* Jamtveit, B., and Yardley, B.W.D., eds., Fluid flow and transport in rocks—mechanisms and effects: London, New York, Chapman and Hall, p. 263–292.
Matthai, S.K., Henley, R.W., Bacigalupo-Rose, Binns, R.A., Andrew, A.S., Carr, G.R., French, D.H., McAndrew, J., and Kavanagh, M.E., 1995, Intrusion-related, high-temperature gold quartz veining in the Cosmopolitan Howley metasedimentary rock-hosted gold deposit, Northern Territory, Australia: Economic Geology, v. 90, p. 1012–1045.
Matthai, S.K., Heinrich, C.A. and Driesner, T., 2004, Is the Mount Isa copper deposit the product of forced brine convection in the footwall of a major reverse fault?: Geology, v. 32, p. 357–350.
McCaig, A.M., 1988, Deep fluid circulation in fault zones: Geology, v. 16, p. 867–870.
——1997, The geochemistry of volatile flow in shear zones, *in* Holness, M.B., ed., Deformation-enhanced fluid transport in the Earth's crust and mantle: London, Chapman and Hall, p. 227–266.
McCuaig, T.C., and Kerrich, R., 1994, P-T-t-deformation-fluid characteristics of lode gold deposits: Evidence from alteration systematics: Geological Association of Canada Short Course Notes, v. 11, p. 339–380.
Meinert, L.D., Dipple, G.M., and Nicolescu, S., 2005, World skarn deposits: Economic Geology 100th Anniversary Volume, p. 299–336.
Meyer, C., Shea, E.P., Goodard, Jr., C.C., and Staff, 1968, Ore deposits at Butte, Montana, *in* Ridge, J.R., ed., Ore deposits of the United States, 1933–1967: New York, American Institute of Mining, Metallurgical and Petroleum Engineers, v. II, p. 1373–1416.
Micklethwaite, S., and Cox, S.F., 2004, Fault segment rupture, aftershock-zone fluid flow, and mineralization: Geology, v. 32, p. 813–816.
Miller, S.A., and Nur, A., 2000, Permeability as a toggle switch in fluid-controlled crustal processes: Earth and Planetary Science Letters, v. 193, p. 133–146.
Miller, S.A., Collettini, C., Chiaraluce, L., Cocco, M., Barchi, M., and Klaus, B.J.P., 2004, Aftershocks driven by a high-pressure $CO_2$ source at depth: Nature, v. 247, p. 724–727.
Muir-Wood, R., and King, G.C.P., 1993, Hydrological signatures of earthquake strain: Journal of Geophysical Research, v. 98, p. 22,035–22,068.
Munroe, S.M., 1995, The Porgera gold deposit, Papua New Guinea: The influence of structure and tectonic setting on hydrothermal fluid flow and mineralisation at a convergent margin: PACRIM '95 Conference, Auckland, New Zealand, Melbourne, Proceedings, p. 413–416.
Murphy, H.D., 1979, Convective instabilities in vertical fractures and faults: Journal of Geophysical Research, v. 84, p. 6121–6130.
Norton, D., and Knight, J., 1977, Transport phenomena in hydrothermal systems: Cooling plutons: American Journal of Science, v. 277, p. 937–981.
Nur, A., and Booker, J.R., 1972, Aftershocks caused by pore fluid flow: Science, v. 175, p. 885–887.
Nur, A., and Walder, J., 1990, Time-dependent permeability of the Earth's crust, *in* Bredehoeft, J.D., and Norton, D., eds., The role of fluids in crustal processes: Washington, D.C., National Academic Press, p. 113-127.
Odling, N., 1997, Fluid flow in fractures rocks at shallow levels in the Earth's crust: An overview, *in* Holness, M.B., ed., Deformation-enhanced fluid transport in the Earth's crust and mantle: London, Chapman and Hall, p. 289–320.
Oliver, N.H.S., 1996, Review and classification of structural controls on fluid flow during regional metamorphism: Journal of Metamorphic Geology, v. 14, p. 477–492.
——2001, Linking of regional and local hydrothermal systems in the mid-crust by shearing and faulting: Tectonophysics, v. 335, p. 147–161.
Oliver, N.H.S., Ord, A., Valenta, R.K., and Upton, P., 2001, The role of rock rheological heterogeneity in fluid flow and epigenetic mineralization, with examples from the Mt Isa district: Reviews in Economic Geology, v. 14, p. 51–74.
Ord, A., and Oliver, N.H.S., 1997, Mechanical controls on fluid flow during regional metamorphism: Some numerical models: Journal of Metamorphic Geology, v. 15, p. 345–359.
Paterson, M.S., and Weiss, L., 1966, Experimental deformation and folding in phyllite: Geological Society of America Bulletin, v. 77, p. 343–374.
Peach, C.J., and Spiers, C.J., 1996, Influence of crystal plastic deformation on dilatancy and permeability development in synthetic salt rock: Tectonophysics, v. 256, p. 101–128.
Peacock, S.M., 1989, Numerical constraints on rates of metamorphism, fluid production and fluid flux during metamorphism: Geological Society of America Bulletin, v. 101, p. 476–485.
——1990, Fluid processes in subduction zones: Science, v. 248, p. 329–337.
Person, M., Raffensberger, J.D., Ge, S., and Garven, G., 1996, Basin-scale hydrologic modeling: Reviews of Geophysics, v. 34, p. 61–87.
Phillipot, R., and Selverstone, J., 1991, Trace element rich brine in eclogite veins: Implications for fluid composition and transport during subduction: Contributions to Mineralogy and Petrology, v. 106, p. 417–430.
Phillips, O.M., 1991, Flow and reactions in permeable rocks: Cambridge, Cambridge University Press, 285 p.
Powell, R., Will, T.M., and Phillips, G.N., 1991, Metamorphism in Archaean greenstone belts: Calculated fluid compositions and implications for mineralization: Journal of Metamorphic Geology, v. 9, p. 141–150.
Powley, D.E., 1990, Pressures and hydrology in petroleum basins: Earth Science Reviews, v. 29, p. 215–226.

Preston, L.A., Creager, K.C., Crosson, R.S., Brocher, T.M., and Trehu, A.M., 2003, Intraslab earthquakes: Dehydration of the Cascadia slab: Science, v. 302, p. 1197–1200.

Ramsay, J.G., 1967, Folding and fracturing of rocks. New York, NY, John Wiley and Sons, 568 p.

——1974, Development of chevron folds: Geological Society of America Bulletin, v. 85, p. 1741–1754.

——1980, The crack-seal mechanism of rock deformation: Nature, v. 284, p. 135–139.

Ramsay, J.G., and Huber, M., 1987, The techniques of modern structural geology: London, Academic Press, 700 p.

Redmond, P.B., Einaudi, M.T., Inan, E.E., Landtwing, M.R., and Heinrich, C.A., 2004, Copper deposition by fluid cooling in intrusive-centered systems: New insights from the Bingham porphyry ore deposit, Utah: Geology, v. 32, p. 217–220.

Rice, J.R., 1992, Fault stress states, pore pressure distributions, and the weakness of the San Andreas fault, *in* Evans, B., and Wong, T.-F., eds., Fault mechanics and transport properties of rocks: London, Academic Press, p. 475–503.

Ridley, J.R., and Diamond, L.W., 2000, Fluid chemistry of orogenic lode gold deposits and implications for genetic models: Reviews in Economic Geology, v. 13, p. 141–162.

Ridley, R.J., Groves, D.I., and Knight, J.T., 2000, Gold deposits in amphibolite and granulite facies terranes of the Archaean Yilgarn craton: Evidence and implications of synmetamorphic mineralization: Reviews in Economic Geology, v. 11, p. 265–290.

Robert, F., and Poulsen, K.H., 2001, Vein formation and deformation in greenstone gold deposits: Reviews in Economic Geology, v. 14, p. 111–155.

Robert, F., Poulsen, K.H., Cassidy, K.F., and Hodgson, C.J., 2005, Gold metallogeny of the Yilgarn and Superior cratons: Economic Geology 100th Anniversary Volume, p. 1001–1033.

Roddy, M.S., Reynolds, S., Smith, B., and Ruiz, J., 1988, K-metasomatism and detachment-related mineralization, Harcuvar Mountains, Arizona: Geological Society of America Bulletin, v. 100, p. 1627–1639.

Rumble, D., 1994, Water circulation in metamorphism: Journal of Geophysical Research, v. 99, p. 15,499–15,502.

Rumble, D., Ferry, J.M., Hoering, T.C., and Boucot, A.J., 1982, Fluid flow during metamorphism at the Beaver Brook fossil locality, New Hampshire: American Journal of Science, v. 282, p. 886–919.

Sahimi, M., 1994, Applications of percolation theory: London, Taylor and Francis, 258 p.

Salier, B.P., Groves, D.I., McNaughton, N.J., and Fletcher, I., 2004, The world-class Wallaby gold deposit, Laverton, Western Australia: An orogenic-style overprint on a magmatic-hydrothermal magnetite-calcite alteration pipe? Mineralium Deposita, v. 39, p. 473–494.

Schaubs, P. M., and Wilson, C.J.L., 2002, The relative roles of faulting and folding in controlling gold mineralization along the Deborah anticline, Bendigo, Victoria: Australia: Economic Geology, v. 97, p. 325–349.

Scholz, C.H., 1990, The mechanics of earthquakes and faulting: Cambridge, Cambridge University Press, 439 p.

Seedorff, E., Dilles, J.H., Proffett, J.M., Jr., Einaudi, M.T., Zurcher, L., Stavast, W.J.A., Barton, M.D., and Johnson, D.A., 2005, Porphyry-related deposits: Characteristics and origin of hypogene features: Economic Geology 100th Anniversary Volume, p. 251–298.

Sibson, R.H., 1987, Earthquake rupturing as a mineralizing agent in hydrothermal systems: Geology, v. 15, p. 710–704.

——1996, Structural permeability of fluid-driven fault-fracture meshes: Journal of Structural Geology, v. 18, p. 1031–1042.

——2001, Seismogenic framework for ore deposition: Reviews in Economic Geology, v. 14, p. 25–50.

Sibson, R.H., Robert, F., and Poulsen, K.H., 1988b, High-angle reverse faults, fluid-pressure cycling, and mesothermal gold deposits: Geology, v. 16, p. 551–555.

Skelton, A.D.L., Graham, C.M., and Bickle, M.J., 1995, Lithological and structural controls on regional 3D fluid flow patterns during greenschist facies metamorphism of the Dalradian of SW Scottish highlands: Journal of Petrology, v. 36, p. 563–586.

Sleep, N.H., and Blanpied, M.L., 1992, Creep, compaction and the weak rheology of major faults: Nature, v. 359, p. 687–692.

Spear, F.S., 1995, The flow of fluids during metamorphism, *in* Spear, F.S., Metamorphic phase equilibria and pressure-temperature-time paths: Mineralogical Association of America Monograph, p. 673–709.

Stegman, C., and Pocock, J., 1996, The Cobar goldfield—a geological perspective, *in* Cook, W.G., Ford, A.J.W., McDermott, J.J., Standish, T.M., and Stegman, T.M., eds., The Cobar mineral field—a 1996 perspective: Melbourne, Australasian Institute of Mining and Metallurgy, p. 229–264.

Stein, R.S., 1999, The role of stress transfer in earthquake occurrence: Nature, v. 402, p. 605–609.

Streit, J.E., and Cox, S.F., 1998, Fluid infiltration and volume change during mid-crustal mylonitisation of Proterozoic granite, King Island, Tasmania: Journal of Metamorphic Geology, v. 16, p. 197–212.

——2000, Asperity interactions during creep of simulated faults at hydrothermal conditions: Geology, v. 28, p. 231–234.

Stuwe, K., Will, T.M., and Zhou, S., 1993, On the timing relationship between fluid production and metamorphism in metamorphic piles: Some implications for the origin of post-metamorphic gold mineralization: Earth and Planetary Science Letters, v. 114, p. 417–430.

Taylor, H.P., Jr., 1990, Oxygen and hydrogen isotope constraints on the deep circulation of surface waters into zones of hydrothermal metamorphism, and melting, *in* Bredehoeft, J.D., and Norton, D., eds., The role of fluids in crustal processes: Washington, D.C., National Academic Press, p. 72–95.

Taylor, W.L., Pollard, D.D., and Aydin, A., 1999, Fluid flow in discrete joint sets: Field observations and numerical simulations: Journal of Geophysical Research, v. 104, p. 28,983–29,006.

Tenthorey, E., and Cox, S.F., 2003, Reaction-enhanced permeability during serpentinite dehydration: Geology, v. 31, p. 921–924.

Tenthorey, E., Cox, S.F., and Todd, H.F., 2003, Evolution of strength recovery and permeability during fluid-rock reaction in experimental fault zones: Earth and Planetary Science Letters, v. 206, p. 161–172.

Thompson, A.B., 1997, Flow and focusing of metamorphic fluid, *in* Jamtveit, B., and Yardley, B.W.D., eds., Fluid flow and transport in rocks—mechanisms and effects: London, Chapman and Hall, p. 297–313.

Tosdal, R.M., and Richards, J.P., 2001, Magmatic and structural controls on the development of porphyry Cu ± Mo ± Au deposits: Reviews in Economic Geology, v. 14, p. 157–181.

Turcotte, D.L., and Schubert, G., 1982, Geodynamics: New York, John Wiley and Sons, 450 p.

Vrolijk, P., 1987, Tectonically driven fluid flow in the Kodiak accretionary complex, Alaska: Geology, v. 15, p. 466–469.

Walther, J.V., and Orville, P.M., 1982, Volatile production and transport in reginal metamorphism: Contributions to Mineralogy and Petrology, v. 79, p. 252–257.

Wannamaker, P.E., Jiracek, G.R., Stodt, J.A., Caldwell, T.G., Gonzalez, V.M., McKnight, J.D., and Porter, A.D., 2002, Fluid generation and pathways beneath an active compressional orogen, the New Zealand southern alps, inferred from magnetotelluric data: Journal of Geophysical Research, v. 107, p. 10.1029/2001 JB 000186.

Watson, E.B., and Brenan, J.M., 1987, Fluids in the lithosphere. I. Experimentally-determined wetting characteristics of $CO_2$-$H_2O$ fluids and their implications for fluid transport, host rock physical properties, and fluid inclusion formation: Earth and Planetary Science Letters, v. 85, p. 497–515.

Wesnousky, S., 1988, Seismological and structural evolution of strike-slip faults: Nature, v. 335, p. 340–343.

Wilde, A.R., Mernagh, T.P., Bloom, M.S., and Hoffman, C.F., 1989, Fluid inclusion evidence on the origin of some Australian unconformity-related uranium deposits: Economic Geology, v. 84, p. 1627–1642.

Wilkins, J.R., Jr., Beane, R.E., and Heidrick, T.L., 1986, Mineralization related to detachment faults: A model: Arizona Geological Society Digest, v. 16, p. 108–117.

Wilkinson, J.J., and Johnston, D.J., 1996, Pressure fluctuations, phase separation, and gold precipitation during seismic fracture propagation: Geology, v. 24, p. 395–398.

Williams, P.J., Barton, M.D., Johnson, D.A., Fontboté, L., De Haller, A., Mark, G., Oliver, N.H.S., and Marschik, R., 2005, Iron oxide copper-gold deposits: Geology, space-time distribution, and possible modes of origin: Economic Geology 100th Anniversary Volume, p. 371–405.

Witherspoon, P.A., Wang, J.S.Y., Iwai, K., and Gale, J.E., 1980, Validity of the cubic law in a deformable rock fracture: Water Resources Research, v. 19, p. 1016–1024.

Yardley, B.W.D., 1986, Fluid migration and veining in the Connemara schists, *in* Walther, J.V., and Wood, B.J., eds., Fluid-rock interactions during metamorphism. Advances in Physical Geochemistry: New York, Springer-Verlag, p. 109–131.

Yardley, B.W.D., Bottrel, S.H., and Cliff, R.A., 1991, Evidence for regional-scale fluid loss events during mid-crustal metamorphism: Nature, v. 349, p. 151–154.

Yardley, B.W.D., and Graham, J.T., 2002, The origins of salinity in metamorphic fluids: Geofluids, v. 2, p. 249–256.

Zhang, S., Paterson, M.S., and Cox, S.F., 1994a, Porosity and permeability evolution during hot isostatic pressing of calcite aggregates: Journal of Geophysical Research, v. 99, p. 15,741–17,560.

Zhang, S., Cox, S.F., and Paterson, M.S., 1994b, The influence of room temperature deformation on porosity and permeability in calcite aggregates: Journal of Geophysical Research, v. 99, p. 15,761–15,775.

Zhang, S., Tullis, T.E., and Scruggs, V.J., 1999, Permeability anisotropy and pressure dependency of permeability in experimentally sheared gouge materials: Journal of Structural Geology, v. 21, p. 795–806.

Zhang, S., Cox, S.F., and Paterson, M.S., 2001, Microcrack growth and healing in deformed calcite aggregates: Tectonophysics, v. 355, p. 17–36.

Zhang, S., FitzGerald, J.G., and Cox, S.F., 2000, Reaction-enhanced permeability during decarbonation of calcite + quartz → wollastonite + carbon dioxide: Geology, v. 28, p. 911–914.

Zhang, X., and Sanderson, D.J., 1994, Fractal structures and deformation of fractured rock masses, *in* Kruhl, J.H., ed., Fractals and dynamic systems in geoscience: Berlin, Springer-Verlag, p. 37–52.

Zhao, C., Hobbs, B.E., Ord, A., Peng, S., Mülhaus, H.B., and Liu, L., 2004, Theoretical investigation of convective instability in inclined and fluid-saturated, three-dimensional fault zones: Tectonophysics, 387, p. 47–64.